Report of Investigations No. 133

Three-Dimensional Ground-Water Modeling in Depositional Systems, Wilcox Group, Oakwood Salt Dome Area, East Texas

Graham E. Fogg, Steven J. Seni, and Charles W. Kreitler

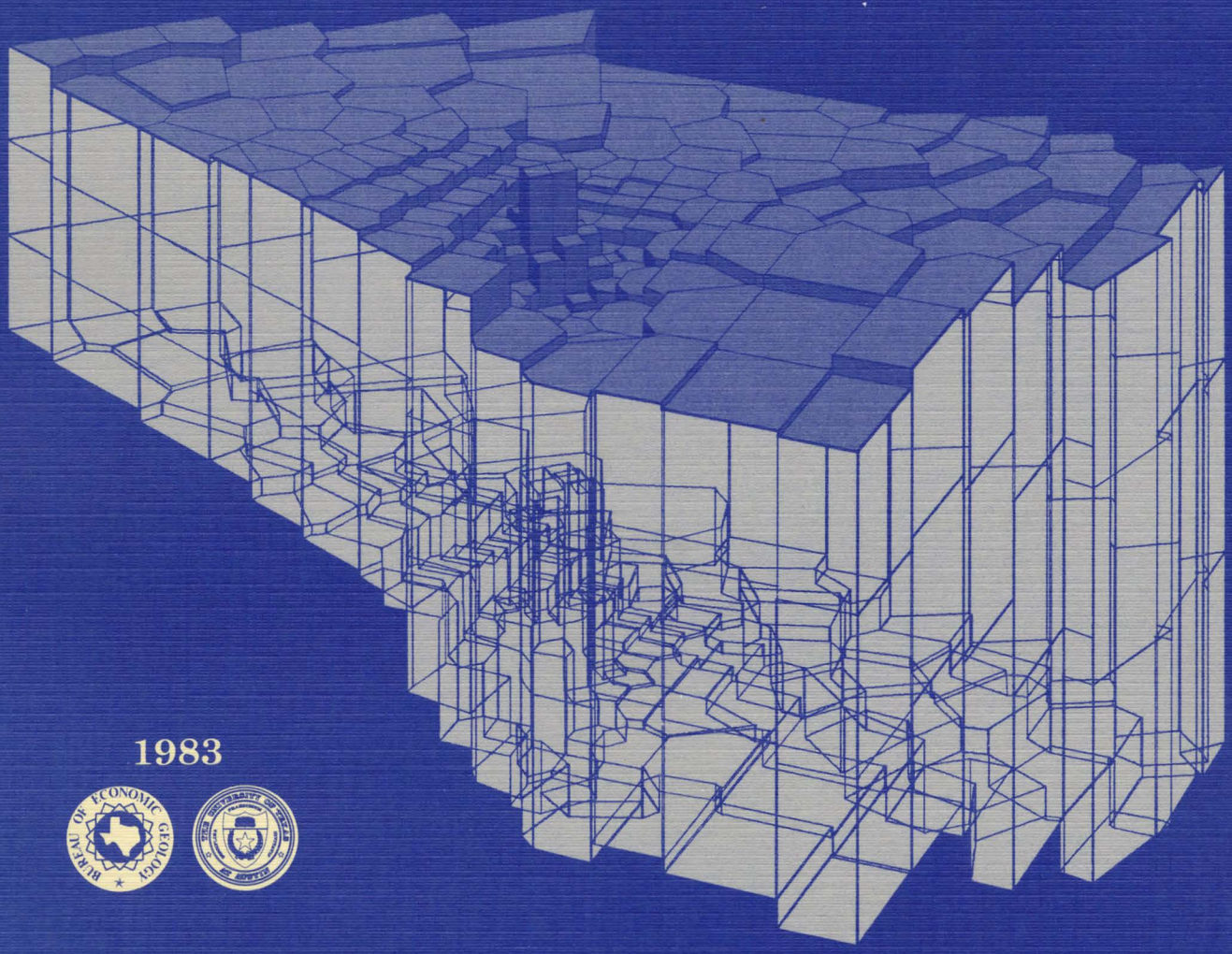

1983

Bureau of Economic Geology • W. L. Fisher, Director

The University of Texas at Austin • Austin, Texas 78712

Report of Investigations No. 133

Three-Dimensional Ground-Water Modeling in Depositional Systems, Wilcox Group, Oakwood Salt Dome Area, East Texas

Graham E. Fogg, Steven J. Seni, and Charles W. Kreitler

Funded by the U. S. Department of Energy,
Office of Nuclear Waste Isolation, under
contract number DE-AC97-80ET46617
and the
Texas Energy and Natural Resources Advisory Council,
under contract number IAC(82-83)-0822

1983

Bureau of Economic Geology • W. L. Fisher, Director
The University of Texas at Austin • Austin, Texas 78712

CONTENTS

Figures

Tables

ABSTRACT

A three-dimensional model was constructed of ground-water flow in the Wilcox-Carrizo aquifer system near Oakwood salt dome to facilitate understanding the hydrogeology around salt domes of the Gulf interior region and ultimately to evaluate the hydrologic suitability of Oakwood Dome for storage of high-level nuclear waste. The data base includes not only measurements of hydraulic head and hydraulic conductivity but also lithofacies maps constructed in a previous study of Wilcox depositional systems.

The Carrizo aquifer is a fairly homogeneous sand sheet overlying the much thicker Wilcox Group, a multiple-aquifer system composed primarily of fluvial channel-fill sand bodies distributed among lower permeability interchannel sands and muds. The interconnectedness of the channel-fill sands, which have predictable values of hydraulic conductivity, strongly influences the rate and direction of ground-water flow. Lateral interconnectedness may depend largely on frequency distributions of channel-fill sands (that is, sand percent). Vertical interconnectedness is apparently poor owing to the horizontal stratification of sand and mud. Simulating observed pressure-depth trends by manipulating values of equivalent vertical hydraulic conductivity (K_v') demonstrates that the ratio of vertical to horizontal conductivity (K_v'/K_h') is very low (approximately 10^{-3} to 10^{-4}). Locally high values of K_v' could result in locally rapid vertical flow, which could in turn be detected using pressure-depth data. Ground-water velocities and travel times computed by the model indicate ground-water residence times of 10^3 to 10^4 years in channel-fill facies and 10^5 to 10^6 years in interchannel facies. Because Oakwood Dome is apparently surrounded by interchannel facies as a result of syndepositional dome growth, the dome may be essentially isolated from circulating Wilcox ground water. A possible exception is where channel-fill facies appear to touch or come close to the northeast flank, coinciding with a brackish-water plume that apparently results from dissolution of salt or cap rock. The northeast orientation of the plume appears to be caused by sand-body distribution and interconnection.

Keywords: ground-water modeling, hydrogeology, Wilcox Group, Carrizo Sand, salt domes, waste disposal, depositional systems, Texas

INTRODUCTION

Oakwood salt dome, located in the southwestern corner of the East Texas Basin (fig. 1), has been studied to evaluate the suitability of salt domes as sites for nuclear waste repositories (Kreitler and others, 1980 and 1981). Hydrologic studies of the salt domes have been conducted to determine whether they are dissolving significantly and to estimate the migration paths and rates of radionuclide transport in the event of a release from a dome repository. Essential to the hydrogeologic system analysis is the construction of numerical models of ground-water flow by which large amounts of data and hypotheses on ground-water circulation can be analyzed collectively. The present study uses such a model for the Wilcox-Carrizo fresh-water aquifer system near Oakwood Dome. The data base includes not only measurements of hydraulic head and conductivity, but also lithofacies maps constructed from an analysis of Wilcox depositional systems by Seni and Fogg (1982).

The purpose of the model is not to make specific predictions about the ground-water flow system, but to assemble large amounts of pertinent data in a form that enables a better understanding of the system. The results can then be used to decide what and where new data are needed to make the model more realistic. Repetition of this procedure can lead to a sufficiently reliable prediction tool.

Unique to the Oakwood modeling study is its combined use of data on depositional systems and hydraulic conductivity to characterize heterogeneity and anisotropy of the Wilcox aquifer. This approach was beneficial because of the complexity of Wilcox geology and the

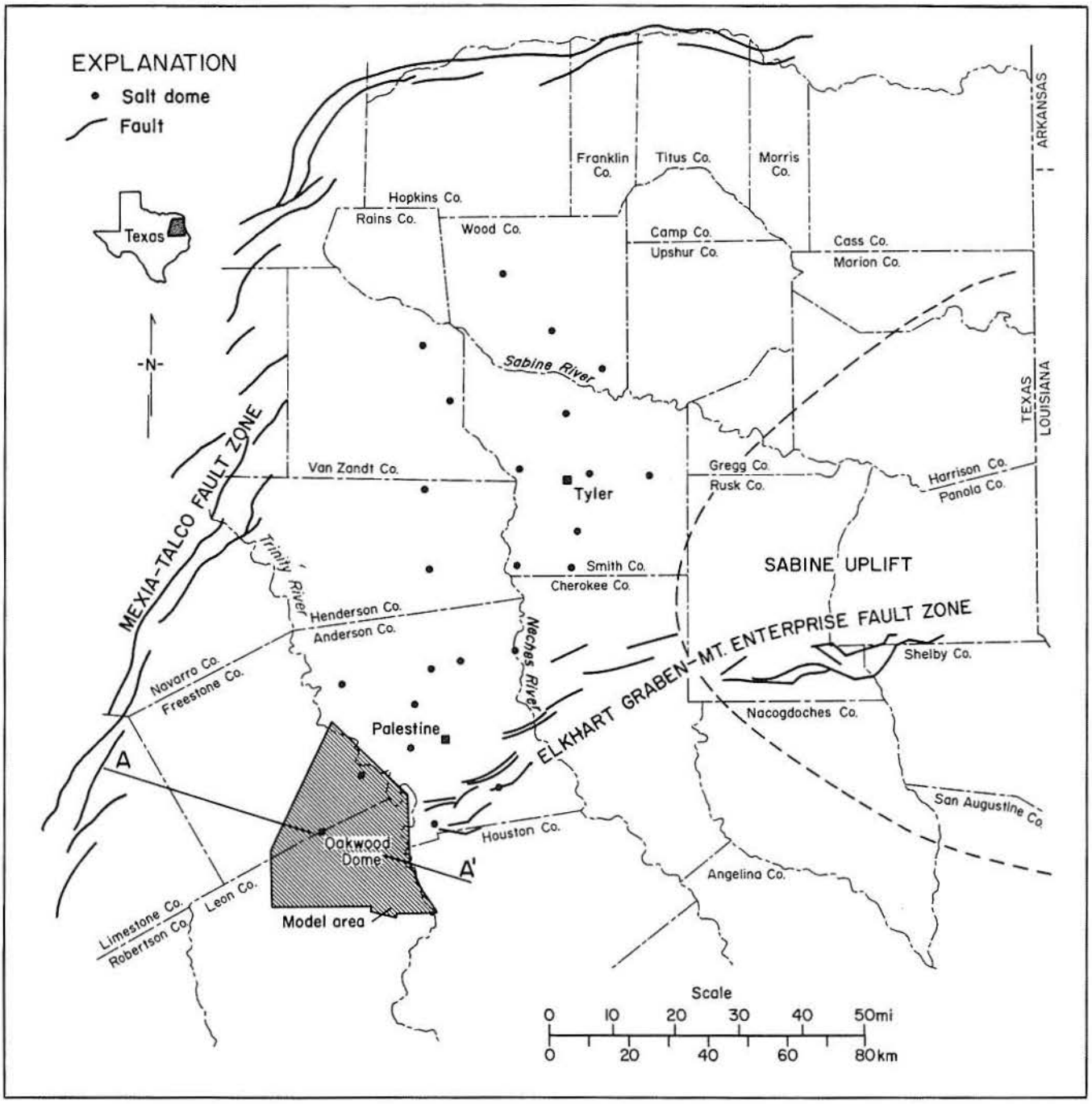

Figure 1. Location of model area.

abundance of geologic data available on the unit. The Wilcox contains thick (approximately 2,000 ft [600 m]) sequences of interbedded, fluvial-deltaic sand and mud bodies. Most of the sands are distributed in a dendritic pattern, indicating a predominantly fluvial depositional environment (Fisher and McGowen, 1967; Kaiser and others, 1978). Detailed maps of sand-body distribution were constructed by Seni and Fogg (1982) for use in the Oakwood model. Field and laboratory measurements of hydraulic conductivity obtained from published sources and from a drilling program conducted around Oakwood Dome in 1979-80 were used to determine permeability of the sands. The maps include only those sands interpreted to have much higher permeability than adjacent sands and muds. Details about how the maps were used in computing equivalent values of hydraulic conductivity for the model will be presented later.

The model was used to simulate several scenarios involving various distributions of hydraulic conductivity of the Wilcox-Carrizo aquifer system and of the Reklaw aquitard. Some of the scenarios appear more realistic than others, but nearly all the results are shown to demonstrate which variables or assumptions have greatest impact on the model. Results are presented in a variety of maps and tables showing (1) contours of hydraulic head, (2) contours of vertical hydraulic gradient, (3) ground-water velocity vectors at each nodal point of the model, (4) boundary fluxes in and out of the model, (5) ground-water travel times, and (6) potential vertical-flow directions in the Wilcox-Carrizo and across the Reklaw aquitard.

The results are pertinent to many other areas of the Gulf Coastal Plain province and to other sedimentary basins where similar hydrogeologic settings exist. Hydrogeologic analysis in these settings is generally complicated owing to (1) aquifer heterogeneity and anisotropy or, more generally, variable sand-body interconnectedness and horizontal stratification of sand-mud complexes, (2) topographic effects on flow, (3) vertical leakage across aquitards, and (4) the meaning of observed three-dimensional trends in hydraulic head and fluid pressure data. The Oakwood model includes all of these factors so that their relative importance and interactions can be observed. The results are also pertinent to the ongoing mining of lignite in the Wilcox Group. Mine dewatering and depressurization problems and environmental impacts are closely tied to the ground-water flow system. The Oakwood model is centered on the deep-basin lignite resource block 8 of Kaiser and others (1980).

HYDROGEOLOGY

Regional Setting

Major fresh-water aquifers in the East Texas Basin are fluvial and deltaic sands of the (youngest to oldest) Queen City Formation, Carrizo Formation, and Wilcox Group (fig. 2). The major saline aquifer is the Woodbine Group, which is separated from the shallower fresh-water systems by 3,000 to 4,000 ft (900 to 1,200 m) of aquitards and aquicludes consisting of clays, shales, and carbonates (Fogg and Kreitler, 1982). Each aquifer consists primarily of thick (approximately 100 ft [30 m]) sands and muddy sands interbedded with mud strata.

The Queen City is a water table system over most of the basin and is separated from the underlying Carrizo Sand by the Reklaw aquitard. In the area of the model, the Reklaw is composed of the Marquez Shale (upper; approximately 90 ft [27 m]) and the Newby Sand (lower; approximately 60 ft [18 m]). Sands and muds of the Reklaw aquitard are typically discontinuous, apparently causing it to be leaky (Fogg and Kreitler, 1982), but in the model area the Marquez Shale appears fairly continuous and thus may form a relatively effective confining bed.

The Carrizo and Wilcox together supply most of the fresh ground water pumped in the basin. The Carrizo Formation is typically a homogeneous sand approximately 100 ft (30 m) thick, whereas the Wilcox Group consists of a heterogeneous distribution of sand and mud facies. Both units occur under predominantly unconfined conditions in outcrops and under confined conditions where overlain by the Reklaw aquitard (fig. 3). The fresh-brackish water interface (1,000 mg/L total dissolved solids) generally lies from 300 to 500 ft (90 to 150 m) above the base of the Wilcox Group. Although the Wilcox and Carrizo are tapped by more than 1,000 wells in the basin, water levels have not declined appreciably, except in a few areas where pumpage rates have been relatively high. Effects of pumpage in the model area have been minimal.

Regional ground-water flow in the Wilcox-Carrizo aquifer system is controlled primarily by geologic structure and topography, as indicated by hydraulic head and water chemistry data (Fogg and Kreitler, 1982). In the Wilcox-Carrizo outcrop areas along the east and west margins of the basin, ground-water flow closely follows topographic gradients; ground water moves away from major recharge areas located at surface watershed divides and toward major discharge areas located along stream valleys. A similar pattern of circulation is apparent in the artesian section (where the Reklaw aquitard is present), but the influence of topography is lessened by the aquitard. Downward leakage from the Queen City to the Wilcox-Carrizo (across the Reklaw) is common except near the Trinity and Sabine Rivers and their tributaries, where upward leakage occurs. Although the directions of vertical leakage have been documented (Fogg and Kreitler, 1982), little information is available on rates of leakage and their significance to the behavior of the system. Correlations between topography and hydraulic head in the artesian section of the

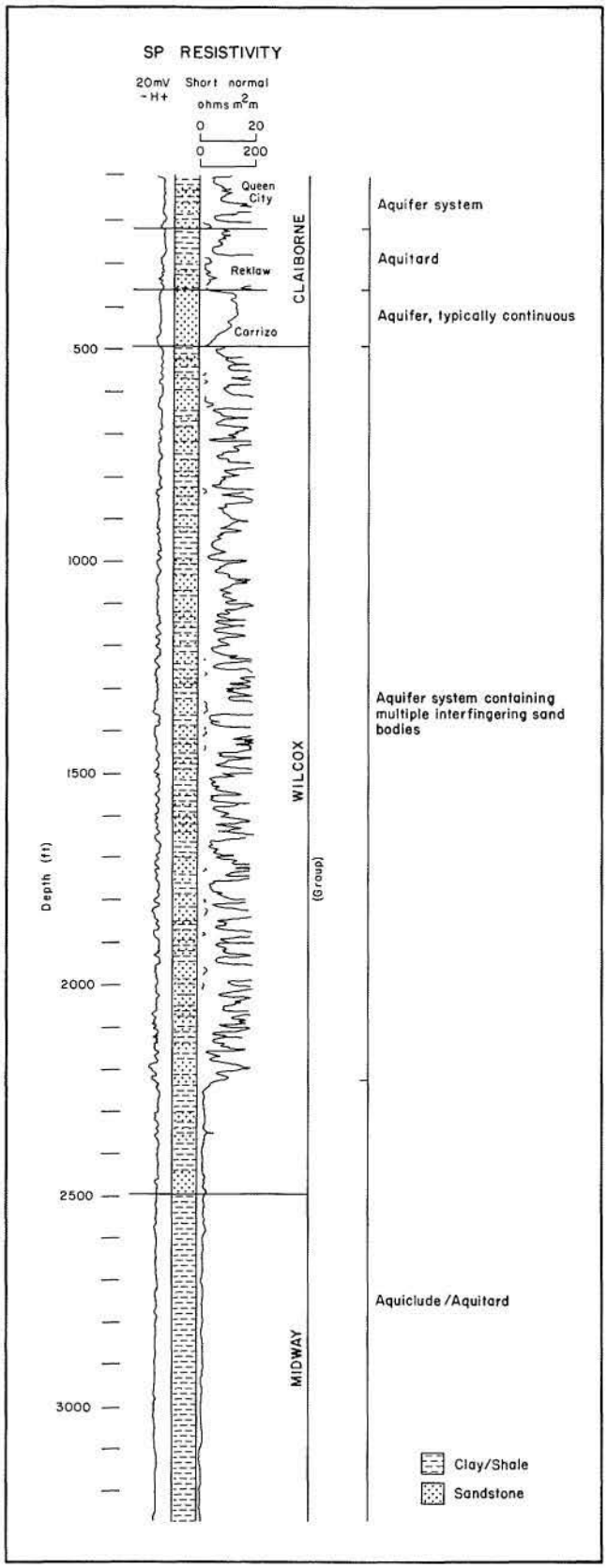

Figure 2. Hydrostratigraphic column showing Tertiary Wilcox and Claiborne Groups and underlying Midway Group. Electric log is from Humble unit number 11, well number 1, Leon County.

Wilcox-Carrizo system suggest that leakage may be significant.

Vertical flow *within* the Wilcox-Carrizo system is another important consideration. Analysis of pressure-versus-depth data indicates potential for downward flow in recharge areas and upward flow in discharge areas (Fogg and Kreitler, 1982).

Oakwood Dome Vicinity

Dome-specific hydrogeology in the East Texas Basin differs from regional hydrogeology in three respects. First, many domes uplift and fault overlying strata, locally creating a more complex aquifer framework. Structural framework around Oakwood Dome is fairly simple compared to that around other domes (fig. 3). Second, in several cases domal uplift has exposed the Wilcox-Carrizo, creating recharge areas over the domes. Third, domes are barriers to ground-water flow. Salt dome dissolution may further alter local conditions by increasing ground-water salinity. The hydrogeology of the Oakwood Dome vicinity has been interpreted using hydraulic-head, geophysical-log, and water-chemistry data.

Hydraulic Head

Fogg and Kreitler (1982) constructed a regional map of the potentiometric surface (head) of the Wilcox-Carrizo aquifer system. More detailed maps have since been constructed of the Wilcox and Carrizo in the vicinity of Oakwood Dome. A head map of the Carrizo aquifer directly over the dome (fig. 4) was made using newly acquired water-level data from 15 test wells drilled in 1979-80 (Fogg, 1981). These new data were also added to the regional data to construct head maps of the Wilcox and Carrizo in the greater Oakwood Dome area (figs. 5 and 6). The Wilcox and Carrizo data are mapped separately rather than collectively so that any differing flow conditions can be observed.

The Carrizo head map of Oakwood Dome (fig. 4) shows a recharge mound where the Carrizo aquifer and Reklaw aquitard have been uplifted and exposed as a result of dome growth. The relatively steep hydraulic gradients on the east side of the mound coincide with faults that were mapped by Collins and others (1981), suggesting that the faults are partial barriers to horizontal flow.

The Wilcox and Carrizo maps of the greater Oakwood Dome area (figs. 5 and 6) do not differ greatly from the regional Wilcox-Carrizo map by Fogg and Kreitler (1982), except that a smaller contour interval is used (25 ft [7.6 m], rather

than 50 ft [15.2 m]). The new maps show some features along the Trinity River that were not previously evident: namely, a potentiometric depression just south of the Carrizo outcrop and, farther south, a west-to-east flow direction across the river. Note, however, that where the Carrizo head map (fig. 6) indicates west-to-east flow, there are practically no Wilcox head data (fig. 5). Thus, the dashed contours in the southeastern part of the Wilcox head map are inferred from the shallower Carrizo data. These contours are considered representative of head in the upper few hundred feet of the Wilcox, but heads deeper in the Wilcox may be considerably different. For example, the one Wilcox data point in the lower right of figure 5 is from a well (well no. 38-35-203; [Tarver, 1966]) completed at a depth of 1,800 ft (549 m) in the lower Wilcox and registers a head of 300 ft (91 m). The Wilcox and Carrizo contours indicate a head of 225 ft (68.6 m) in the same area. This data point was ignored during contouring because it was so anomalous and was not supported by other data. As will be demonstrated using the pressure-versus-depth data, a head of 300 ft (91.4 m) at this depth is not unrealistic, and heads throughout the Wilcox Group should be expected to vary considerably with depth.

Queen City head data are too sparse to allow contour mapping of the Queen City water table. We know, however, that Queen City heads are primarily a function of topography, as illustrated by the plot of head versus land surface in figure 7. This plot, together with topographic maps, was used to synthesize a Queen City water table map used in an upper boundary condition for the model (fig. 27).

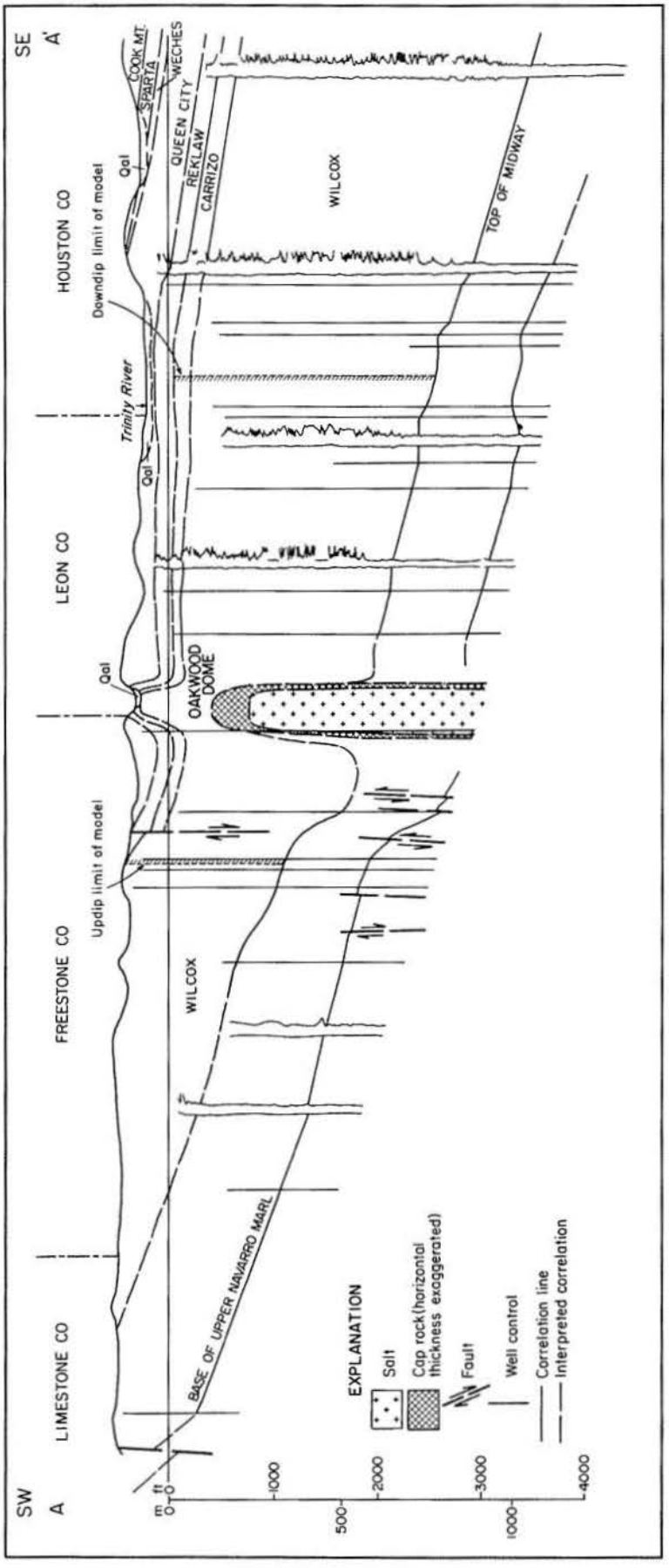

Figure 3. Regional structural cross section through the study area (modified from Wood and Guevara, 1981). See figure 1 for location of section. The model area is in the artesian section of the Wilcox-Carrizo system, immediately downdip of the unconfined outcrop.

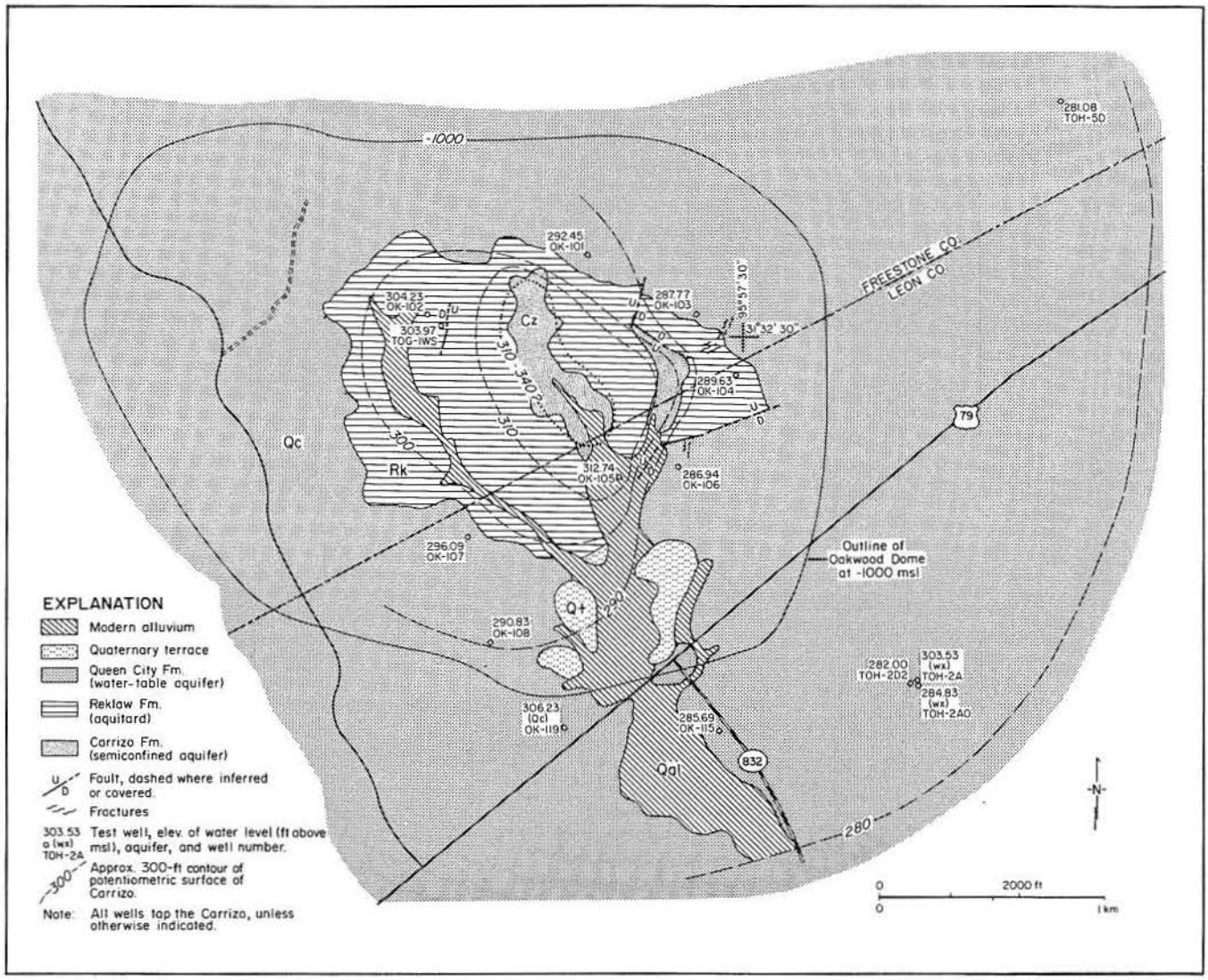

Figure 4. Potentiometric surface map for the Carrizo aquifer over Oakwood salt dome (geology from Collins and Hobday, 1981). Uplift of the dome has exposed the Carrizo and created the observed recharge mound.

Pressure Versus Depth

Fluid pressure versus depth (P-D) relationships have been derived from water well monitoring data and used in the East Texas Basin by Fogg and Kreitler (1982) to study potential for vertical flow in the Wilcox-Carrizo system. Results showed that (1) there is generally potential for downward fluid movement in the East Texas Basin, (2) potential for downward flow increases toward higher elevations and from the artesian section to the outcrops, and (3) there is potential for upward flow beneath the Trinity River floodplain. In general, the P-D data show consistent, predictable trends. These trends are used in the model to assign prescribed head boundary conditions as a function of depth.

Table 1 summarizes the P-D data for the vicinity of the model. The values of slope (m) given for each data group are derived from least-squares linear regression analyses and indicate direction of the vertical-flow component: when $m > 1$, potential for vertical flow is upward and when $m < 1$, potential for vertical flow is downward. Note that many of the m values in table 1 have 95-percent confidence intervals ranging from <1 to >1, suggesting an indeterminate value of m. As discussed by Fogg and Kreitler (1982), however, the general trends represented in the P-D data appear reliable because of the strong correlation between m values, topography, and confining conditions.

Most of the m values in table 1 are from Fogg and Kreitler (1982), except those given for data

within 2 mi (3.22 km) of the Carrizo-Reklaw outcrop boundary (fig. 8) and for data at drill site TOH-2 (fig. 9), which is about 2,000 ft (610 m) southeast of Oakwood Dome (fig. 4). The P-D trend near the Carrizo-Reklaw boundary is important because this boundary coincides with the northwest margin of the model. The corresponding m value of 0.96 indicates potential for downward flow and is transitional between lower m values for the Wilcox and Carrizo outcrop to the northwest ("Freestone County — unconfined" in table 1) and higher m values for the confined section to the southeast ("Freestone and Leon Counties — confined" and "Trinity River").

The only P-D data indicating potential for upward flow are those along the Trinity River (m = 1.10), from Houston and Anderson Counties in the surface-elevation range of 250 to 350 ft (76 to 107 m) (m = 1.05 to 1.07), and from drill site TOH-2 (m = 1.02). The latter value is close enough to 1.00 to suggest that Oakwood Dome lies in a transition zone where potential for vertical flow changes from downward to upward.

Table 1. Pressure-versus-depth (P-D) relationships. Refer to figure 1 for locations of counties.

Area	Slope (m) and 95% confidence interval	Depth range (ft)	Correlation (r)	No. of points
*Freestone Co. (unconfined) land surface (ft):				
300-350	0.95±.13	17-306	0.98	8
350-400	0.79±.09	28-330	0.97	16
400-450	0.85±.04	23-525	0.99	26
450-500	0.80±.04	16-668	0.99	42
500-550	0.86±.06	20-822	0.99	20
*Freestone Co. (confined) land surface (ft):				
300-350	0.95±.33	295-856	0.97	4
350-400	0.94±.10	480-800	0.99	4
*Leon Co. (unconfined) land surface (ft):				
350-400	0.91±.34	614-724	0.85	11
400-450	0.96±.12	337-840	0.99	6
*Houston Co. (confined) land surface (ft):				
250-300	1.05±.02	360-1,800	0.99	3
450-500	0.89±.47	735-903	0.91	5
*Anderson Co. (confined) land surface (ft):				
250-300	1.07±.17	215- 835	0.97	9
300-350	1.07±.14	260- 614	0.99	7
350-400	0.88±.04	136-1,345	0.99	16
400-450	0.96±.05	420-1,745	0.99	17
450-500	0.98±.05	462-2,120	0.99	10
500-550	0.94±.03	600-1,855	0.99	7
*Trinity River (confined)	1.10±.13	359-1,230	0.98	10
Carrizo-Reklaw outcrop boundary	0.96±.08	230- 800	0.98	17
Site TOH-2 (near Oakwood Dome)	1.02±.01	500-2,100	0.99	6

*from Fogg and Kreitler (1982).

The Trinity River vicinity is particularly important because it coincides with a boundary of the model and is a potential discharge area. Unfortunately, the Trinity River m value of 1.10 is based almost entirely on data from north of the Elkhart Graben (fig. 1). The Houston County value of 1.05, however, is based on data from near the river south of the Elkhart Graben and will be assumed to be representative of the southeastern corner of the model. This value is based on only three data points (including well 38-35-203) but has a relatively narrow, 95-percent-confidence interval of ± .02 (table 1). The depth range of these data is 360 to 1,800 ft (110 to 549 m), or from the Carrizo to the middle of the Wilcox.

Total Dissolved Solids

Although Oakwood Dome is in contact with the Wilcox Group (fig. 3), Wilcox ground water around the dome is primarily fresh (<1,000 mg/L total dissolved solids). This is also true of most other domes in the basin (Fogg and Kreitler, 1982), suggesting that the domes are generally isolated from ground-water circulation in the Wilcox. Possible causes of such isolation are salt dome cap rock (Kreitler and Dutton, 1983) and relatively muddy, low-permeability facies surrounding the domes (Seni and Fogg, 1982). Of all the domes, however, only Oakwood is associated with a ground-water plume of anomalously high salinity that is thought to be caused by dome dissolution. The plume has not been verified by water sampling, but interpretation of electrical-resistivity-log data strongly indicates that the plume consists of moderately brackish water (1,000 to 4,000 mg/L) (fig. 10).

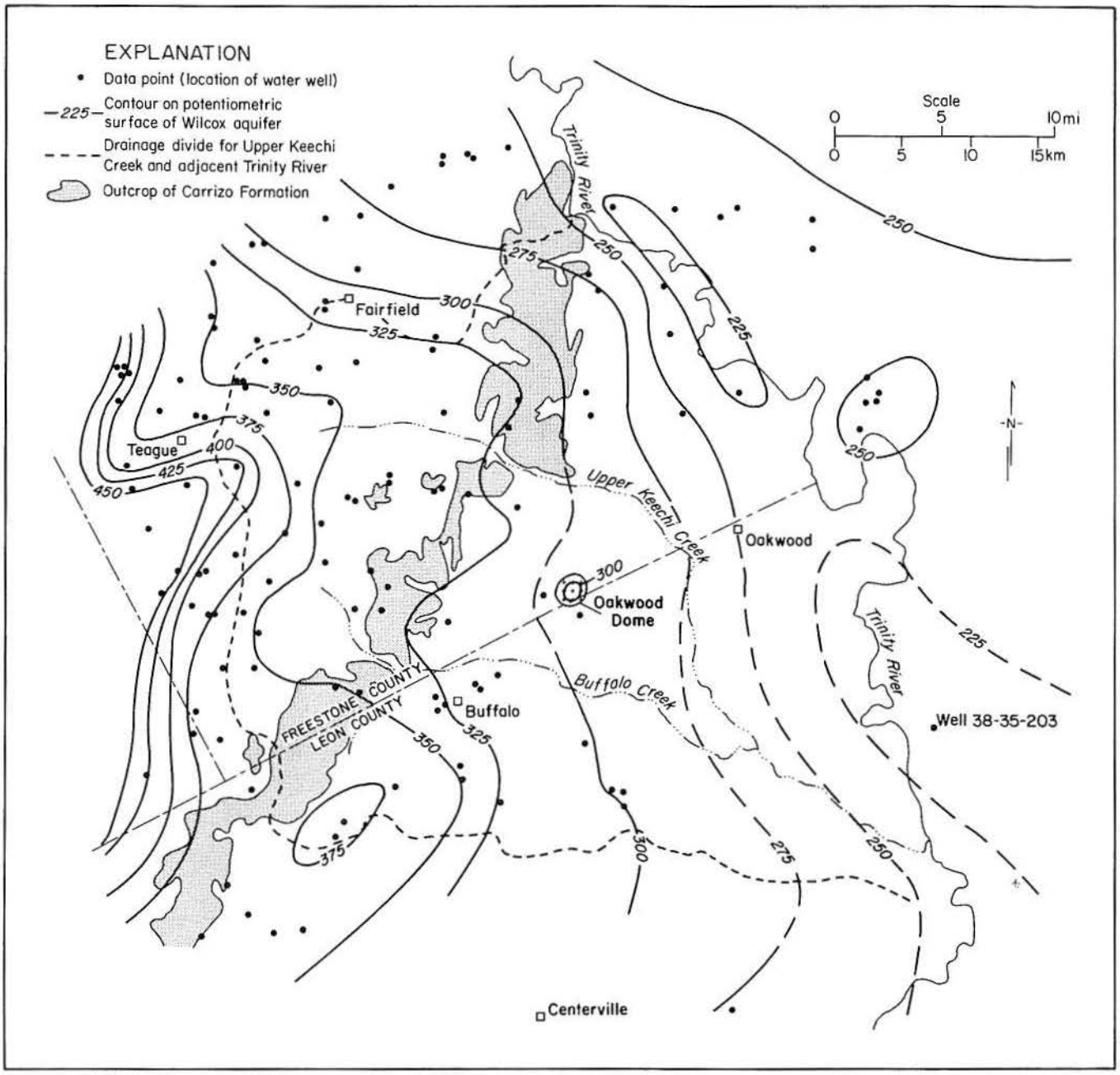

Figure 5. Potentiometric surface map for the Wilcox aquifer in the Oakwood Dome vicinity. Dashed contours in the southeastern quadrant are inferred from the Carrizo map (fig. 6) and are representative primarily of the upper Wilcox Group. Head tends to increase with depth in this quadrant, as evidenced by well 38-35-203 (just east of the Trinity River), which registers a head of 300 ft (91 m).

The electrical-resistivity log data also suggest a brackish plume southwest of the dome, but the existence of this plume is questionable because it is based on only two data points. The rest of the report will refer only to the plume northeast of the dome.

The plume implies a northwestward groundwater flow direction that conflicts with east/southeast flow directions indicated by regional potentiometric surface mapping (Fogg and Kreitler, 1981 and 1982). However, this discrepancy is apparently an artifact of the regional mapping scale. The more detailed potentiometric surface maps in figures 5 and 6 indicate an east/northeast flow direction away from the dome and thus are in general agreement with the plume orientation.

Before we constructed the model, we hypothesized that the east/northeast flow component away from the dome might be caused

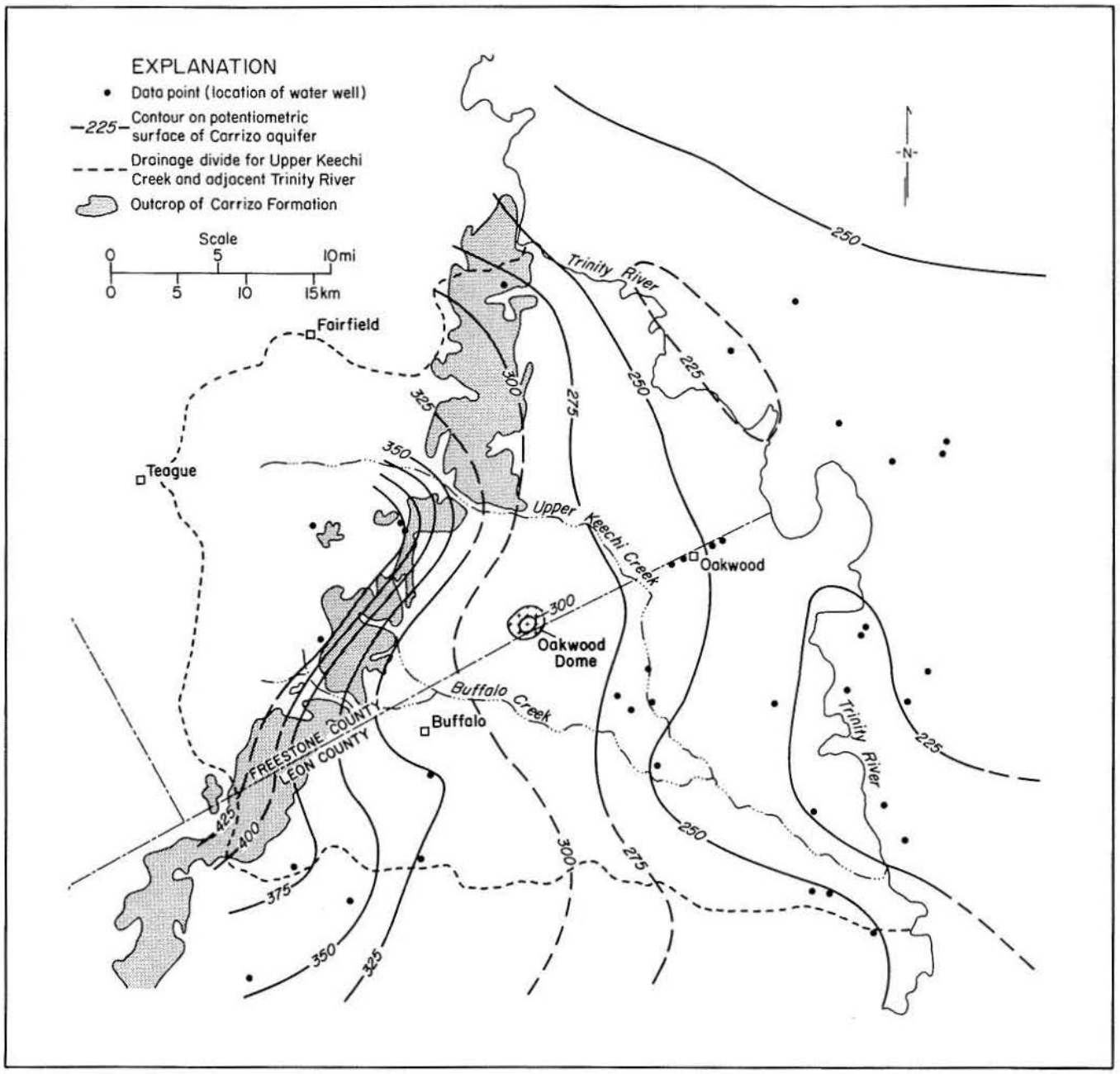

Figure 6. Potentiometric surface map for the Carrizo aquifer in the Oakwood Dome vicinity.

by flow toward possible ground-water discharge areas located along either the Trinity River or Upper Keechi Creek, or both. Discharge to the creek was thought to be especially plausible because the creek (1) coincides with the terminus of the plume and (2) incises the Reklaw aquitard near the plume (fig. 19), thereby increasing the likelihood of Wilcox-Carrizo ground-water discharge to the creek. The model, however, indicates that neither the Trinity River nor Upper Keechi Creek significantly influences ground-water flow near the dome and that the orientation of the plume is the result of Wilcox sand facies influencing ground-water flow.

Ground-Water Chemistry

A geochemical evolution of Wilcox-Carrizo ground water in the East Texas Basin has been documented (Kreitler and Wuerch, 1981a; Fogg and Kreitler, 1982) and can be used to evaluate anomalous flow conditions in the aquifer. As ground water flows from recharge areas to discharge areas, it is consistently altered

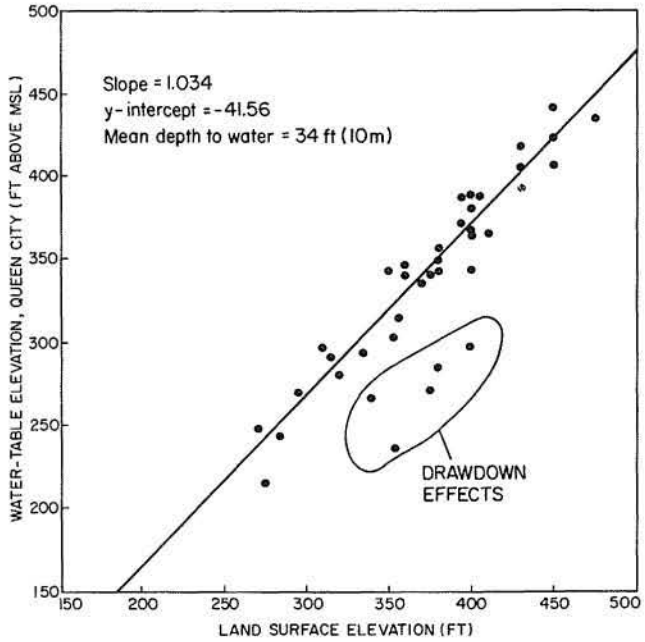

Figure 7. Relationship between elevation of the water table and land surface in the Queen City aquifer, Leon and Freestone Counties. Data are from Guyton and Associates (1972) and Peckham (1965). Circled points are anomalous owing to drawdowns caused by pumping.

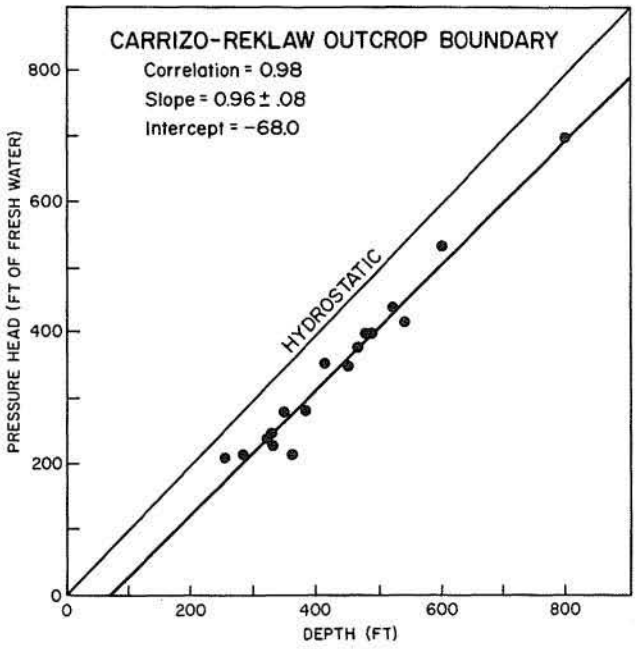

Figure 8. Pressure-versus-depth relationship for data within 2 mi (3.22 km) of the Carrizo-Reklaw surface contact (southeast boundary of the Carrizo outcrop in fig. 6). This boundary corresponds approximately to the northwest margin of the model. The slope (m) indicates potential for downward flow.

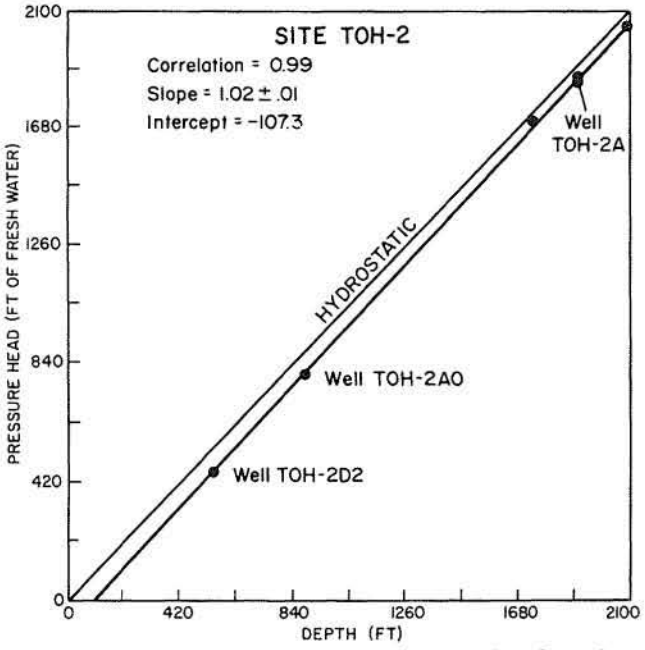

Figure 9. Pressure-versus-depth relationship based on water level and pressure measurements made at drill site TOH-2, 2,000 ft (610 m) southeast of Oakwood salt dome. The unlabeled points are open-hole pressure measurements from a Schlumberger Repeat Formation Tester. Because the value of m is so close to 1.00, the dome appears to lie in a transition zone where potential for vertical-flow changes from downward to upward.

chemically from an acidic, oxidized calcium-magnesium-bicarbonate-sulfate-type water to a basic, reduced, sodium-bicarbonate water. This change in the water chemistry is controlled predominantly by calcite dissolution and cation exchange with montmorillonitic clays. Water that departs from regional patterns of chemical change indicates anomalous hydrologic conditions, such as relatively high rates of recharge to the artesian part of the Wilcox-Carrizo.

Water-chemistry data from monitoring wells completed in the Carrizo aquifer at Oakwood Dome characteristically display chemical composition indicative of shallow recharge water and are anomalous in comparison to Carrizo water chemistry in the greater Oakwood Dome area (Kreitler and Wuerch, 1981a; Fogg and Kreitler, 1982). Water-chemistry data from deeper Wilcox wells near the dome do not indicate recharge or vertical mixing with overlying Carrizo waters.

Carbon-14 age dates of water samples from the Oakwood Dome monitoring wells support the water-chemistry interpretations (Kreitler and Wuerch, 1981b). Youngest waters are found closest to the recharge area over the dome, and ages generally increase with depth and with distance away from this area.

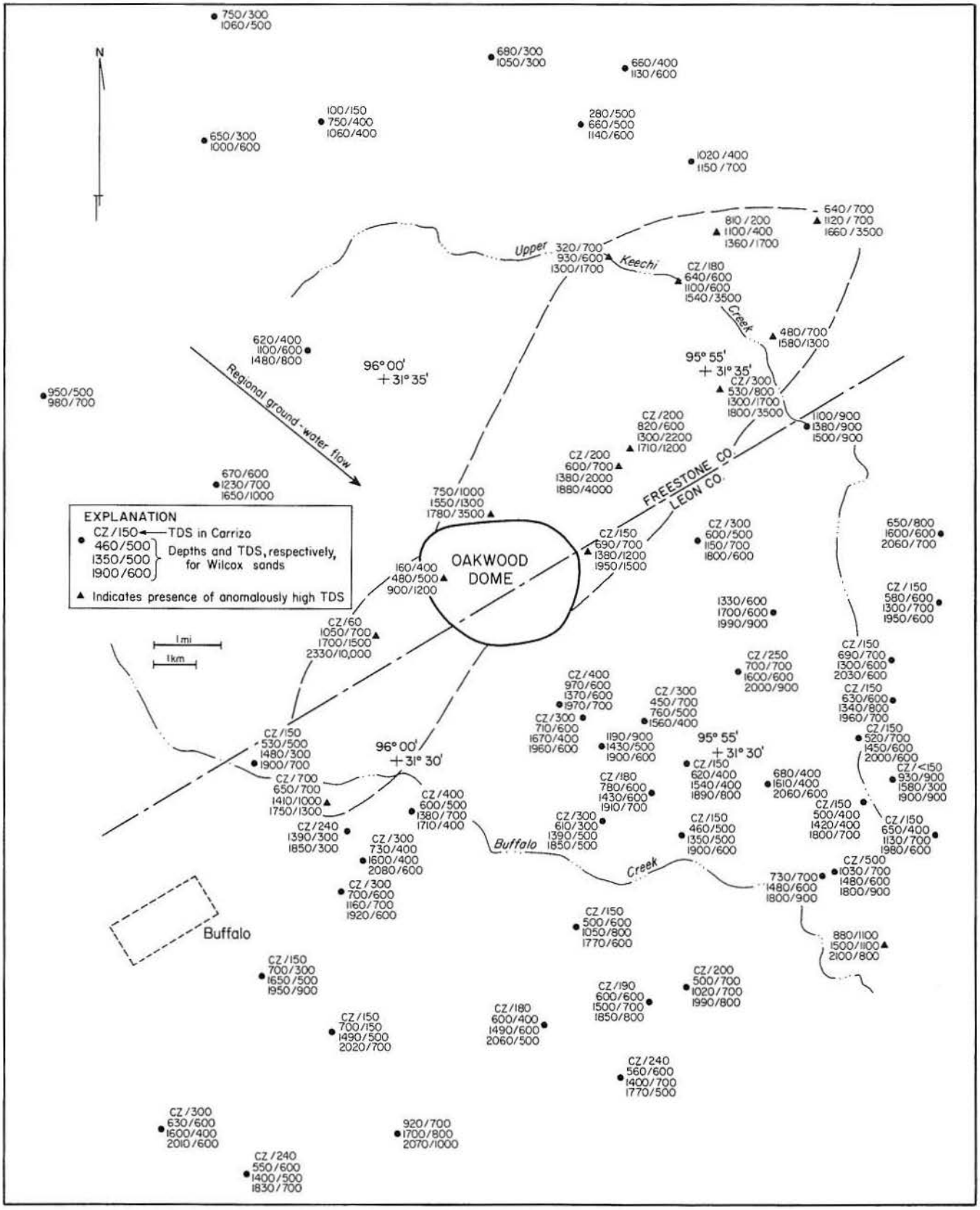

Figure 10. Electrical-resistivity-log estimates of total dissolved solids (TDS; mg/L) in Wilcox-Carrizo sands around Oakwood Dome. Water-chemistry analyses have shown these estimates to be accurate within 250 mg/L (Fogg and Kreitler, 1982, fig. 44). Anomalously high values are encircled by the dashed line. The high values southwest of the dome may not be reliable.

Table 2. Field pumping test results from the model area and vicinity (sources: Myers, 1969; Guyton and Associates, 1972; and Fogg, 1981).

Well number[a]	Aquifer	Hydraulic conductivity (K) ft/day	m/day	Resistivity of produced sand (ohm-m)
		Freestone County		
39-15-601	Wilcox	7.0	2.1	32-40
39-15-802	Wilcox	3.7	1.1	n.d.
39-15-902	Wilcox	10.7	3.3	25-50
39-16-502	Wilcox	3.7	1.1	n.d.
39-22-901	Wilcox	2.3	0.70	31-39
39-23-301	Wilcox	4.8	1.5	n.d.
39-23-302	Wilcox	5.9	1.8	n.d.
39-23-303	Wilcox	9.5	2.9	12-43
39-23-404	Wilcox	2.8	0.85	n.d.
TOG-1WS	Carrizo	8.9	2.7	50[b]
TOH-5D	Carrizo	23.0	7.0	50-100[b]
		Leon County		
TOH-2A	Wilcox	0.69-0.89	0.21-0.27	14-17.5[b]
TOH-2AO	Wilcox	20.7	6.3	25-30[b]
TOH-2D2	Carrizo	22.6	6.9	30-40[b]
38-43-101	Carrizo	23.0	7.0	n.d.
38-26-102	Carrizo	40.1[c]	12.2[c]	85-95
		Anderson County		
38-02-302	Wilcox	19.0	5.8	n.d.
38-03-701	Wilcox	19.9	6.1	32-35[b]
38-09-601	Wilcox	8.7	2.7	n.d.
38-11-801	Wilcox	10.8	3.3	60-90
38-11-901	Wilcox	10.4	3.2	70
38-11-902	Wilcox	9.1	2.8	n.d.
38-19-301	Wilcox	6.6	2.0	25-47
38-21-703	Wilcox	45.2	13.8	25
38-21-704	Wilcox	41.8	12.7	n.d.
34-60-602	Carrizo	21.1	6.4	n.d.
38-13-106	Carrizo	25.3	7.7	n.d.
38-19-802	Carrizo	23.5	7.2	n.d.
38-20-801	Carrizo	23.4	7.1	n.d.
38-21-706	Carrizo	28.6	8.7	n.d.

[a]Seven-digit numbers are state well numbers, and "TO-" wells were constructed for this project.
[b]Indicates induction-resistivity (other values are from 64-inch long-normal resistivity logs).
[c]Hydraulic conductivity was calculated from a transmissivity value given in Myers (1969) and an aquifer thickness determined from the electric log.
n.d. indicates no data.

Hydraulic Conductivity

Characterizing hydraulic conductivity of the Wilcox Group is difficult because the Wilcox contains a complex distribution of sand and mud facies. Fortunately, cumulative thickness of the sands is mappable on a regional scale using electric logs and interpretations of depositional environments (Kaiser and others, 1978; Fisher and McGowen, 1967). In this study, we used results of field pumping tests and laboratory tests on core samples to estimate hydraulic conductivity of different sand facies in the Wilcox. These sand facies were then mapped by Seni and Fogg (1982) in two ways: (1) as sand-percent maps corresponding to each layer of the model and (2) as cross sections showing vertical distribution of sand bodies. Distribution of equivalent hydraulic conductivity in each layer of the model was calculated using these maps and cross sections, the field and laboratory measurements, and certain assumptions regarding sand-body interconnectedness. Equivalent hydraulic conductivity (K′) as used here refers to the calculated resultant conductivity of strata containing layers of different hydraulic conductivity (K) (refer to Freeze and Cherry, 1979, or Bear, 1972).

Field Pumping Tests

In 1979 and 1980, pumping tests were carried out in five test wells that were completed in Wilcox and Carrizo sands near Oakwood Dome (wells TOH-2A, TOH-2AO, TOH-2D2, TOH-5D, and TOG-1WS; fig. 4). Each well fully penetrates a sand body and was pumped for approximately 24 hours. Values of transmissivity (T), hydraulic conductivity (K), and storativity were obtained by analyses of drawdown and recovery data using methods of Theis (1935) and Cooper and Jacob (1946), and results are summarized in table 2. Alternative methods of analysis that account for effects of barrier boundaries and leakage across confining beds were not applied, because either these conditions or data necessary to detect them were lacking. Refer to Fogg (1981) for details of well construction and additional discussion of the data analysis.

Values of K obtained from the pumping tests near Oakwood Dome are in very close agreement with published values (table 2), as illustrated in the histogram on the right-hand side of figure 11. In the histogram, K values are plotted on a log scale. Note the narrow range of values, 75 percent of which lie between 3.3 and 33 ft/d (1 and 10 m/d). An important characteristic of the sands represented by these data is that they generally register a resistivity (R_o) value greater than 20 ohm-m on borehole resistivity logs (log normal or induction) (table 2). The only known exception is the sand tested by well TOH-2A, which registers an R_o value just under 20 ohm-m and yields the

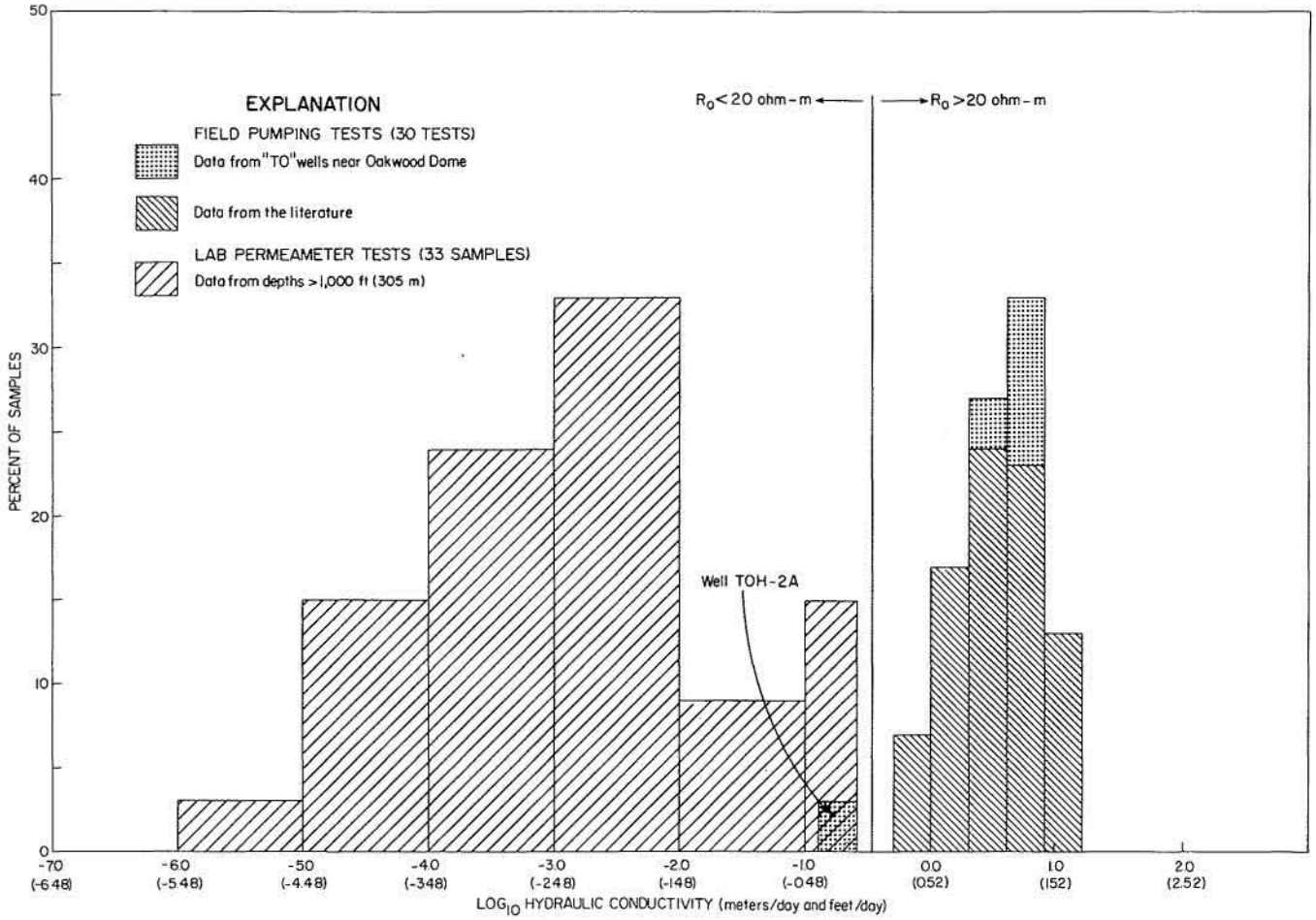

Figure 11. Histograms showing hydraulic conductivity (K) distributions from pumping tests and laboratory permeameter tests. With the exception of well TOH-2A, all pumping test results are from relatively permeable channel-fill sands. Laboratory permeameter results are from less permeable interchannel sands.

lowest K value of all the wells (0.69-0.89 ft/d; 0.21-0.27 m/d). Water well drillers and consultants who develop Wilcox and Carrizo ground-water resources in the East Texas Basin consistently target the sands of highest resistivity for water production wells, because these sands are generally thought to have the highest K values and to contain the freshest ground water. Thus, it is safe to assume that K values for which R_o data are not available in table 2 are from sands registering R_o values greater than 20 ohm-m.

The higher resistivity sands also appear significant with respect to depositional environments in the Wilcox Group. Owing to their relatively coarse apparent grain size and blocky character on electric logs, these sands are interpreted to be fluvial channel-fill facies (Seni and Fogg, 1982). The lower resistivity ($R_o < 20$ ohm-m) sands of the Wilcox are typically thinner and are typical of interchannel deposition. Data on K of interchannel facies are available from laboratory permeameter testing.

Laboratory Permeameter Tests

During the fall of 1979 approximately 1,700 ft (518 m) of continuous core 3 inches (7.6 cm) in diameter was drilled in the Wilcox at site TOH-2AO (fig. 4). Core Laboratories, Inc., was contracted by the Bureau of Economic Geology to extract 46 plug samples from specified points of the core and to measure the horizontal hydraulic conductivity and porosity of each sample. Plug dimensions were approximately 1 inch (2.5 cm) wide by 2 inches (5.1 cm) long. Results of these tests are shown in figure 12, along with results of pumping tests at the same site and the induction-resistivity and gamma logs of the cored hole. Values of K measured in the core samples range from 1.10×10^{-4} to 6.63 ft/d (3.35×10^{-5} to 2.02 m/d).

The broad scatter of K values is to be expected in heterogeneous fluvial and deltaic sediments such as the Wilcox Group. Much of this scatter, however, may stem from disturbance of in situ conditions of cored sediments during drilling or

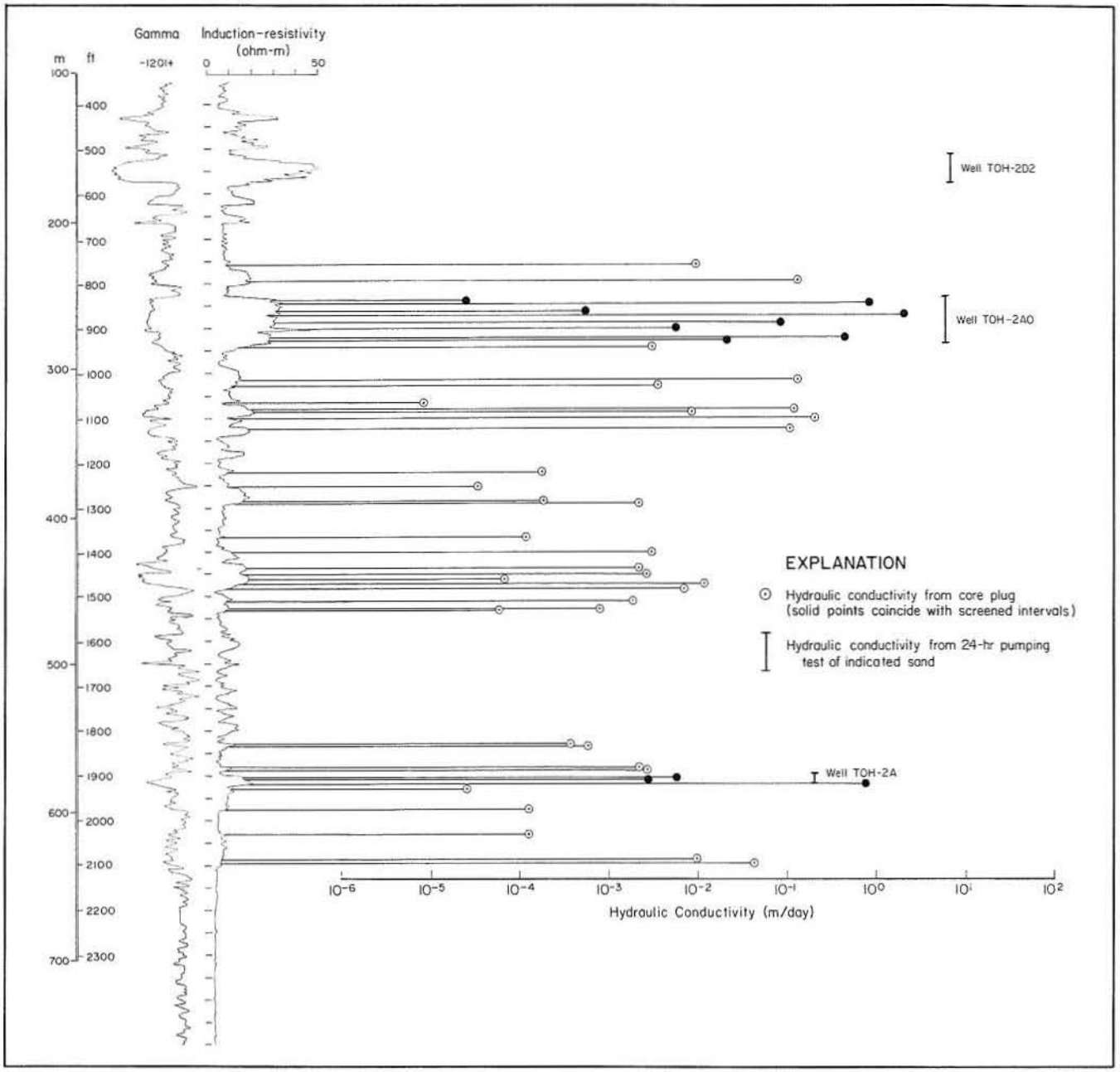

Figure 12. Results of laboratory permeameter tests conducted on Wilcox core and of pumping tests conducted in adjacent water wells. Above a depth of about 1,000 ft (300 m) the laboratory-conductivity values are presumed unreliable owing to disturbance of relatively loose, unconsolidated sediment. Average measured porosity of the core samples is 33.5 percent; there appears to be no trend with depth.

sample preparation. Disturbance during coring was minimized by use of a coring method designed especially to recover unconsolidated sediments, which involved an expandable rubber sleeve that encases and protects the core as it enters the core barrel. Consequently, more than 85 percent of the cored section was recovered, and small-scale sedimentary structures such as ripple marks and laminations were preserved in the core (Seni and Fogg, 1982). Care was also taken to minimize disturbance of the core and samples during sample preparation, but there was significant disturbance of samples shallower than about 1,000 ft (305 m) (Core Laboratories, Inc., personal communication, 1980). Above this depth, the cored sediments were fairly noncohesive and considerable rearrangement and repacking of grains may have occurred during both coring and plug extraction.

Disturbance of in situ conditions in samples shallower than 1,000 ft (305 m) may be responsible for the discrepancy between laboratory-measured K values and K values from field pumping tests for the Wilcox sand body in the interval 835 to 945 ft (254.5 to 288.0 m) (fig. 12). Most of the plug K values are lower than the pumping-test value (which is considered accurate) by a factor of 10^2 to 10^3. Possible explanations for the discrepancy are (1) Rearrangement of grains during coring or plug extraction might result in poor sorting of grain sizes (and hence lower K values) by mixing of silty lamina with previously well-sorted sand lamina. Many of the sands are laminated with alternating fine and coarse sediment (Seni and Fogg, 1982). (2) Drilling mud invasion of the core could have deposited fines in the pores and hence lowered K. Core Laboratories, Inc., flushed each plug sample with several pore volumes of fresh water before each permeability test, but this remedy may not have been totally successful. (3) Because the distribution of K is typically log-normal for geologic materials (Freeze, 1975, p. 728), random plug samples could preferentially represent the lower K sediments (refer to fig. 13). More specifically, in a log-normal K distribution, most of the K values are relatively small; consequently there is a greater probability that the less abundant high-K intervals will be missed during sampling. To minimize chances of this happening, we selected most of the sample points in intervals that were interpreted to be relatively permeable using the micro-resistivity log that was run in the cored hole. (Refer to Schlumberger, 1974, for an explanation of how the micro-resistivity log can be used for permeability interpretation.)

At depths below 1,000 ft (305 m), the core permeameter data are considered fairly reliable, because these K values are somewhat less scattered[1] (fig. 12), and in the interval 1,900 to 1,920 ft (579.1 to 585.2 m), the mean K value agrees closely with the corresponding pumping-test result from well TOH-2A. Less scatter can be attributed to greater cohesiveness of these sands and, in turn, less disturbance of in situ conditions (Core Laboratories, Inc., personal communication, 1980). Mean value of the three plug K values in the interval 1,900 to 1,920 ft (579.1 to 585.2 m) is 0.82 ft/d (0.25 m/d), which agrees with the field-derived K values of 0.69 to 0.89 ft/d (0.21 to 0.27 m/d) from TOH-2A, located about 50 ft (15.2 m) from the cored hole (table 2). Note in figure 12, however, that the three plug K values are widely scattered about the mean; the K values are (in order of increasing depth) 1.89×10^{-2} ft/d (5.76×10^{-3} m/d), 5.74×10^{-3} ft/d (1.75×10^{-3} m/d), and 2.46×10^{-1} ft/d (7.51×10^{-1} m/d). This does not imply that the agreement between core-plug and pumping-test K values is merely coincidental, because the variation in plug K values is directly related to the variation in lithology. Size of the sand decreases upward from a fine-grained sand to a very fine grained sand (fig. 12, and Seni and Fogg, 1982). Accordingly, the deepest plug sample yielded a much higher K value than did the two shallower plug samples. During pumping of TOH-2A, the more permeable, lower sections of the sand yielded most of the water, and, as a result, the pumping test yielded a K value that is closest to that of the lower section, but slightly skewed toward K of the upper section.

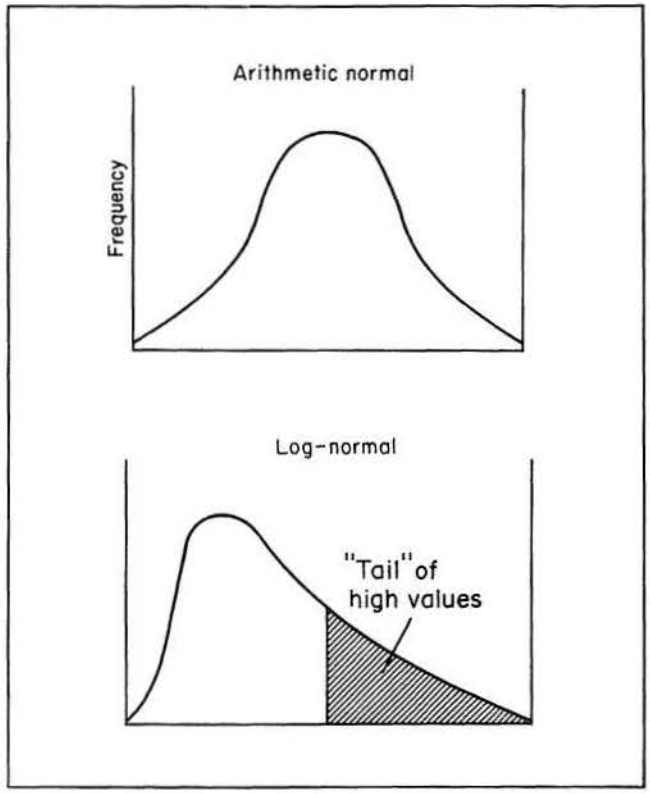

Figure 13. Comparison of arithmetic-normal and log-normal frequency distributions. Random sampling of a log-normal distribution will tend to miss the tail of higher values.

Comparison of Field and Laboratory Tests

The laboratory-derived K values from depths greater than 1,000 ft (305 m) and the field-derived K values are summarized in two separate

[1]Standard deviation of K values above 1,000 ft (305 m) is 0.60 and below 1,000 ft (305 m) is 0.14.

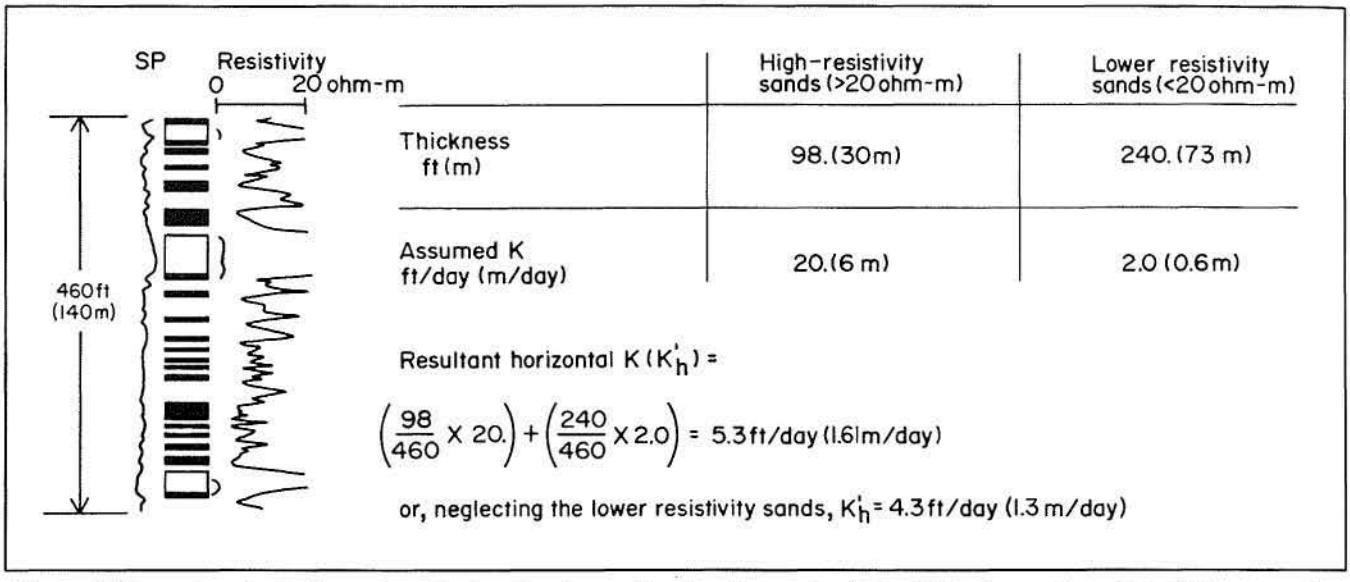

Figure 14. Sample calculations of equivalent horizontal hydraulic conductivity (K_h') of a section of the Wilcox aquifer. The lower resistivity interchannel sands are abundant but contribute little to the overall K_h' of the section. The channel-fill (high resistivity) sands control K_h' values.

histograms in figure 11. Laboratory values from depths less than 1,000 ft (305 m) are excluded because of their unreliability. Note that the histograms barely overlap and that their median values differ by a factor of about 10^3. This contrast supports the interpreted relationship between depositional facies and electric-log resistivity values of the Wilcox Group. As mentioned earlier, all the field-derived K values (except for the one from well TOH-2A) are apparently from thick, channel-fill sand bodies that consistently register electric-log resistivities (R_o) greater than 20 ohm-m. The laboratory-derived values, however, are from thinner sand bodies that consistently register R_o values less than 20 ohm-m (fig. 11). The thinner sands were probably deposited in interchannel environments ranging from floodplains to tributary channels of major streams (Seni and Fogg, 1982).

Thus, it appears that in the Wilcox, the K value of channel-fill sands is typically greater than that of interchannel sands by a factor of 10^1 to 10^3. Moreover, the channel-fill sands are indicated by electric-log resistivities (R_o) greater than 20 ohm-m. To demonstrate the hydrologic significance of this K contrast, two calculations of equivalent hydraulic conductivity (K′) of a section of Wilcox, 460 ft (140 m) thick, are made in figure 14 by assuming K of interchannel sands is (1) less than that of channel-fill sands by a factor of 10^1 and (2) equal to zero. The two values of K′, 5.3 and 4.3 ft/d (1.61 and 1.30 m/d), differ negligibly from each other, suggesting that K′ of the Wilcox can be approximated in the manner of the second calculation, which is simply the product of thickness percent and K of the channel-fill sands. The numbers used in these calculations were chosen to maximize the difference between the two K′ values. In reality, this difference might approach zero because thickness percent of sands with $R_o > 20$ ohm-m can be as great as 60 (but is only 21 percent in the example), and K of sands with $R_o < 20$ ohm-m can be much lower than 2.0 ft/d (0.6 m/d) (fig. 11).

Calculations of K′ for the model were therefore based on percent thickness of sands having $R_o > 20$ ohm-m (channel-fill sands) and the approximate log-mean K of these sands (20 ft/d [6 m/d]). A key assumption here is that K of the interchannel sands is indeed lower by a factor of 10^1 to 10^3. This assumption should be tested with additional field pumping tests of the interchannel sands.

Aquifer Mapping

Because of the apparent significance of the channel-fill sands, their distribution was mapped in the study area and vicinity by Seni and Fogg (1982). Seni and Fogg mapped the sand percent of channel-fill sand bodies ($R_o > 20$ ohm-m) for each of the three layers of the model (figs. 15, 16, and 17). Each layer represents one-third of the Wilcox thickness. The sand-percent maps show dip-oriented belts of sand-rich facies that reflect a predominantly fluvial depositional environment.

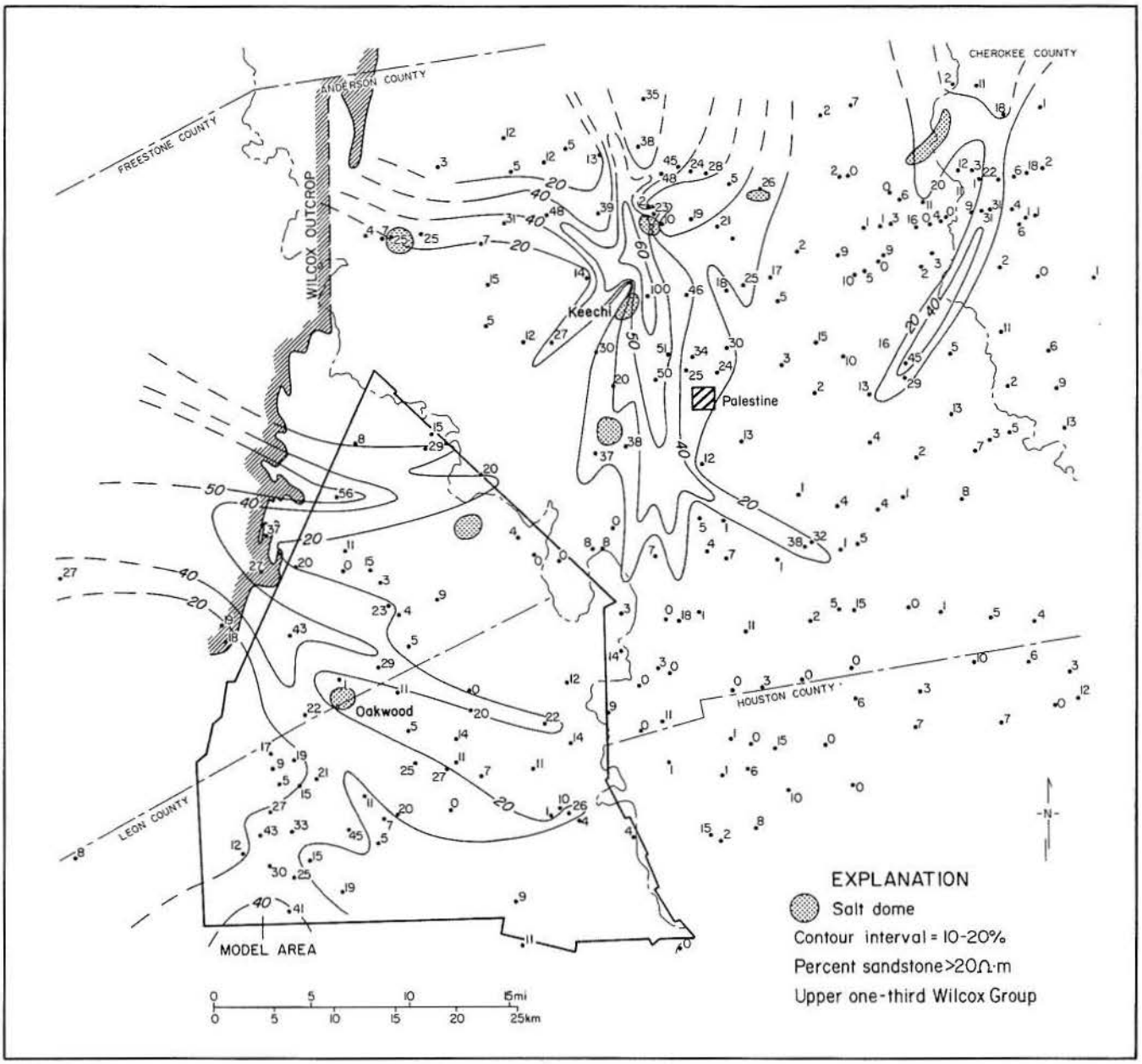

Figure 15. Sand-percent map of channel-fill sands ($R_o > 20$ ohm-m) for upper layer of the model (from Seni and Fogg, 1982). Low sand percentages around Oakwood Dome are theorized to be the result of syndepositional dome growth. Numbers at data points are sand-percent values.

Thinner deltaic sands occur at the base of the Wilcox, but are not included in the maps because of their lower resistivity.

Interestingly, Oakwood Dome is located in predominantly interchannel facies where channel-fill sand is less than 20 percent of total thickness (figs. 15, 16, and 17). This is interpreted to be a result of syndepositional dome growth. The dome was growing and forming a topographic high during Wilcox Group deposition and, consequently, deflected away the major streams of deposition, leaving relatively muddy, interchannel facies around the dome (Seni and Fogg, 1982).

The muddy facies represent an additional deterrent to ground-water circulation around Oakwood Dome that was not previously evident. The muddy facies together with salt dome cap rock (Kreitler and Dutton, 1983) may effectively isolate Oakwood Dome and other salt domes from circulating ground water, thus explaining the lack of saline water in the Wilcox aquifer where it comes in contact with the domes. As will be demonstrated in some of the model simulations,

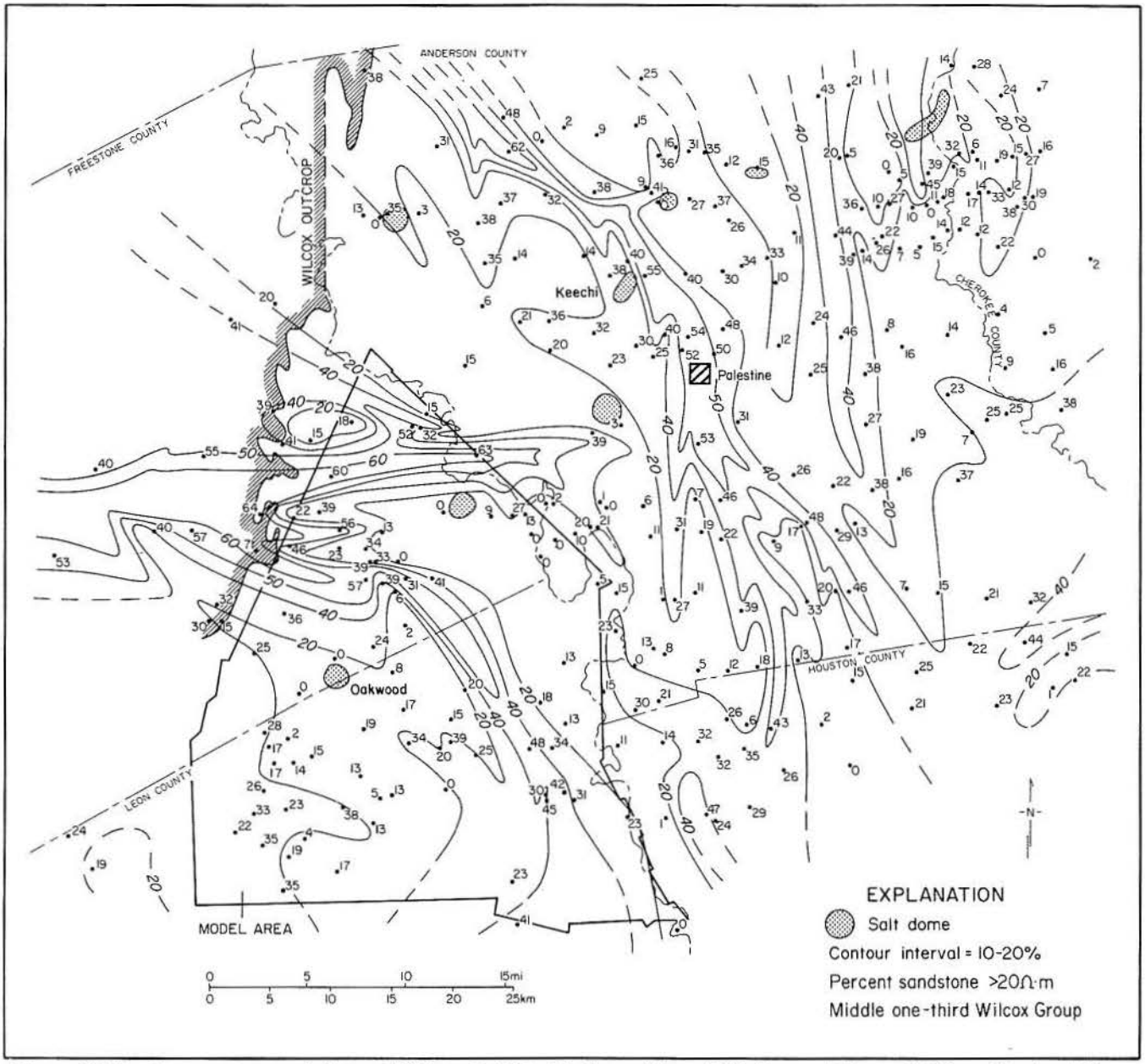

Figure 16. Sand-percent map of channel-fill sands ($R_o > 20$ ohm-m) for middle layer of the model (from Seni and Fogg, 1982). Low sand percentages around Oakwood Dome are theorized to be the result of syndepositional dome growth. Numbers at data points are sand-percent values.

ground-water velocities in this facies may indeed be very low if channel-fill sand bodies lying within the muddy facies are assumed to be disconnected.

Sand-Body Interconnectedness

Intuitively one might expect that where channel-fill sand bodies are sparsely distributed, they could be totally disconnected from one another, resulting in a value of equivalent hydraulic conductivity (K′) much lower than would otherwise be calculated using the product of the thickness fraction and K of channel-fill sands. To investigate this problem, several cross sections were designed specifically to study sand-body interconnectedness (Seni and Fogg, 1982). Each cross section was subdivided according to the model layers, and attempts were made to correlate laterally each channel-fill sand with surrounding channel-fill sands. To account for possible changes in thickness and vertical migration of units, adjacent sand bodies were assumed to be interconnected wherever they were offset vertically by less than 100 ft (30 m). It was

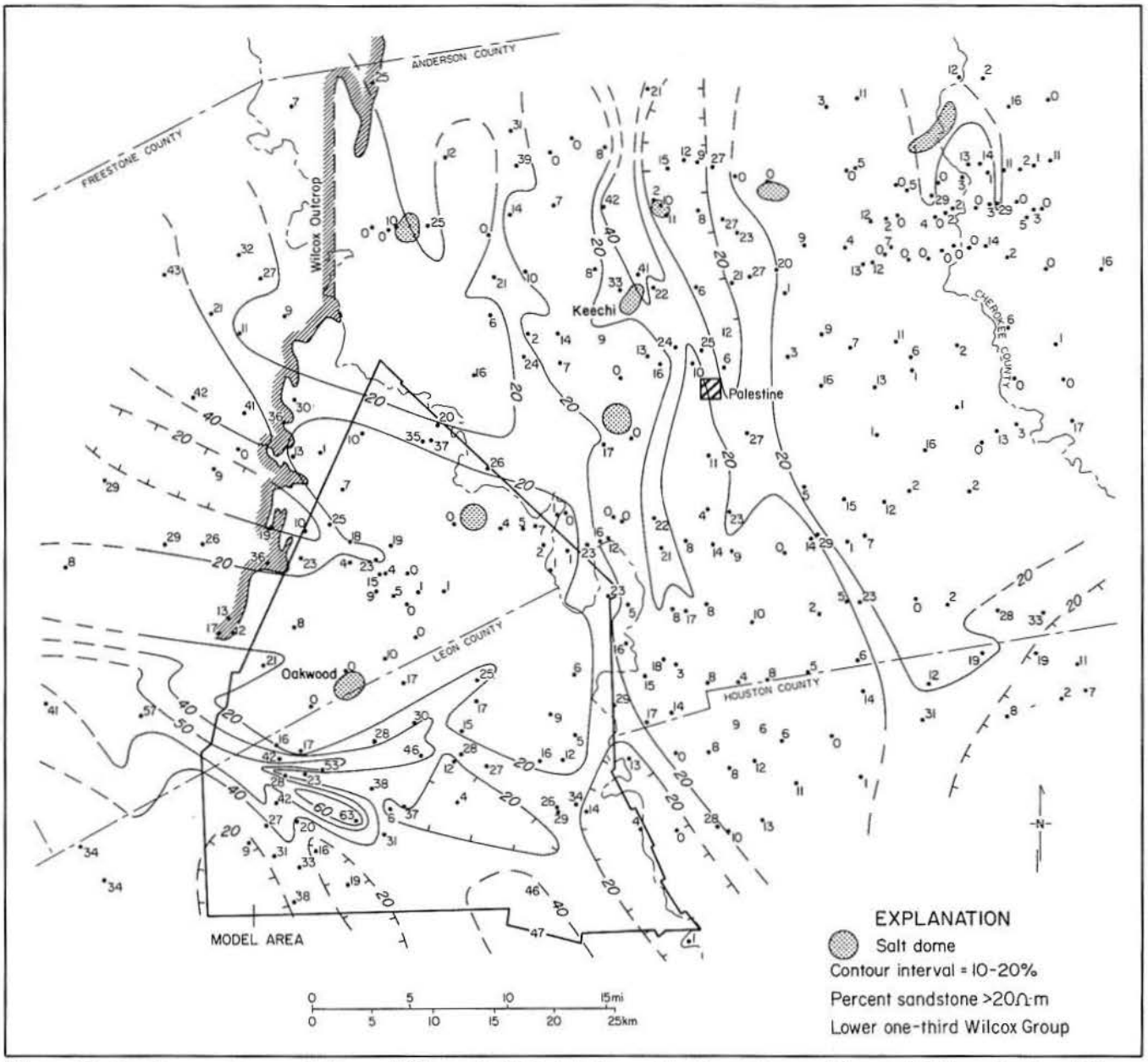

Figure 17. Sand-percent map of channel-fill sands ($R_o > 20$ ohm-m) for lower layer of the model (from Seni and Fogg, 1982). Low sand percentages around Oakwood Dome are theorized to be the result of syndepositional dome growth. Numbers at data points are sand-percent values.

observed that the channel-fill sand bodies appear to be laterally interconnected where sand percent exceeds 20 and disconnected where sand percent is less than 20 (figs. 15, 16, and 17).

Determining interconnectedness of Wilcox sands remains a major problem, and semi-quantitative methods are needed that employ concepts of both geostatistics and depositional systems to reduce or evaluate the degree of uncertainty. The sands may interconnect in a very complex pattern that does not necessarily correspond to patterns of sand percent. To better document the role played by discontinuous sand bodies on the model, different simulations were made assuming that either (1) all sands are laterally interconnected or (2) sands are laterally interconnected only in areas where sand percentages are higher than 20. Also, simulations were made that test assumptions regarding vertical interconnectedness of sands.

Vertical interconnection between Wilcox sands is generally precluded by intervening silts and clays at any given locality. The model results indicate lack of vertical interconnection on a regional scale as well.

COMPUTER PROGRAMS

Computer programs we used are the ground-water flow simulator (TERZAGI), the integrated finite difference mesh generator (OGRE), an automatic contouring algorithm (CPS-1), and a line-drawing algorithm (NCAR).

TERZAGI, which was developed at Lawrence Berkeley Laboratory and Lawrence Livermore Laboratory, California, employs an integrated finite difference (IFD), mixed explicit-implicit numerical scheme for solving problems of one-, two-, or three-dimensional fluid movement in fully or partially saturated porous media with vertical consolidation in the saturated zone. The theory behind TERZAGI, description of its algorithm, and its applications to problems can be found in literature describing its two related programs, TRUST and FLUMP. Described by Narasimhan and Witherspoon (1977 and 1978) and Narasimhan and others (1978b), TRUST is identical to TERZAGI, except that it includes vertical consolidation in both the fully and partially saturated zones. FLUMP, described by Fogg and others (1979), Narasimhan and others (1977 and 1978a), and Neuman and Narasimhan (1977), was developed from a version of TRUST by replacing the IFD matrix generator with a finite-element matrix generator. TERZAGI was chosen for this project because it is a flexible program that yields numerically accurate answers to complex ground-water flow problems. The program is used to solve the steady-state ground-water flow equation in three dimensions:

$$\frac{\partial}{\partial x}\left(K_h \frac{\partial h}{\partial x}\right) + \frac{\partial}{\partial y}\left(K_h \frac{\partial h}{\partial y}\right) + \frac{\partial}{\partial z}\left(K_v \frac{\partial h}{\partial z}\right) = 0$$

where K_h and K_v are horizontal and vertical hydraulic conductivity and h is hydraulic head.

OGRE was developed at Lawrence Berkeley Laboratory by Weres and Schroeder (1978) for use with TERZAGI, TRUST, and related IFD programs. It accepts, as input data, digitized nodal point locations and produces an IFD mesh in one, two, or three dimensions. Figure 18 is a two-dimensional example showing how OGRE works for one point surrounded by four other points. The program (1) connects adjacent points with line segments, (2) finds perpendicular bisectors for each line segment, and (3) finds the intersections of adjacent perpendicular bisectors, resulting in a polygon representing the nodal volume. When applied to an entire field of nodes, OGRE produces a mosaic of polygonal elements. To generate a three-dimensional mesh, one need only specify a three-dimensional distribution of nodes.

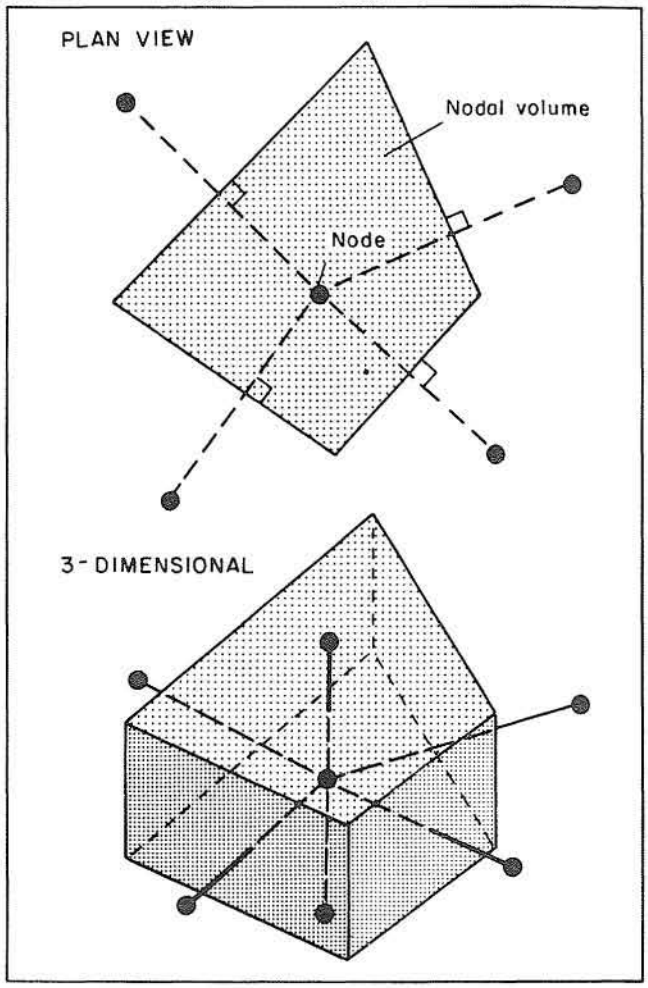

Figure 18. Example of how the integrated finite difference (IFD) mesh is generated with program OGRE.

OGRE automatically stores its results in forms that can be used to digitally plot the mesh and to specify the mesh as input data in TERZAGI. TERZAGI accepts the mesh data in the form of distances and cross-sectional areas between nodes and volumes of nodal elements (fig. 18).

CPS-1 (Unitech Inc., 1978) and NCAR (Wright, 1978) are general-purpose graphics programs that are supported and maintained by The University of Texas at Austin Computation Center. CPS-1 was used to generate contour maps of hydraulic head and vertical hydraulic gradients computed by the model. NCAR was used to generate plots of the IFD mesh and of ground-water velocity vector fields computed by the model.

MODELING PROCEDURE

The modeling procedure entails five phases: (1) selecting locations of model boundaries, (2) constructing the integrated finite difference (IFD) mesh, (3) assigning boundary conditions (for example, prescribed head or prescribed flux), (4) assigning values of hydraulic conductivity to elements of the mesh, and (5) simulating various scenarios of flow conditions.

Many modeling studies also include a calibration phase wherein the input data (usually hydraulic conductivity or transmissivity) are adjusted to "optimal values" that produce results (usually in the form of hydraulic head) that agree reasonably well with measured data. The model in this study was calibrated only slightly, because the hydraulic head data are generally too sparse and because there are too many unknowns that could be adjusted to produce the same results (for example, vertical and horizontal hydraulic conductivity of the Wilcox-Carrizo and the Reklaw and boundary conditions in lower parts of the Wilcox where data are scarce). If hydraulic conductivity is to be adjusted in a calibration, there should be a fairly dense distribution of hydraulic head data: Calibration of more than one item simultaneously in a model is very difficult and usually unwise.

Our data base is quite different from that of most other models because it includes so much three-dimensional geologic data. Moreover, we have unusual detail on regional pressure-versus-depth trends. Thus, the philosophy behind this study has been to assimilate all these hydrologic and geologic data in a model that will improve our understanding of the system, and not to build a model that will merely mimic certain aspects of system behavior.

Lateral Boundaries

The lateral boundaries of the integrated finite difference (IFD) mesh (fig. 19) were generally placed along certain hydrologic boundaries (that is, no-flow, recharge, or discharge boundaries) in the dome vicinity. The east-northeast boundary is along the Trinity River and the southern boundary is along the southern drainage divide of the Upper Keechi Creek watershed. Much of the southern boundary can be treated as a no-flow boundary condition because the potentiometric surface maps (figs. 5 and 6) indicate that flow is generally parallel to the boundary. No-flow boundary conditions are easiest to handle because they do not require knowledge of the hydraulic head or the magnitude of a non-zero flux.

The west-northwest boundary was placed approximately along the outcrop contact between the Carrizo aquifer and the Reklaw aquitard (fig. 19). Thus, updip of the model, the Wilcox-Carrizo is essentially an unconfined system; within the model area, it is a confined (artesian) system. The model was not extended into the unconfined section because (1) the complex, topographically controlled ground-water circulation patterns in this section would be difficult to model accurately and would not be pertinent to hydrogeology of the dome vicinity and (2) abundant hydraulic head data near the boundary can be used to assign prescribed head boundary conditions to simulate flow between the outcrop belt and the model area. South of Buffalo Creek, the west-northwest boundary lies slightly downdip of the Carrizo-Reklaw contact. This boundary placement was done to simplify mesh construction and does not detract from the accuracy of the model.

Integrated Finite Difference Mesh Construction

The IFD mesh was constructed by specifying nodal points at desired locations and using OGRE to automatically construct the three-dimensional network of volume elements. Node distribution in the horizontal plane was designed to accommodate the geometry of lateral boundaries, stream courses of Upper Keechi and Buffalo Creeks, and structural complexities around Oakwood Dome. Nodes were placed directly over the two creeks because they are potential ground-water discharge areas. Node spacing generally decreases from a maximum of about 4 mi (7.4 km) near the mesh margins to 0.71 mi (1.3 km) at the dome (fig. 19).

Distribution of nodes along the vertical was designed to accommodate the geometry of the Wilcox-Carrizo aquifer system as defined by structure-contour maps for the base of Carrizo and Wilcox units (figs. 20 and 21). Elevation of top of the Carrizo Sand can be estimated from elevation of its base, using the fairly uniform thickness of the Carrizo (approximately 90 ft [27 m]) in the study area. The Wilcox-Carrizo was divided into three layers of equal thickness with nodal points specified at the elevation of the midpoint of each

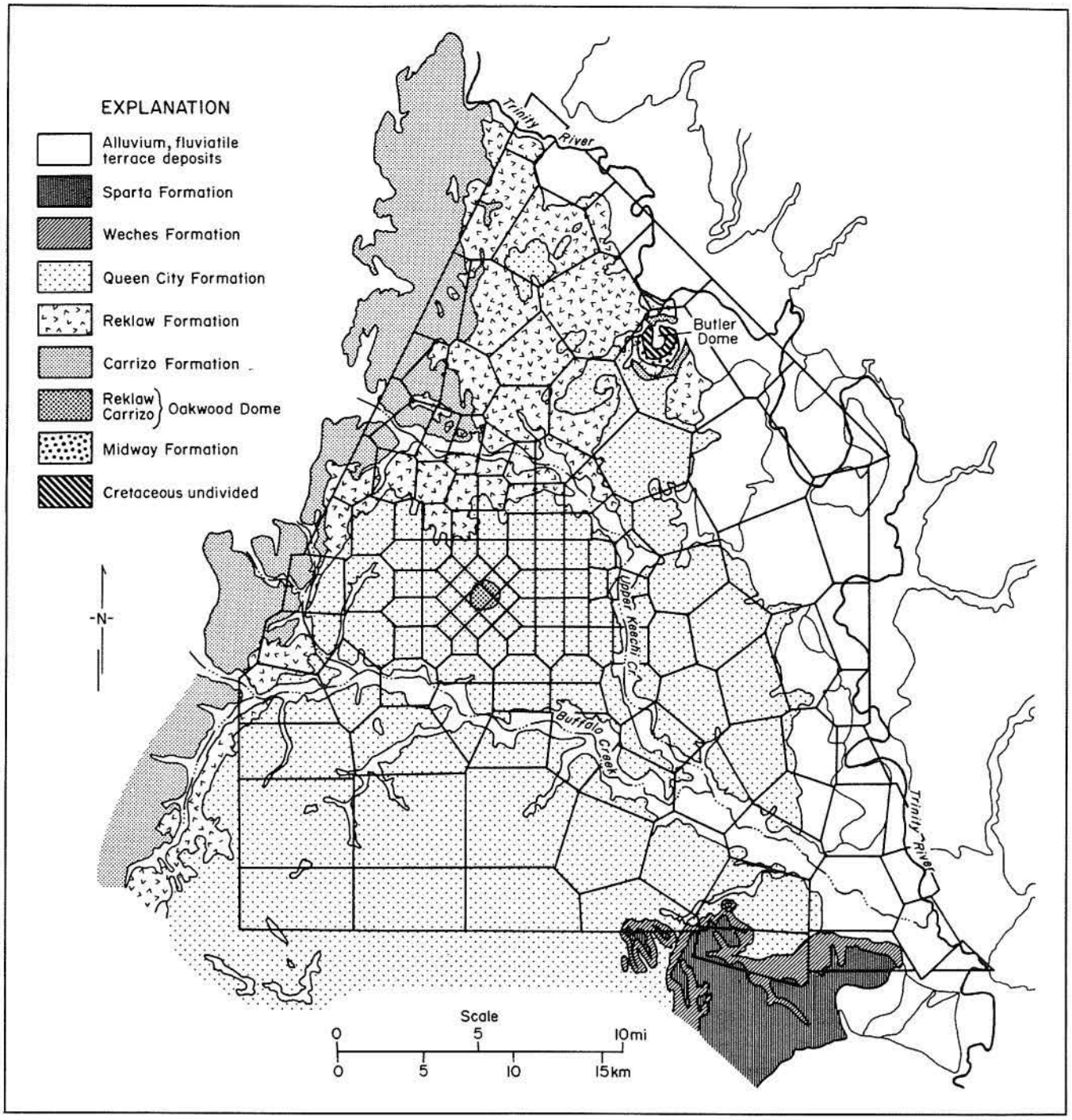

Figure 19. Plan view of the IFD mesh and surface geology from Barnes (1967 and 1970).

layer (fig. 26). The outer surface of the resulting three-dimensional mesh generated by OGRE and plotted using NCAR is shown from a southwest perspective in figure 22. The upper and lower surfaces of the mesh represent the upper and lower surfaces of the Wilcox-Carrizo; a clearer view of the upper surface is shown in figure 23. Compare these three-dimensional plots with the structure maps (figs. 20 and 21) and note that the mesh includes the uplift and rim syncline associated with Oakwood Dome and the observed geometry and attitude of the system.

The chief advantage of this mesh is that it accurately represents the structural complexities of the aquifer and the desired node distribution using only 425 nodes. To achieve comparable

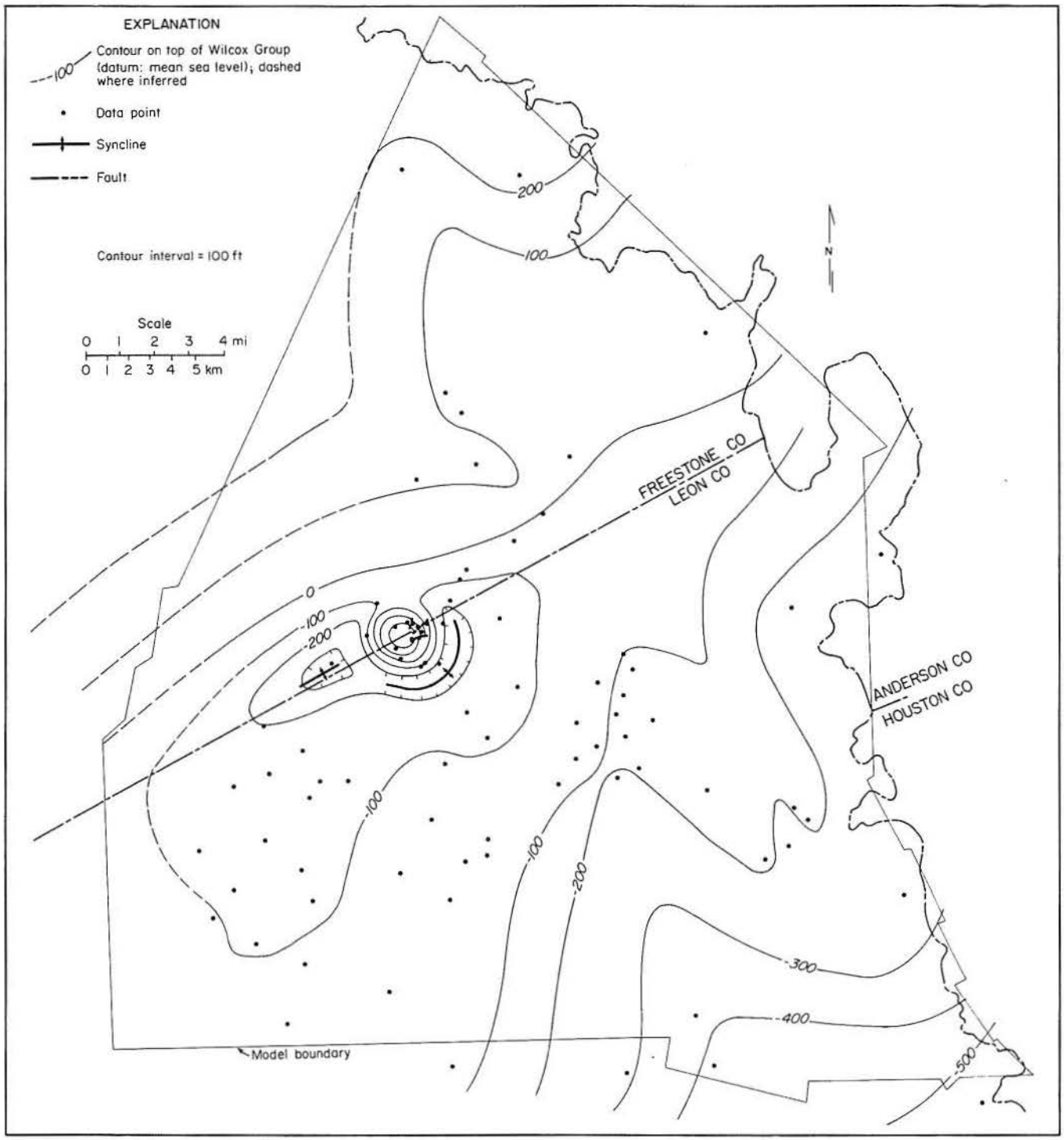

Figure 20. Structure-contour map on top of Wilcox Group (base of Carrizo Sand). Details around Oakwood Dome are from Giles and Wood (in preparation).

representation of the aquifer using a conventional finite-element or finite-difference grid would require thousands of nodes.

Primary limitations of the mesh are: (1) Structural complexities associated with Oakwood Dome are somewhat simplified, owing to a node spacing too coarse to represent all the details. (2) The Carrizo is grouped with the Wilcox in the upper layer, but because of its fairly uniform thickness and lithology, the Carrizo should be represented as an additional layer. (3) The uplift associated with Butler Dome (figs. 19 and 21) is not

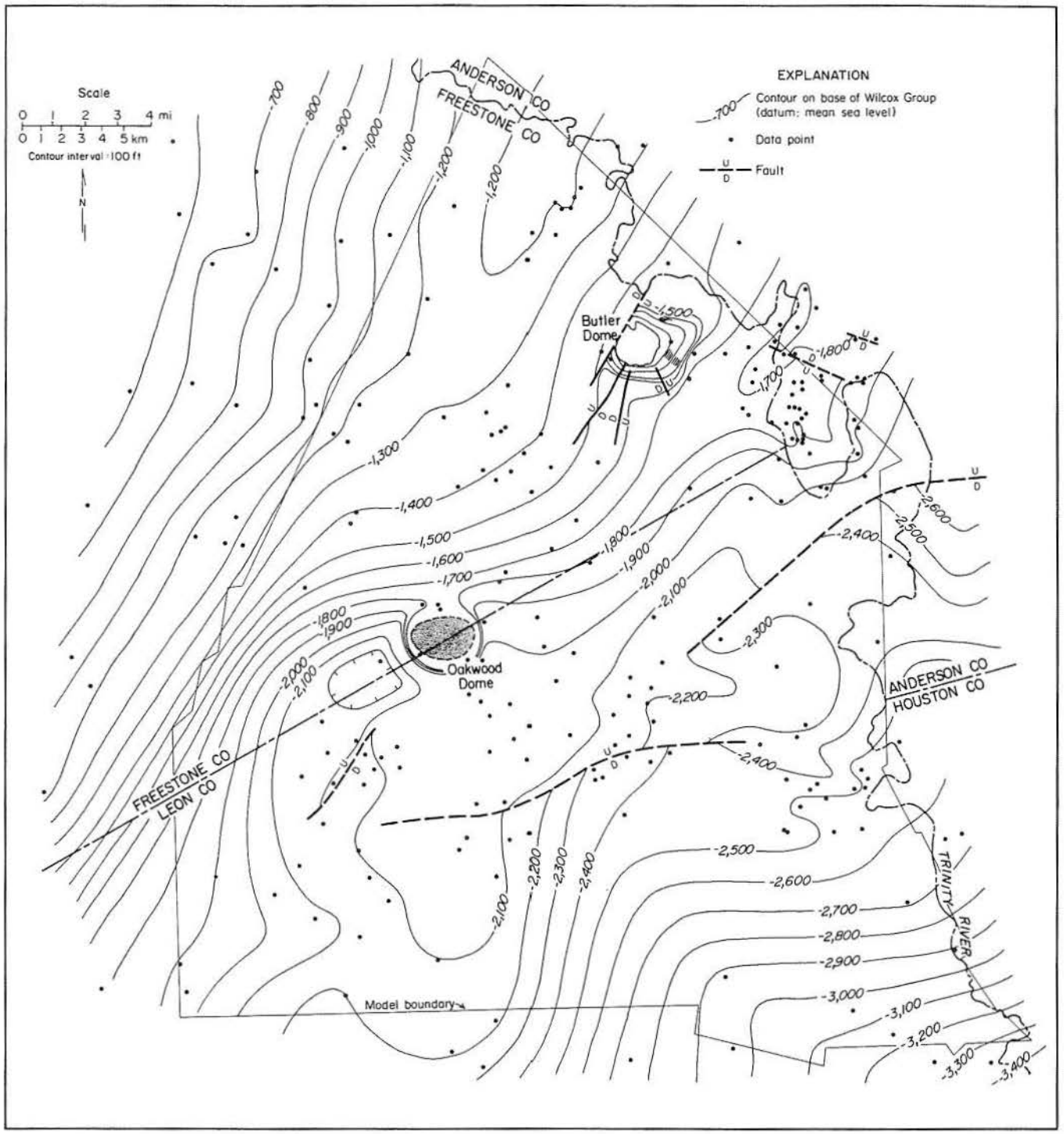

Figure 21. Structure-contour map on base of Wilcox Group. Details around Oakwood Dome are from Giles and Wood (in preparation).

accounted for. (4) The three layers of the mesh are much thicker than the individual layers of sand and mud in the Wilcox, and therefore values of hydraulic conductivity assigned to the model must represent volume-averaged, equivalent hydraulic conductivities of layered media. All these limitations stem from the ultimate limitations of computer storage space and computer time; theoretically, they could have been avoided by using a mesh containing many more nodes. If the model were being constructed today, a mesh consisting of 1,000 nodes, or even many more,

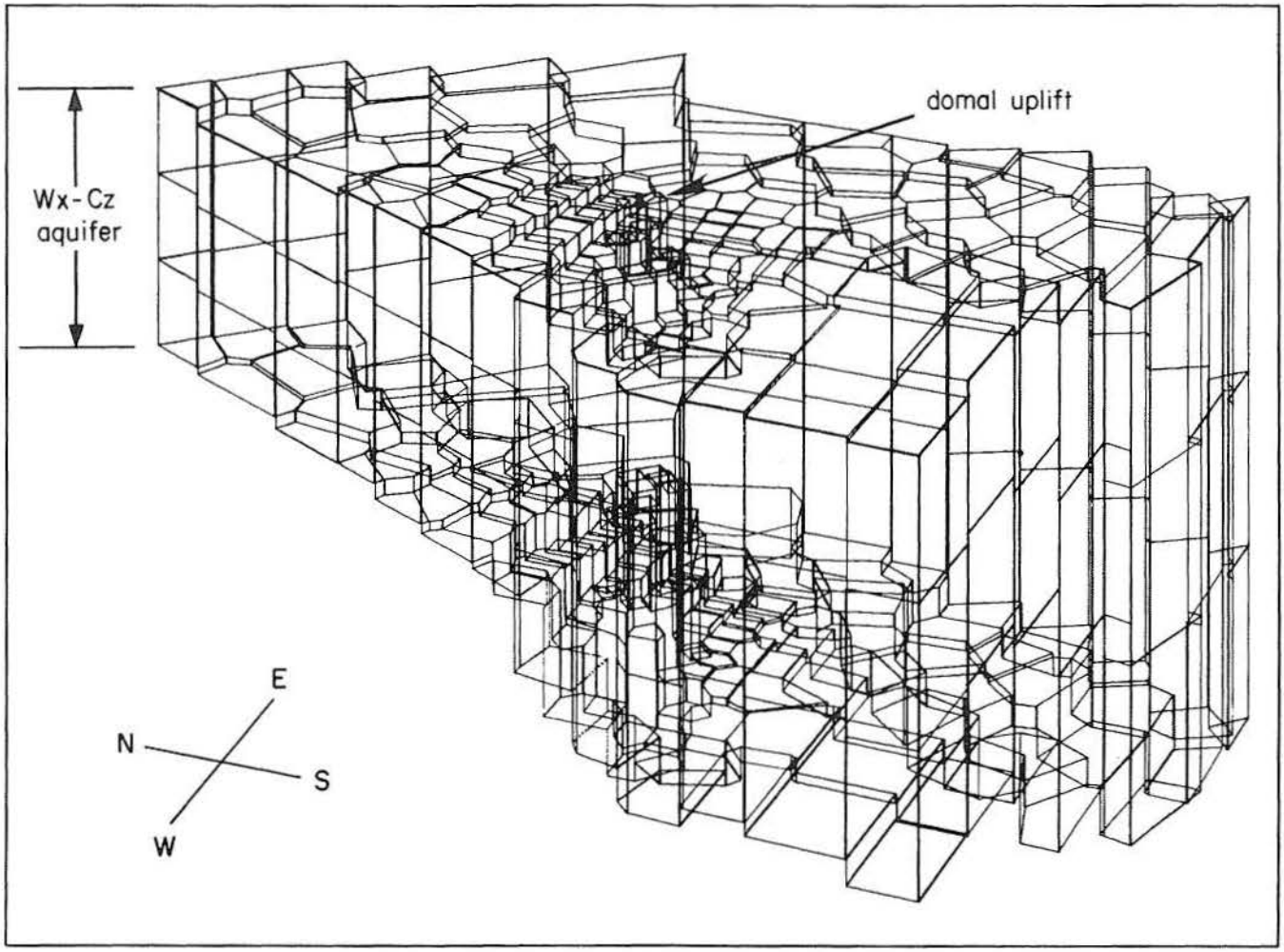

Figure 22. Three-dimensional perspective from the southwest of the outer surface of the IFD mesh generated from the structure-contour maps using program OGRE.

would be considered quite feasible, because the limit on computer storage for The University of Texas CDC Dual Cyber 170/750 computer system was recently raised, and because the present model proved to be surprisingly economical for a three-dimensional model (execution times of approximately 120 seconds per steady-state simulation).

Despite its limitations, the mesh did not seriously handicap the ability of the model to simulate realistic ground-water conditions. The major structural features included in the mesh near Oakwood Dome proved to have only a minor effect on ground-water flow; thus, inclusion of additional details would have been a minor improvement. Combining the Carrizo with the upper Wilcox caused an averaging of ground-water conditions between two quite different aquifer lithologies. This effect was obvious in the results and had to be carefully considered when interpreting them. The uplift associated with Butler Dome could be regionally significant if, by disruption of the Reklaw aquitard and muds in the Wilcox, it causes increased rates of ground-water discharge to the Trinity River and floodplain. Such discharge is taken into account using a boundary condition (see next section).

The limitation of representing heterogeneous, layered media as volume-averaged, equivalent hydraulic conductivities is a problem inherent in any ground-water model of a real-world system. How we have handled this problem will be discussed in the section "Equivalent Hydraulic Conductivity."

Boundary Conditions

Boundary conditions are often considered of secondary importance in ground-water modeling

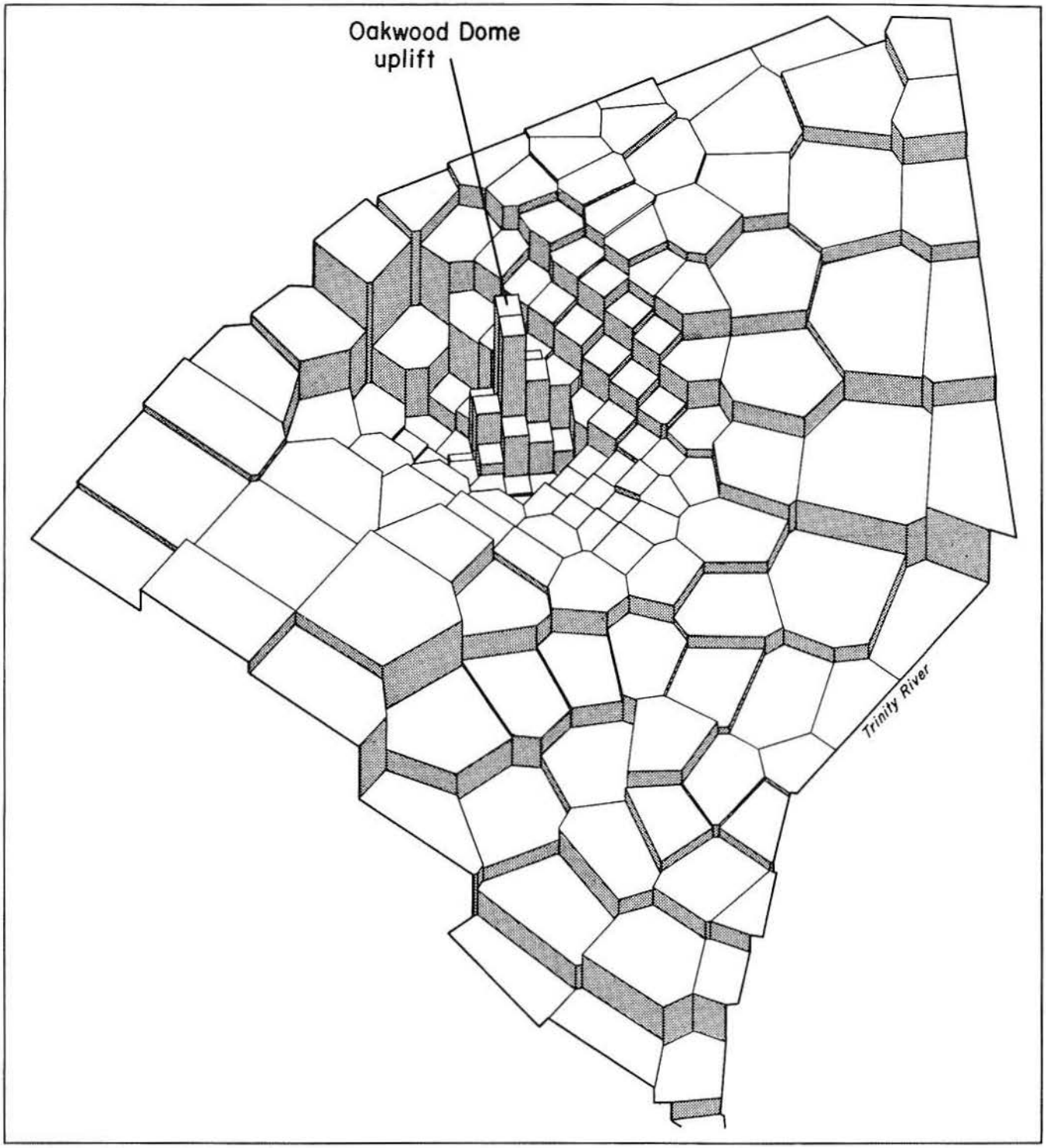

Figure 23. Three-dimensional perspective from the southeast of the upper surface (top of Carrizo aquifer) of the IFD mesh.

studies but can be most decisive to modeling results. Boundary conditions dictate where fluid will enter or leave the model and, in turn, what the model's general fluid circulation pattern will be. The modeler generally has the option of choosing from among three types of boundary conditions: (1) prescribed head (Dirichlet condition), (2) prescribed flux (Neumann condition), or (3) a mixed boundary condition, involving a combination of the Dirichlet and Neumann conditions in which both head and flux are allowed to vary on the boundary and the flux is

made a function of head. In the model, prescribed head boundary conditions are used to account for all flow across boundaries. Prescribed flux boundary conditions would have been used if any of the fluxes (that is, lateral flow across boundaries and vertical leakage) had been known with reasonable certainty. As is usually the case, flux is the least accurately known quantity and hydraulic head is relatively well known. One of the most important outputs of the model is a computed value for flux at each node where a prescribed head or mixed boundary condition is applied. The accuracy of these fluxes chiefly depends on the accuracy of aquifer parameters and heads assigned to the model.

Lateral Boundary Conditions

For convenience, names of lateral boundary segments will be abbreviated as indicated in figure 24: "W-NW" for the combined west and northwest boundaries; "TR-N" for the northern two-thirds of the Trinity River boundary; "SE" for boundaries at the southeast corner, including the lower one-third of the Trinity River boundary; and "S" for the straight segment of the south boundary.

Except where no-flow boundary conditions (that is, prescribed flux = 0) were assumed, hydraulic head was prescribed on lateral boundaries using data from the potentiometric surface maps (figs. 5 and 6) and pressure-versus-depth (P-D) relationships (table 1 and figs. 8 and 9). No-flow conditions were prescribed along the TR-N and S boundaries. The potentiometric surface maps indicate that ground-water flow does not cross these boundaries; flow appears roughly parallel to S and converges symmetrically on TR-N. The major inflow and outflow boundaries, where heads were prescribed, are the W-NW and SE boundaries, respectively.

The P-D data were used to estimate variations in head with depth on lateral, prescribed head boundaries. As discussed earlier, these P-D data and similar data from the entire East Texas Basin strongly indicate that head generally decreases with depth in the higher elevations and increases with depth in the lower elevations, owing to effects of topography. A similar pattern is evident for the area of the model but is difficult to quantify for approximately the lower one-half of the system (most of the head data are from the upper half of the system) and in the vicinity of the southeastern corner of the model, where Wilcox data are practically absent.

The W-NW boundary corresponds to a P-D slope (m) of 0.96 (fig. 8), and the Houston County P-D data for surface elevations 250 to 300 ft (76 to 91 m) (table 1) suggest an m value of 1.05 for the SE boundary. If these values are applied to the entire thickness of the model, however, we get unreasonable hydraulic gradients in the lower layer, as illustrated in figure 25, which shows a hypothetical head distribution plotted on a cross section through the southern boundary of the model. A horizontal head drop (Δh) of 105 ft (32.0 m) along the upper layer is measured from the potentiometric surface maps of the Wilcox and Carrizo (figs. 5 and 6). Based on m values of 0.96 and 1.05 at the updip and downdip ends of the section, respectively, Δh would decrease to 40 ft (12.2 m) in the middle layer and then to -30 ft (-9.1 m) in the lower layer. The negative value of Δh in the lower layer would indicate an updip flow direction, which is considered improbable in this case. Flow updip might be possible if the portion of the Wilcox immediately south-southeast of the model contained abnormally high fluid pressure (geopressured conditions), but this is not the case. A more plausible scenario is that Δh decreases with depth but does not become negative; in other words, velocity decreases in magnitude with depth (as commonly occurs in ground-water systems) and maintains a downdip flow direction.

Thus, to impose more realistic boundary conditions on the lower layer, it was assumed that vertical head differentials between the middle and lower layers are less than those predicted by the P-D data; that is, values of m between these layers are closer to 1.00. These values were assumed to be approximately 0.97 and 1.02 at the northwest and southeast boundaries, respectively. The resulting values of prescribed head imposed on the lateral boundaries are shown in figure 24. From the middle to the lower layer, values of prescribed head generally drop by 10 ft (3.0 m) at the northwest boundary and increase by 10 ft at the southeast boundary. The importance of these imposed vertical hydraulic gradients and the consequences of assuming they are zero (m = 1.00) will be discussed in "Results and Discussion."

Vertical-Leakage Boundary Condition

Vertical leakage across the Reklaw aquitard was accounted for using the boundary condition described in figure 26. This leakage boundary condition involved adding another layer of nodes (external boundary nodes) and connecting them to the upper surface of the mesh. Prescribed heads representing the Queen City water-table aquifer were assigned to each of the external boundary nodes, and each connection to the mesh was assigned a conductance term that includes vertical

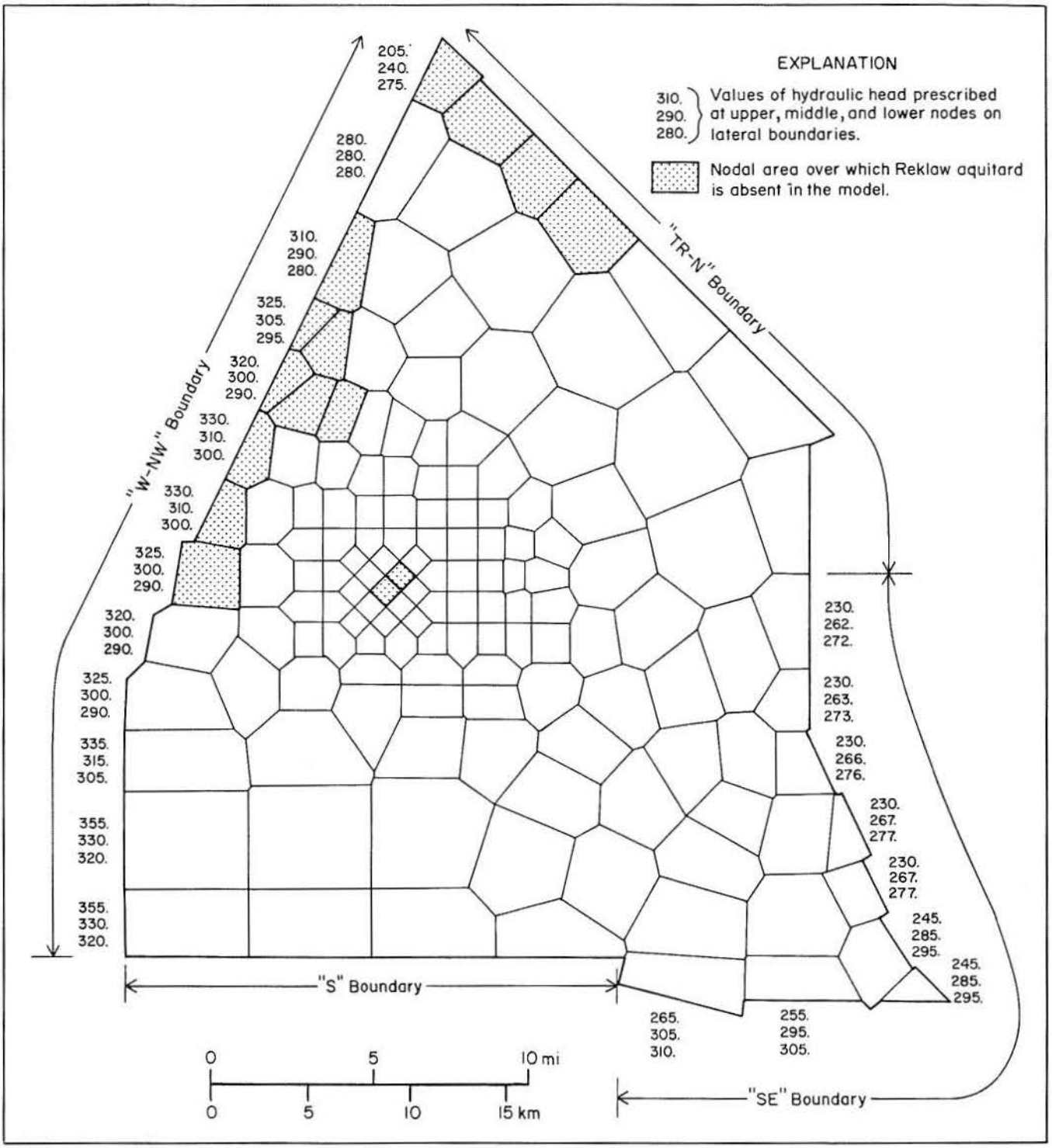

Figure 24. Map of IFD mesh, values of hydraulic head prescribed on lateral boundaries, and nodal areas where the Reklaw aquitard is absent in the model. Boundaries where head values are absent ("S" and "TR-N" boundaries) are no-flow boundaries.

hydraulic conductivity (K_v) and thickness of the Reklaw aquitard (b in fig. 26) and the cross-sectional area of vertical flow (A in fig. 26). This conductance term is then combined in Darcy's equation with the vertical head drop between the water table and the potentiometric surface to simulate leakage at each node location. Fixed values of head on the water table are assigned to external boundary nodes, and heads on the potentiometric surface are computed by the model.

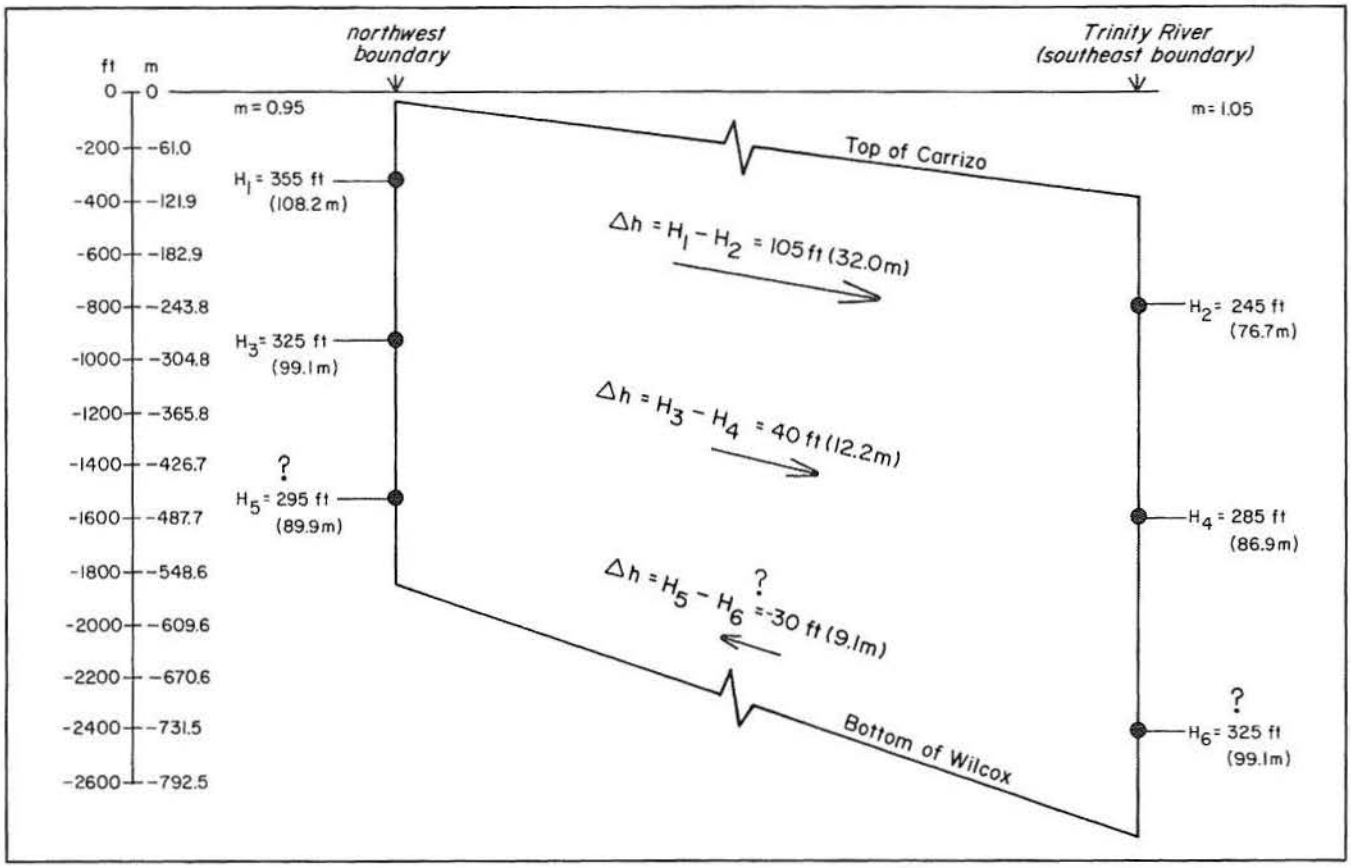

Figure 25. Schematic cross section showing values of horizontal head differential (Δh) that would occur if pressure-depth (P-D) slopes (m) were assumed to be uniformly equal to 0.95 and 1.05 at updip and downdip boundaries, respectively. This is unrealistic because it results in updip flow on a regional scale in the lower third of the system. A more realistic scenario is that the P-D slope approaches a value of 1.00 toward the base such that horizontal hydraulic gradients decrease downward but do not reverse directions.

Application of the leakage boundary condition requires a detailed map of the Queen City potentiometric surface, but the head data alone are too sparse to use in constructing such a map. Because Queen City heads correlate closely with topography, however, we were able to construct the potentiometric surface map based solely on topographic maps and the observed relationship between head and topography (fig. 7).

The Queen City potentiometric surface used in the model (fig. 27) was created by overlaying a plan view of the IFD mesh on USGS topographic maps (scale 1:250,000), calculating the average land-surface elevation within each nodal area, and assigning a corresponding head value from the graph in figure 7. Note that the resulting surface is most complex in the vicinity of Oakwood Dome. This is merely an artifact of the closer node spacing around the dome and does not affect the results significantly.

Other data needed to simulate leakage are thickness and vertical hydraulic conductivity of the Reklaw aquitard. Effective confining thickness of the Reklaw is assumed to be equal to thickness of mud strata that make up the unit. This thickness in the model area is about 60 to 160 ft (18.3 to 48.8 m) (Fogg and Kreitler, 1982), and thus a uniform value of about 100 ft (30.5 m) was used in the model. It is not worthwhile to assign a precise variation in thickness to the model because any such variation is rendered meaningless by uncertainty regarding hydraulic conductivity (K) of the Reklaw, which could vary by several orders of magnitude.

Hydraulic conductivity (K) of the Reklaw has not been measured, and consequently it had to be inferred from knowledge of the lithology. Accuracy of the estimated K is, of course, very tenuous and therefore a range of values was tested to indicate the sensitivity of the model to K of the Reklaw. The range used is 2.6×10^{-4} to 2.6×10^{-6} ft/d (7.9×10^{-5} to 7.9×10^{-7} m/d). These values are reasonable for clays or shales (Freeze and Cherry, 1979).

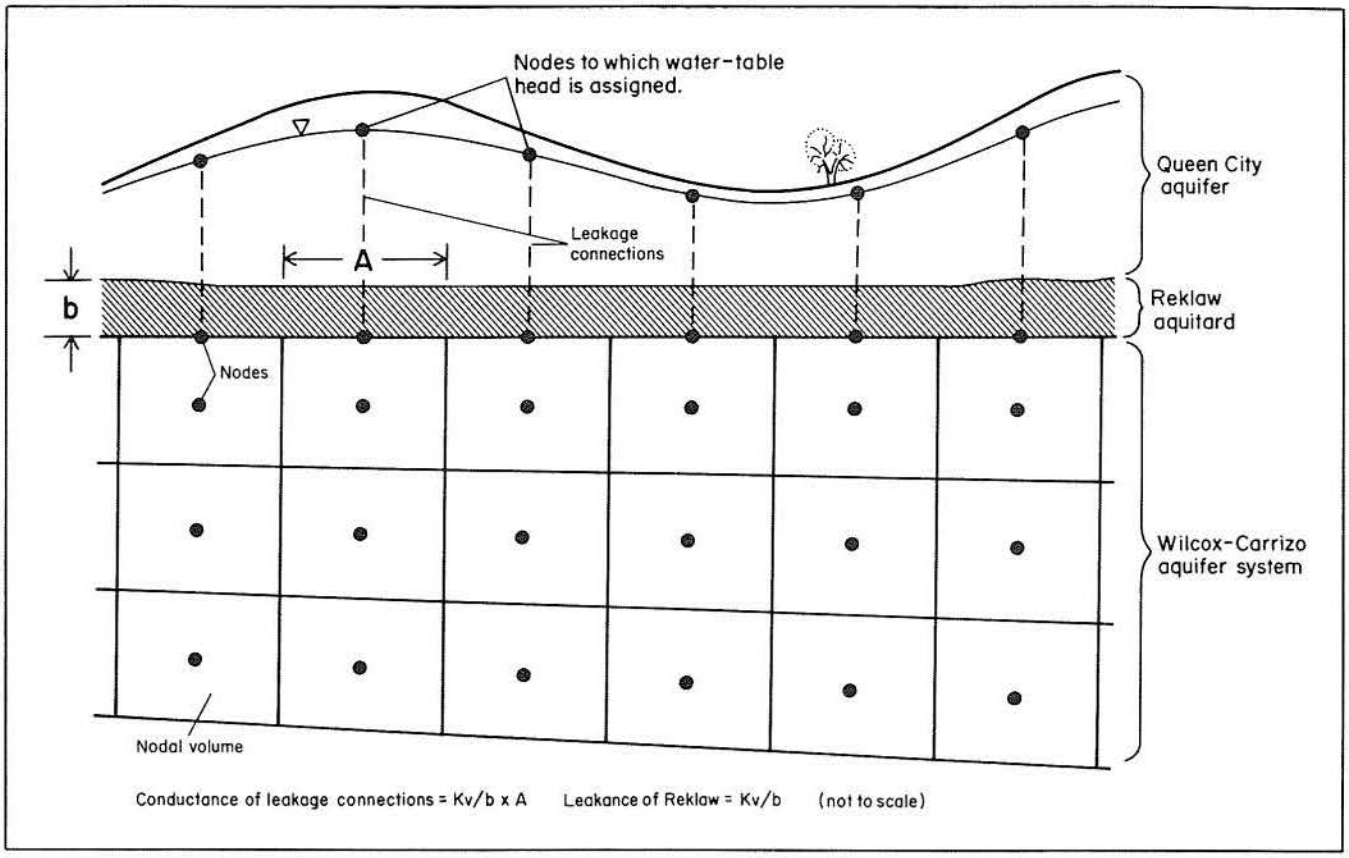

Figure 26. Schematic cross section depicting how vertical-leakage boundary condition was prescribed.

In areas where the Reklaw has been partially or completely eroded away, it was not included in the model. These areas (fig. 24) are (1) along certain segments of the W-NW boundary, (2) over Oakwood Dome, and (3) along the northernmost four nodes of the TR-N boundary. The Reklaw is present along the entire TR-N boundary but is incised by the Trinity River along the northern section of the boundary, thereby increasing the probability of having unimpeded hydraulic communication between the river and the Wilcox-Carrizo system. The potentiometric depression along this reach (figs. 5 and 6) further suggests such communication. As will be demonstrated, however, presence or absence of the Reklaw has little effect on the model results because vertical conductivity of the Wilcox-Carrizo itself is so low.

Equivalent Hydraulic Conductivity

To each volume element of the mesh, a value of hydraulic conductivity must be assigned that is equivalent to that of the interbedded sand and mud facies of the Wilcox-Carrizo aquifer system. Values of equivalent hydraulic conductivity in the horizontal direction (K_h') were calculated using the maps of channel-fill sand-percent (figs. 15, 16, and 17) and the hydraulic conductivity data (fig. 11). The value of K_h' for a horizontally layered porous medium can theoretically be calculated as a weighted arithmetic mean of K values of individual layers (fig. 14). Because K of the interchannel sands is much lower than that of the channel-fill sands (discussed on p. 16), the interchannel sands contribute negligibly to the value of K_h'; thus, K_h' can be approximated as the product of percent thickness and K of channel-fill sands if all these sands are interconnected. If the channel-fill sands are disconnected, K_h' will essentially be controlled by the interchannel sands, which were assumed to be generally lower in permeability by a factor of 100 or more (fig. 11). In areas where thickness of channel-fill sand is less than 20 percent (figs. 15-17), the sand bodies appear to be disconnected (discussed on pages 18 and 19); hence, values of K_h' in these areas were lowered by a factor of 100 relative to adjacent areas.

The resulting calculated values of K_h' are shown in figure 28 for each layer of the model. The Carrizo

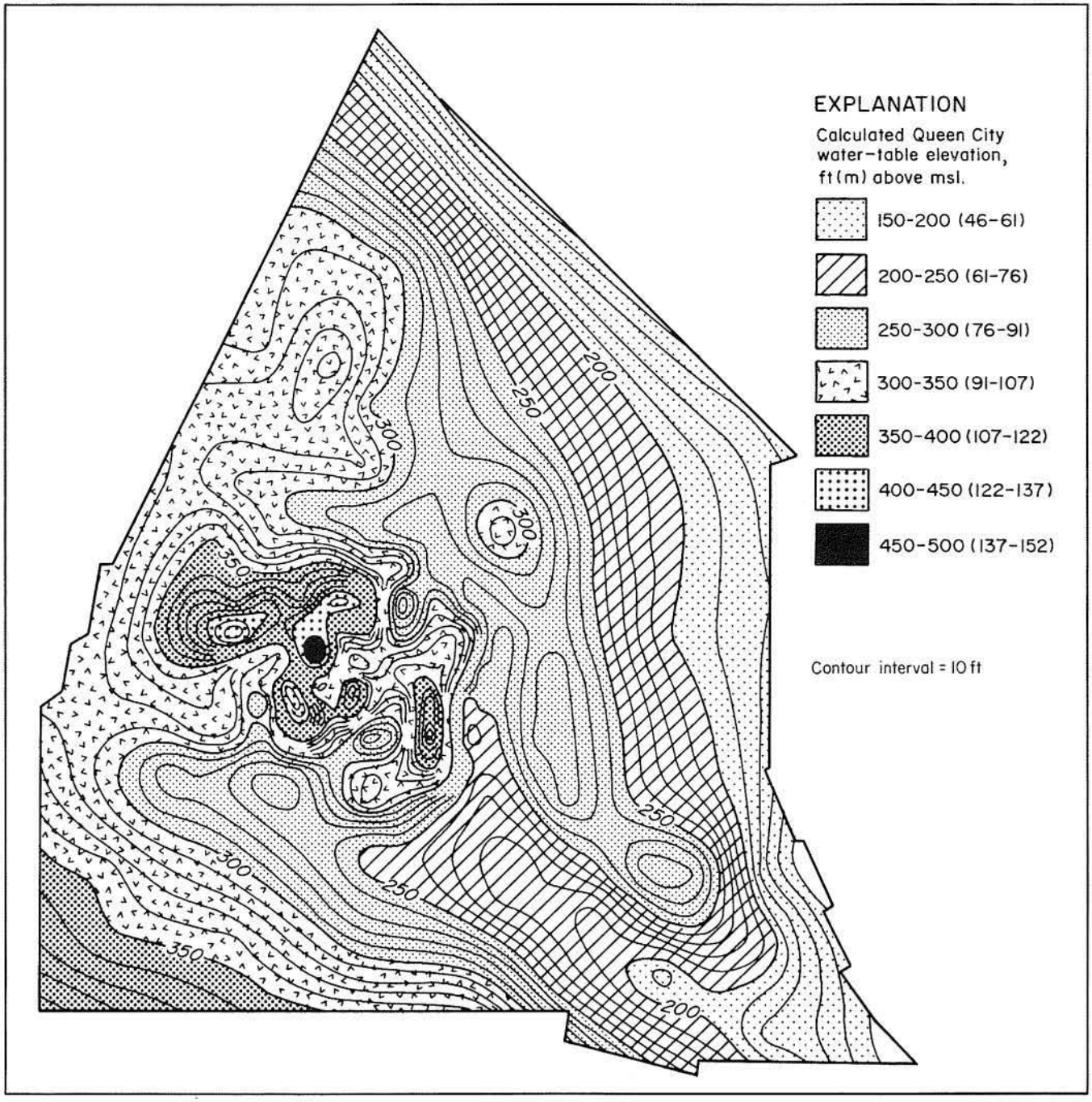

Figure 27. Map of Queen City water table calculated from the observed water-table/topography relationship shown in figure 7.

aquifer is averaged in with the upper layer, causing a fairly minor variation in K_h' in the upper layer. Effects of having a homogeneous K_h' distribution and of assuming that all channel-fill sands are interconnected will be shown.

Equivalent hydraulic conductivity in the vertical direction (K_v') could only be guessed at initially. From the simulations, however, we learned that the values of vertical head differential computed between layers by the model were extremely sensitive to the assigned values of K_v'. Maximum values of K_v' were estimated using a calibration procedure in which the ratio K_v'/K_h' was adjusted until the computed vertical hydraulic gradients agreed with those indicated by the pressure-depth (P-D) data. (The vertical hydraulic gradient equals the slope of the P-D line minus 1.00.)

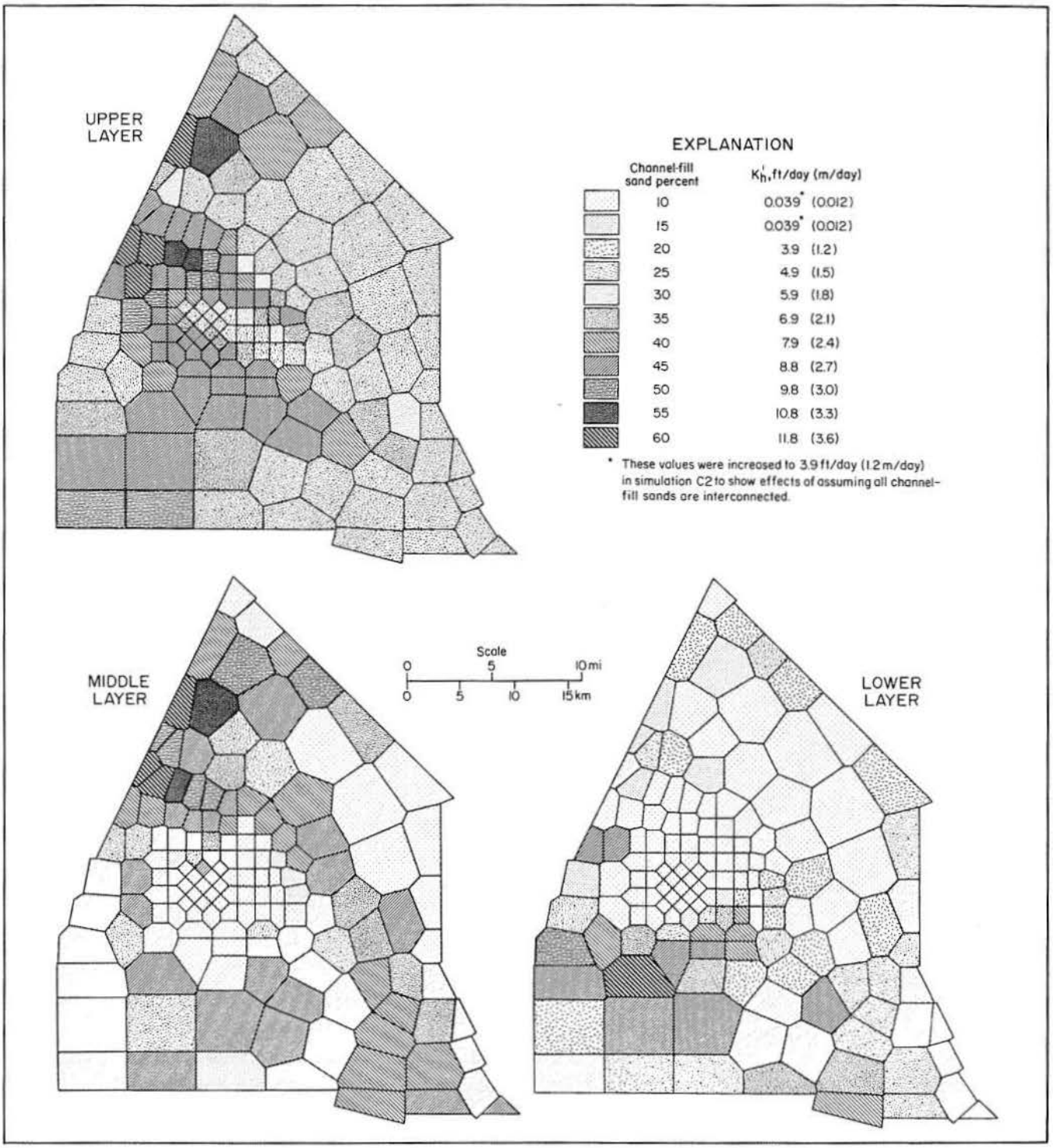

Figure 28. Values of equivalent horizontal hydraulic conductivity (K_h') calculated for each layer of the model. Where all channel-fill sands are interconnected, K_h' = (channel-fill sand percent) × (mean K of the channel-fill sands). Where channel-fill sand percent is less than 20, K_h' is reduced by a factor of 100 relative to adjacent areas. The Carrizo aquifer is included in the upper layer.

Simulations

Seven simulations were run in order to test the sensitivity of the model. Simulation A (table 3) can be considered a reference simulation that is convenient to compare with the others. The other simulations involve (1) adjustments of K_v'/K_h' (B1 and B2), (2) adjustments of K_h' with respect to

Table 3. Summary of conditions imposed during each simulation.

Conditions	Simulations						
	A	B		C		D	E
		1	2	1	2		
$K_v'/K_h' = 10^{-2}$		X					
$K_v'/K_h' = 10^{-4}$	X			X	X	X	X
$K_v'/K_h' = 10^{-6}$			X				
K_h' homogeneous				X			
All channel-fill sands interconnected					X		
Channel-fill sands disconnected in interchannel areas	X	X	X			X	X
K of Reklaw = 2.6×10^{-4} ft/day	X	X	X	X	X		
K of Reklaw = 2.6×10^{-6} ft/day						X	
High K_v' inserted near Butler Dome ($K_v'/K_h' = 1$)							X

sand-body interconnectedness (C1 and C2), (3) adjustment of K of Reklaw from 2.6×10^{-4} to 2.6×10^{-6} ft/d (7.9×10^{-5} to 7.9×10^{-7} m/d) (D), and (4) insertion of good vertical hydraulic continuity at the Trinity River boundary near Butler Dome (E).

Adjustments of K_v'/K_h' were made in attempts to reproduce the vertical hydraulic gradients that are indicated by the pressure-depth data. The best reproduction occurs when $K_v'/K_h' = 10^{-4}$, which is therefore used in all but simulations B1 and B2. As a result, average values of K_v' in simulation A are approximately 2.6×10^{-4} ft/d, which was in turn assumed to be a maximum K value for the Reklaw aquitard. K of the Reklaw is unknown, but it is presumably no greater than K_v' of the Wilcox. In order to maximize effects of leakage on the model results, K of the Reklaw was set equal to K_v' of the Wilcox in all but simulation D, in which it was reduced by an additional two orders of magnitude.

To test the effects of having a local zone of good vertical hydraulic communication from the bottom of the Wilcox through the Reklaw aquitard in a potential discharge area, K_v' of the Wilcox-Carrizo was increased in simulation E by a factor of 10^4 at a node location just north of Butler salt dome at the Trinity River boundary (fig. 35). The Reklaw aquitard is already assumed to be breached in the model at this location (fig. 24). Relatively high values of vertical conductivity are possible in this area because the nearby Butler Dome uplift has caused faulting and uplift of Tertiary strata (fig. 21). The faults may provide vertical pathways for flow, and the uplift may have caused the Trinity River to incise locally through the Reklaw Formation and into the Carrizo Formation.

A simulation similar to E was also run in which good vertical conductivity was inserted near the terminus of the brackish-water plume at Upper Keechi Creek (fig. 10). The results are not presented because they show no significant change in heads and fluxes.

RESULTS AND DISCUSSION

Vertical Interconnection of Sand Bodies

Vertical interconnection of sand bodies in the Wilcox-Carrizo aquifer system is manifested in the vertical equivalent hydraulic conductivity (K_v'). There are virtually no data on K_v', but by inserting different values of K_v' and observing vertical hydraulic gradients ($\partial h/\partial z$) computed by the model, we are able to estimate a maximum reasonable value.

Values of $\partial h/\partial z$ computed between the upper and middle layers and the middle and lower layers are contoured in figure 29 for simulations B1, A, and B2, respectively (refer to table 3). The value of $\partial h/\partial z$ equals the slope of the pressure-depth line (table 1) minus 1.00; thus, negative and positive values of $\partial h/\partial z$ indicate downward- and upward-

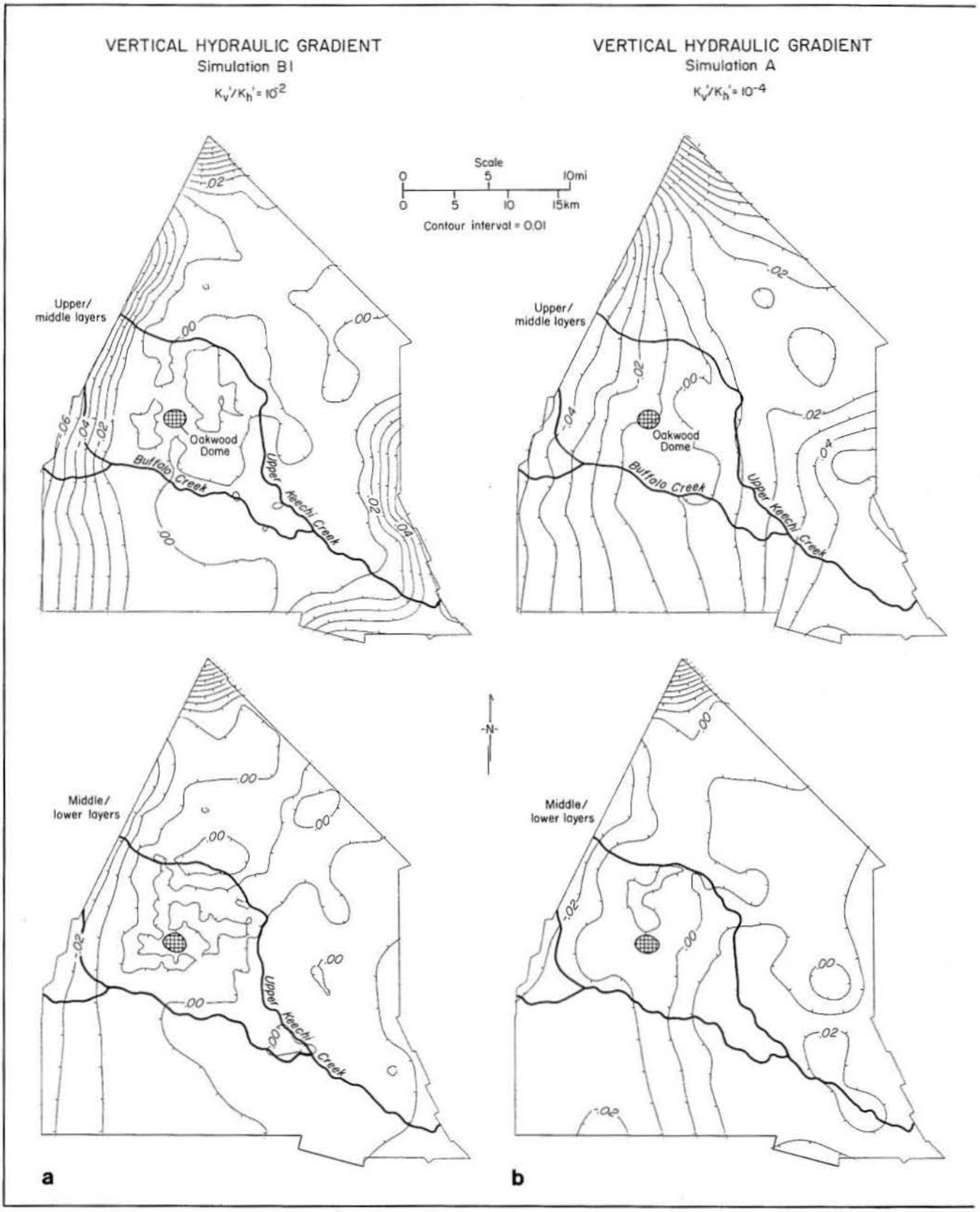

Figure 29. Contour maps of vertical hydraulic gradient ($\partial h/\partial z$) computed between upper and middle and middle and lower layers in simulations (a) B1, (b) A, and (c) B2. Simulation B1 produced $\partial h/\partial z$ values equal to zero everywhere but on the boundaries where they are imposed with boundary conditions, while simulations A and B2 produced a more realistic, gradual variation in $\partial h/\partial z$ across the area. Thus, a K_v'/K_h' value of 10^{-2} is too high.

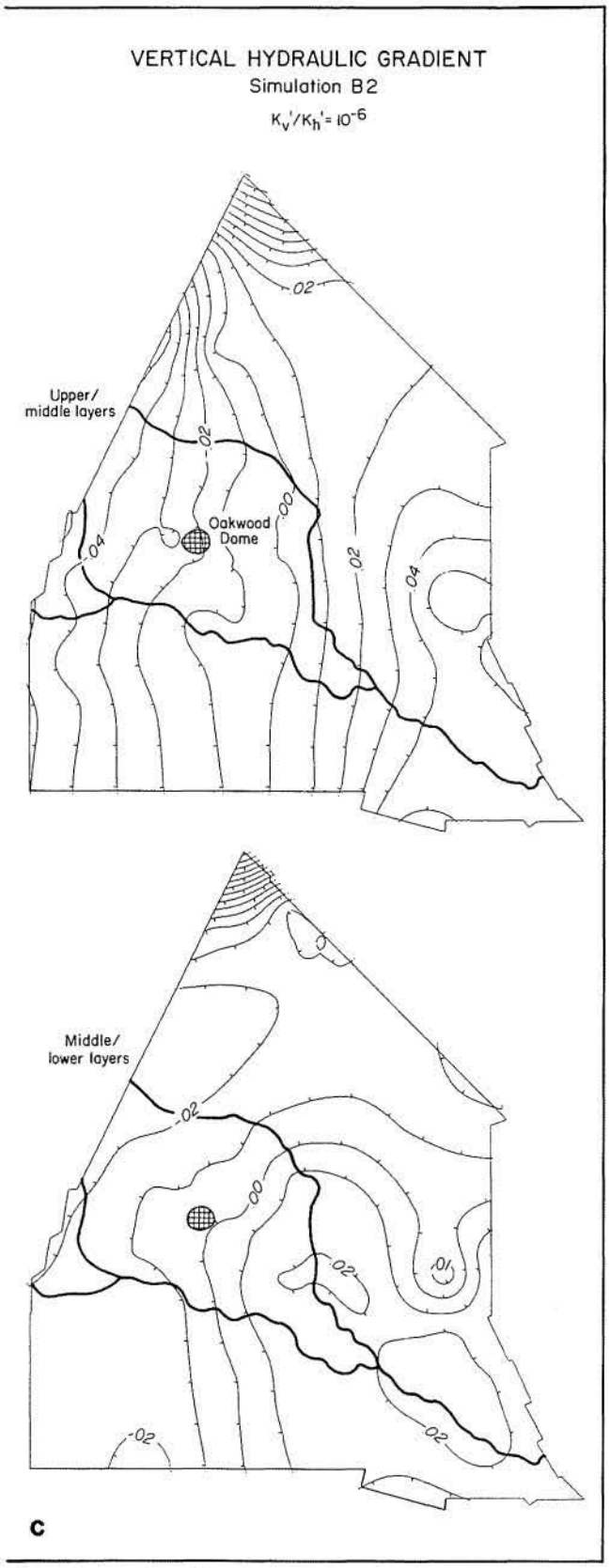

Fig. 29 (continued)

flow potentials, respectively. On the basis of the pressure-depth data, we would expect $\partial h/\partial z$ to generally be non-zero and to vary gradually from negative values near the Wilcox-Carrizo outcrop area to positive values further downdip in the artesian section. Such a trend was produced by simulations A and B2 ($K_v'/K_h' = 10^{-4}$ and 10^{-6}, respectively) but not by B1 ($K_v'/K_h' = 10^{-2}$).

In simulation B1, $\partial h/\partial z$ is non-zero only near the boundaries, where it is being imposed by the boundary conditions, but rapidly shifts to zero toward the interior of the model. This indicates that the value of K_v'/K_h' is too high (K_v' is too high) and is allowing potentials (heads) to equilibrate readily along the vertical. The same does not happen along the horizontal, because of the great horizontal distances involved. (Recall from Darcy's equation that for a given flow rate [Q], the hydraulic head differential between two points is proportional to the distance between them and inversely proportional to hydraulic conductivity and cross-sectional area of flow.)

Decreasing K_v'/K_h' from 10^{-2} to 10^{-4} in simulation A effectively lowered K_v' below some critical range, thus allowing $\partial h/\partial z$ values imposed on the boundaries to propagate across the entire model. Therefore, a maximum reasonable value for K_v'/K_h' is on the order of 10^{-4} to 10^{-3}. The minimum reasonable value is more difficult to estimate, but the map of $\partial h/\partial z$ between the middle and lower layers from simulation B2 (fig. 29c) suggests that it is greater than 10^{-6}. The map shows that the zero contour of $\partial h/\partial z$ bends southward near the Trinity River such that, contrary to the pressure-depth data (table 1), $\partial h/\partial z$ is primarily negative (or the pressure-depth slope is less than 1.0) beneath the Trinity River where it borders the northern half of the model area. Apparently, K_v' is so low in this case that it totally segregates adjacent layers of the model and allows negative values of $\partial h/\partial z$ imposed on the W-NW boundary to propagate all the way to the Trinity River.

This anisotropy ratio (K_v'/K_h') of 10^{-4} is much smaller than the commonly assumed values of 0.5 to 0.1 for sandstone aquifers. However, the Wilcox-Carrizo is composed not of a single sand unit but of multiple sand bodies interfingered with mud and lignite. Because the muds may be of lower permeability than the sands by many orders of magnitude, the muds can result in very low values of K_v'. Before the modeling study, we had assumed that K_v' would be very low at most localities, but that because of the generally high sand content of the Wilcox-Carrizo, vertical interconnection of sand bodies would be adequate to yield regional values of K_v' within one or two orders of magnitude

of K_h'. On the contrary, the very low values of K_v' derived from the model indicate that the mud facies are laterally extensive enough to effectively prevent much vertical interconnection of sands.

Although we have bracketed a probable value of K_v' using model calibration, the model tells us nothing about possible variations in K_v' over the region. Because K_v' is merely a regional average, it may result from a complex distribution of both very high and very low K_v' values. The high values, however, probably occur over a very small part of the model area. For example, let us assume that, relative to the apparent regional K_v' value of approximately 2.6×10^{-4} ft/d (7.9×10^{-5} m/d), local values of K_v' are either (1) very low (10^{-6} ft/d [10^{-7} m/d]) owing to laterally extensive clay/shale units or (2) very high (10^{0} ft/d [10^{-1} m/d]) owing either to local areas of good vertical interconnection of sand bodies or to fault planes serving as avenues of flow. All the geologic evidence suggests that condition 1 is by far the more common because of the omnipresent clay/shale strata (Seni and Fogg, 1982). If these two conditions occur in discrete zones, the regional value of K_v' can be calculated as a weighted arithmetic mean (otherwise, a weighted geometric mean might be more appropriate [Bear, 1972]):

$$K_v' = \frac{A_1}{A}[K_v']_1 + \frac{A_2}{A}[K_v']_2 = 2.6 \times 10^{-4} \text{ ft/d}$$

where A_1 and A_2 are the horizontal areas over which conditions 1 and 2 occur, A is total area of the model, $[K_v']_1$ is K_v' for condition 1, and so on. Since $[K_v']_1$ is only 10^{-6} ft/d, it is negligible in the calculation and can be omitted. Thus, if $[K_v']_2 = 10^{0}$ ft/d, A_2/A is only 2.6×10^{-4}; that is, good vertical hydraulic communication occurs over only .026 percent of the aquifer, and if $(K_v') = 10^{-2}$, over only 2.6 percent of the aquifer, and so on.

This type of calculation could be useful for quantifying the probability of local zones of rapid, vertical ground-water flow, which would in turn be useful in assessing the risks of contaminants escaping to the biosphere. Insufficient data exist to render the calculations accurate, but the exercise helps define what new data would be needed to enable a risk assessment. For example, it seems that pressure-depth and K_h' data are particularly important because they can be used to determine regional (and perhaps local) values of K_v'/K_h'.

Lateral Interconnection of Sand Bodies

In the simulations discussed previously, channel-fill sand bodies are assumed to be interconnected everywhere but in interfluve areas, where sand percent is less than 20 and the sand bodies generally appear to be disconnected (fig. 28). Additionally, we have assumed that where the sands are disconnected, equivalent horizontal hydraulic conductivity (K_h') should be lowered by a factor of 10^2 relative to the K_h' value that would otherwise be assumed. Comparison of hydraulic heads and Darcy velocity (specific discharge) vectors computed by the model in simulations A (channel-fill sands disconnected in interfluve areas) and C2 (all channel-fill sands interconnected) shows the importance of the interconnectedness assumptions (figs. 30, 31, 32, and 33). Results of simulation C1, in which distribution of K_h' is homogeneous, are not shown because they are practically identical to results of C2. Thus, although the K_h' distribution is heterogeneous in C2, the contrasts in K_h' values are insufficient to significantly affect ground-water flow. Interconnectedness of sand bodies is therefore a key variable.

Hydraulic head in simulation A is more irregular than, but not strikingly different from, that in simulation C2 (figs. 30 and 31). Hydraulic head generally is not very sensitive to hydraulic conductivity variations, especially in a three-dimensional model. The upper layer is not included in figure 31 because it is nearly identical to that in figure 30; the similarity is caused by the minor variations in K_h' that result from inclusion of the laterally continuous Carrizo Sand in the upper layer.

Contrasts between runs A and C2 are most obvious in ground-water velocity computed for the middle and lower layers (figs. 32 and 33). The assumption that sands are disconnected in interchannel areas causes a reduction of ground-water flow rates in these areas by a factor of 10^2 to 10^3 and significant changes in flow direction. In fact, flow in the middle layer for simulation A is roughly parallel to the brackish-water plume northeast of Oakwood Dome, as a result of a low-conductivity interchannel section located immediately southeast of the plume. The interchannel section is a partial barrier, thus diverting flow to the northeast. The plume is located in approximately the middle and lower layers of the model. Note that just off the northeast flank of the dome, where the plume probably originates, the low-conductivity interchannel section is narrow and velocity is fairly high in the middle layer. This suggests that relatively rapidly circulating ground water may come in contact with the northeast flank of the dome, thereby dissolving salt and/or cap rock and producing the brackish water in the plume.

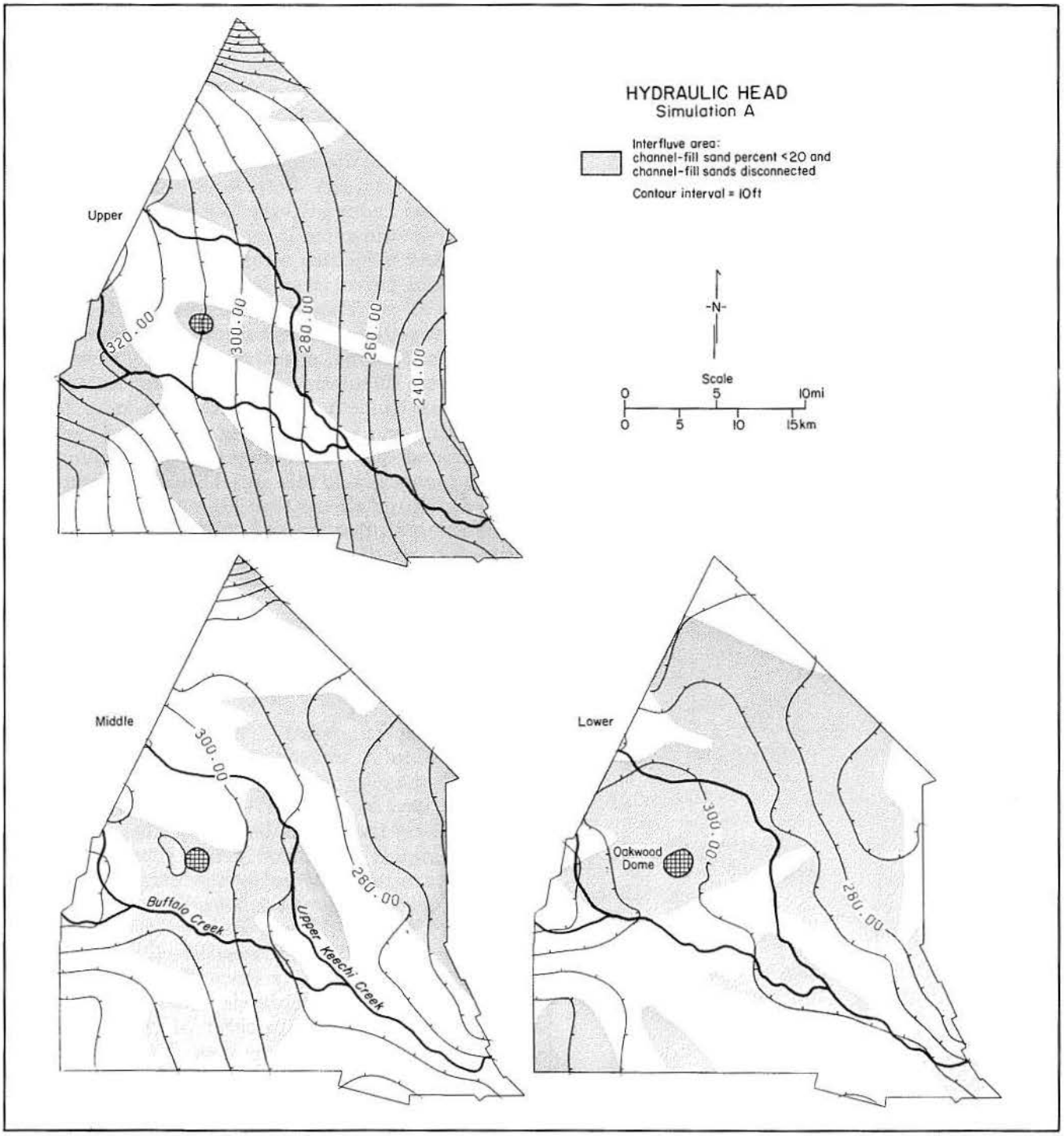

Figure 30. Contour maps of hydraulic head computed in simulation A. The potentiometric depression midway along the right margin of the lower layer is caused by an overlying topographic depression. The feature is less pronounced in upper layers because they have higher values of K_h'. Correlation between a potentiometric surface and surface topography does not necessarily indicate good vertical hydraulic communication between the two.

Preliminary results of the model presented in Kreitler and others (1981) showed that flow in the direction of the plume did not occur, even though the same assumptions about lateral interconnectedness of sand bodies were used. The reason is that values of K_v' were too high, thus allowing fluid in the model to move vertically over low K_h' obstructions rather than flowing around them in the horizontal plane. At the time of that report, we had not fully interpreted the pressure-

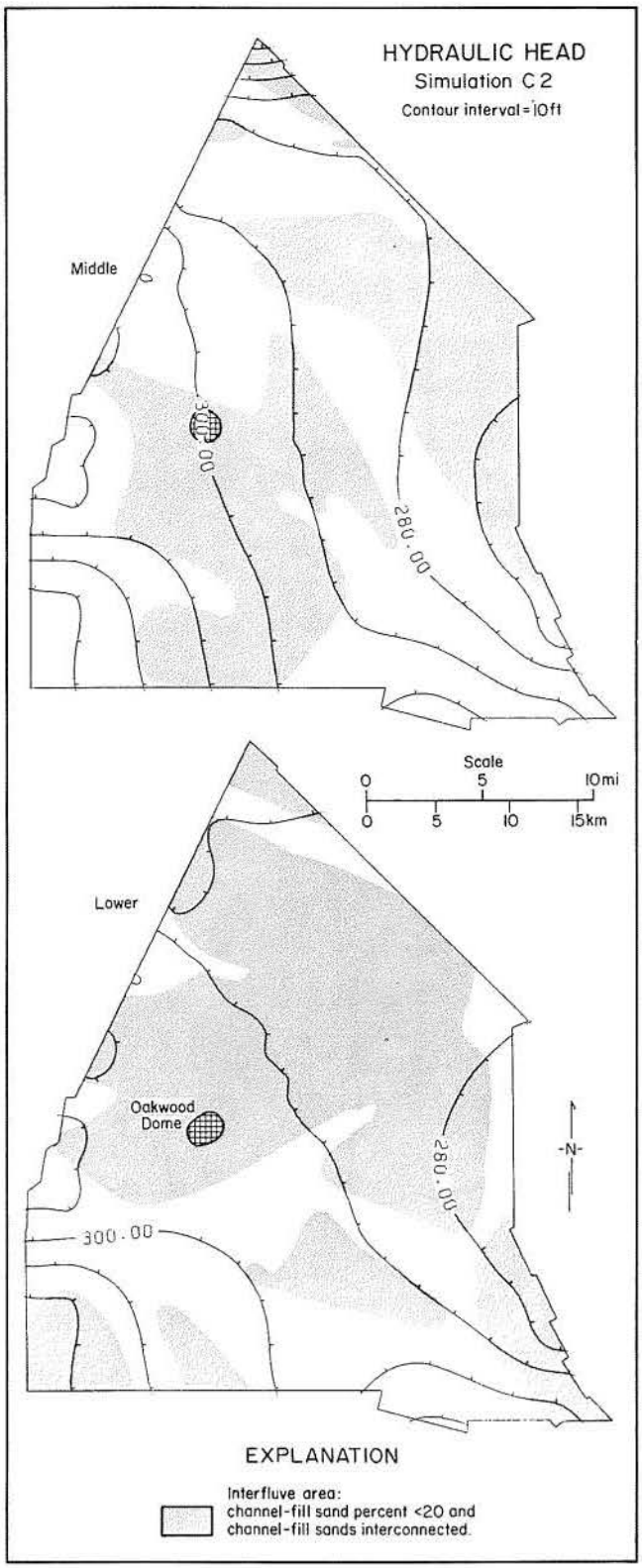

Figure 31. Contour maps of hydraulic head computed in simulation C2. Differences between these maps and figure 30 are caused by differences in K_h' distributions, which are relatively uniform in this case because all channel-fill sands are assumed interconnected. Results for the upper layer are not shown because they are practically identical to those from simulation A.

depth data, and therefore had no basis for assuming the low values of K_v'/K_h' used in simulation A. Hydrologic testing and sampling of water in the plume and vicinity would still be necessary in order to verify the scenario indicated by run A.

Outside of the plume area in simulation A (fig. 32), ground-water flow rates computed around Oakwood Dome are very low. (The dome does not penetrate the upper layer.) As will be shown later, such low velocities would theoretically result in very long travel times in the dome vicinity, about 10^5 to 10^6 yr. Thus, it is conceivable that the cap rock, together with low sand percentages around Oakwood Dome, effectively isolates most of the salt from circulating Wilcox ground water.

Note that the computed head map for the middle layer of run A (fig. 30) would not have indicated flow in the direction of the plume. The head map misses this detail because it represents hydraulic gradients that are regionally averaged by interpolation between node points. A velocity vector, on the other hand, represents a flux averaged about a single point and is therefore more definitive.

Topographic Effects and Updip Flow Directions

Other important features exhibited by simulation A include (1) lack of effect of local topography on computed heads and (2) ground-water flow to the west-northwest (up structural dip) along the W-NW boundary (figs. 30 and 32). Topographic effects on heads computed by the model are generally not evident except in the lower layer, midway along the boundary paralleling the Trinity River. Here, a depression in the head surface (fig. 30) correlates directly with a wide section of the Trinity River floodplain (fig. 19), implying that the depression results from upward flow and eventual discharge of ground water in this topographically low area. The depression is not closed at the model boundary to the east, but a no-flow boundary condition is imposed on this segment of the boundary, which means the flux must be upward somewhere inside the depression. Accordingly, the lateral component of velocity in the depression appears nonexistent in the lower layer (fig. 32).

Interestingly, the depression begins to die out in the middle layer and is totally absent in the upper layer. This is at first counterintuitive, because if discharge to the floodplain is lowering heads at the bottom of the system, one would expect to see the same feature (but perhaps larger) in higher layers. We checked the node-to-node

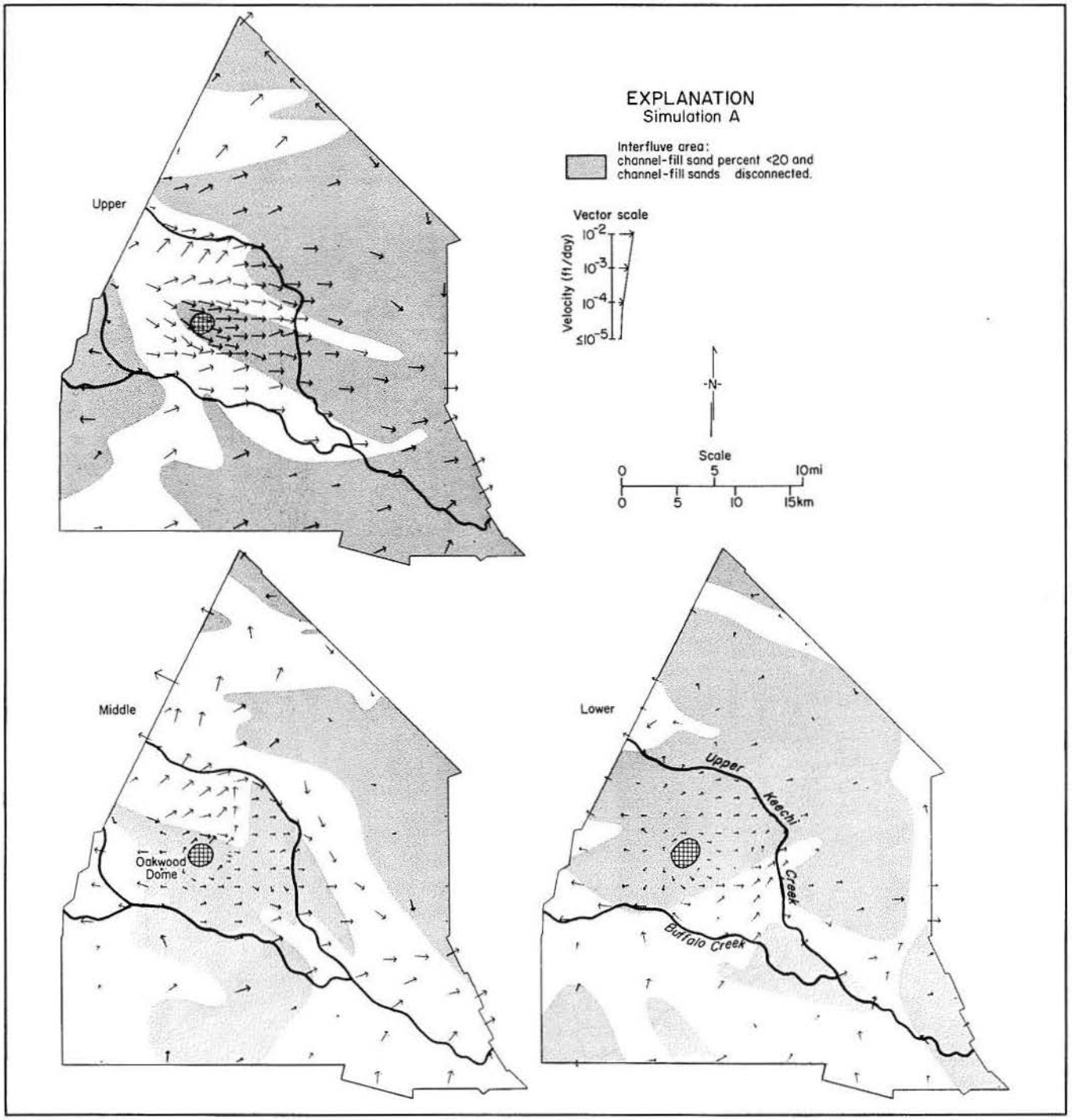

Figure 32. Maps showing ground-water velocity vectors (specific discharge) computed in simulation A. Uniform velocities in the upper layer are caused by inclusion of the Carrizo aquifer in that layer. Updip flow directions along the west-northwest boundary may be caused by errors in the boundary conditions or they may reflect a natural phenomenon. Northeastward flow away from the dome in the middle layer coincides with the brackish-water plume (fig. 10). Compare velocity vectors with head maps in figure 30 and note that the latter miss important details.

fluxes listed on the computer printouts of the model and verified that vertical fluxes at the depression are indeed relatively high in all layers. The explanation becomes obvious given the vertical variations in hydraulic conductivity (K_h') in the vicinity of the depression (fig. 28). Values of K_h' decrease from the upper to lower layers at the site. Theoretically, removal of a given amount of water from a local area of an aquifer by upward discharge (or pumping from a well) will result in a

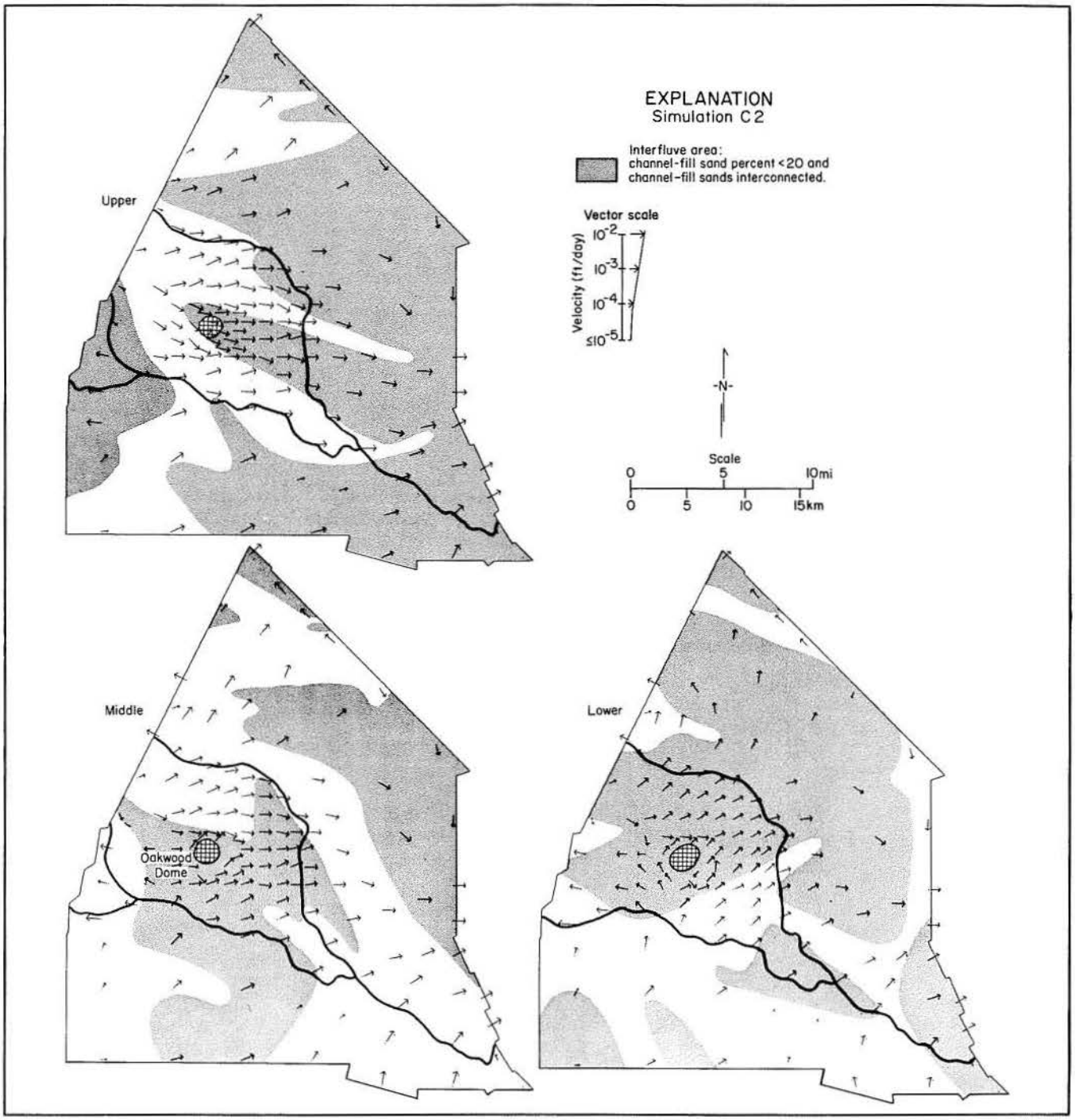

Figure 33. Maps of ground-water velocity vectors (specific discharge) computed in simulation C2. Uniform magnitudes of velocity are caused by assuming that all channel-fill sand bodies are interconnected.

horizontal head drop (or a "cone of depression") having a magnitude inversely proportional to the value of K_h'. Hence, the depression is accentuated in the middle and lower layers because of their lower K_h' values.

Nevertheless, vertical upward fluxes in the depression are very small (10^{-5} to 10^{-6} ft/d [10^{-4} to 10^{-5} m/d]). Correlation between topography and hydraulic head in a deep ground-water system indicates a certain amount of hydraulic communication with the shallow water-table system, but does not necessarily indicate large-scale vertical transfer of fluids. Topographic effects on heads are a complex function of both

topographic relief and three-dimensional distributions of hydraulic conductivity.

The updip flow directions along the W-NW boundary occur primarily in the middle and lower layers beneath topographically low areas in valleys of Upper Keechi and Buffalo Creeks (fig. 32). The phenomenon can be attributed to errors in the prescribed head boundary conditions that were applied, but it might also reflect natural conditions. Errors may stem from the fact that head was prescribed to decrease with depth uniformly along the entire W-NW boundary. Beneath the creeks, however, head may decrease with depth at a lower rate or it may increase with depth. If values of head prescribed beneath the creeks were increased in the model, the updip flow components would diminish in magnitude or would reverse themselves.

Note that the largest updip flow component occurs just northeast of Upper Keechi Creek on the W-NW boundary. Here, the Reklaw aquitard is not assigned (fig. 24), and because of the locally large thicknesses of channel-fill sands in both upper and middle layers (figs. 15 and 16), K_v' was set equal to K_h' in order to reflect the possible vertical interconnection of sands. Since heads are prescribed to decrease with depth at this location, the net effect in the model is that an unrealistically large amount of water cycles in through the upper node and then immediately out (updip) through the middle node. This cycling is only a local phenomenon; it creates no significant errors in fluxes and heads farther downdip or in water budgets computed by the model, because the rapid inflow and outflow cancel each other. A net flux in the downdip direction results.

A certain amount of updip flow may be occurring, however, because ground water seeks the path of least resistance, regardless of the dip of the aquifer. As ground water enters the system along the W-NW boundary and flows downdip, it encounters increasing resistance to flow owing to greater confinement and deeper burial. Generally, the more deeply an aquifer is buried, the more difficult it is for fluids to escape. Thus, after recharge waters flow a few miles downdip from outcrop beneath the Reklaw aquitard or Wilcox muds, the easiest course might be to veer laterally and flow updip to where a creek incises the outcrop boundary between the aquifer and the aquitard. This outcrop boundary is a transition zone from outcrop/water-table conditions to deep artesian conditions, and within that zone ground water may flow into the artesian section at topographic highs and out of it at topographic lows.

Hydraulic Conductivity of the Reklaw Aquitard

Effects of lowering hydraulic conductivity of the Reklaw aquitard from 2.6×10^{-4} to 2.6×10^{-6} ft/d (7.9×10^{-5} to 7.9×10^{-7} m/d) are shown in head maps computed by the model for simulation D (fig. 34). The velocity vectors produced by this run differ only slightly from those of simulation A and are therefore not shown.

Only a few small changes can be seen in the heads. The most noteworthy is the disappearance of the topographically induced depression that was discussed earlier. Also, a small potentiometric mound west of the dome in the middle layer of run A (fig. 30) disappeared in run D. This mound too was caused by topographically influenced leakage in the model.

If the Reklaw hydraulic conductivity (K) used in run D is realistic, the Reklaw aquitard may effectively isolate the Wilcox-Carrizo from any local topographic influence. Perhaps the most realistic scenario is that K of the Reklaw is normally very low but may be locally high owing to disruption by faults or lateral facies changes (Fogg and Kreitler, 1982).

Effects of Inserting Locally High Vertical Conductivity Values at the Trinity River Boundary

In simulation E, K_v' of the Wilcox-Carrizo was increased at a nodal area located near the Trinity River to values approximately equal to the local value of K_h'. The increased K_v' allowed relatively unhindered hydraulic communication between land surface and bottom of the model in a potential discharge area. This would be realistic at this site, as discussed previously (refer to p. 33). Resulting computed heads and velocity vectors are shown in figures 35 and 36. Not surprisingly, the area of increased vertical conductivity becomes a major ground-water discharge area and attracts flow from all directions.

Vertical hydraulic gradients ($\partial h/\partial z$) from simulation E (fig. 37) approach a value of zero at the site of increased vertical conductivity, owing to the lower hydraulic gradient required to move fluids vertically through high-conductivity materials. Thus, where field data show a value of $\partial h/\partial z$ that is locally near zero and is surrounded by values that are greater in absolute value, that locality is probably an area of relatively intense vertical fluid movement.

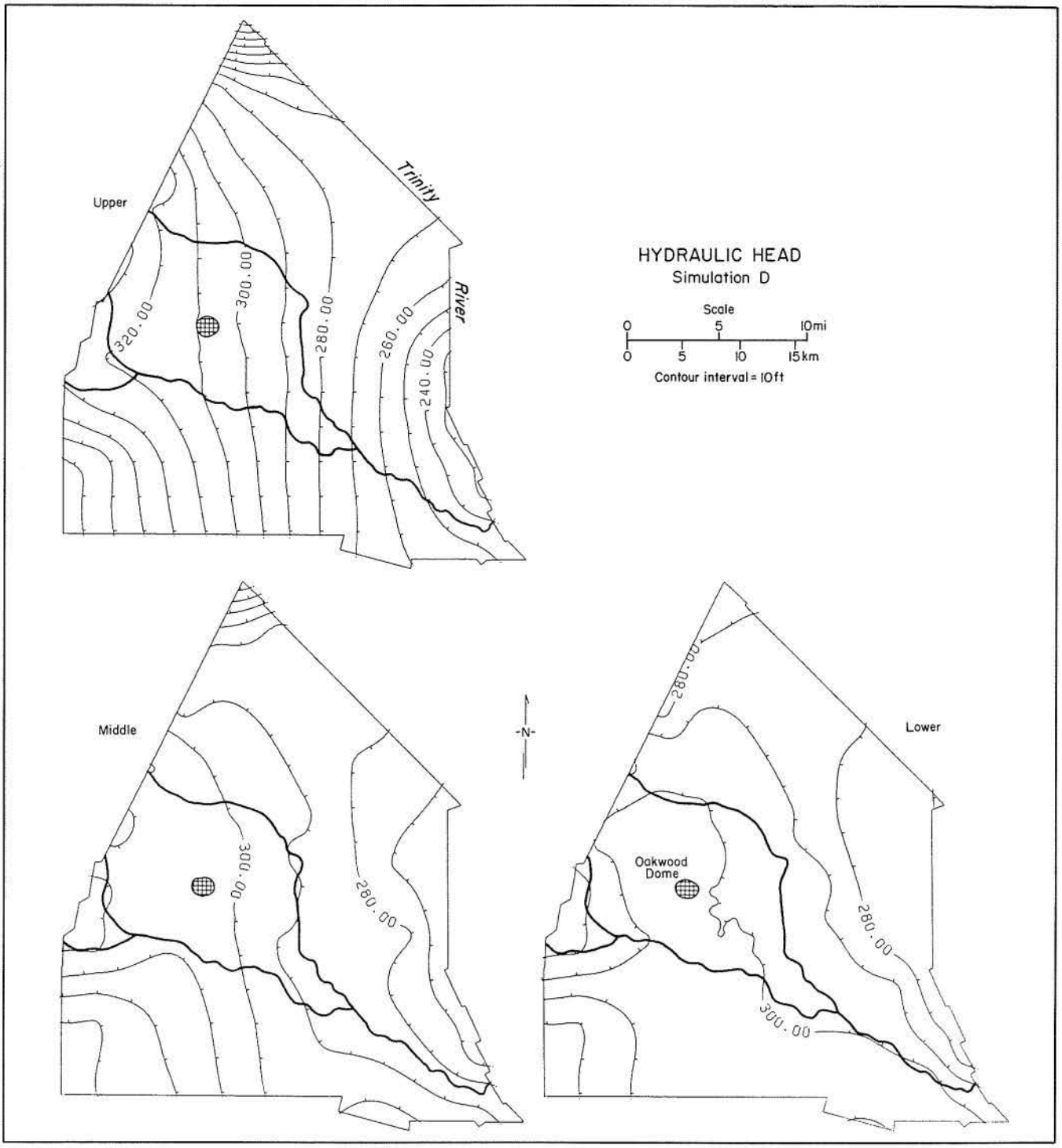

Figure 34. Contour maps of hydraulic head computed in simulation D showing effects of reducing hydraulic conductivity of the Reklaw aquitard from 2.6×10^{-4} to 2.6×10^{-6} ft/d (7.9×10^{-5} to 7.9×10^{-7} m/d). Compare with figure 30 and note that topographic effects along the Trinity River and near Oakwood Dome have essentially disappeared.

Whether a locally high value of K_v' causes intense vertical movement depends on location in the regional flow field. In certain areas of the flow field, no driving force will be present to move fluids vertically. For example, we made a simulation where vertical conductivity of the system was increased at a node located approximately at the intersection between Upper Keechi Creek and the contour of $\partial h/\partial z = 0.00$ (fig. 37). The results of the simulation are not shown because very little

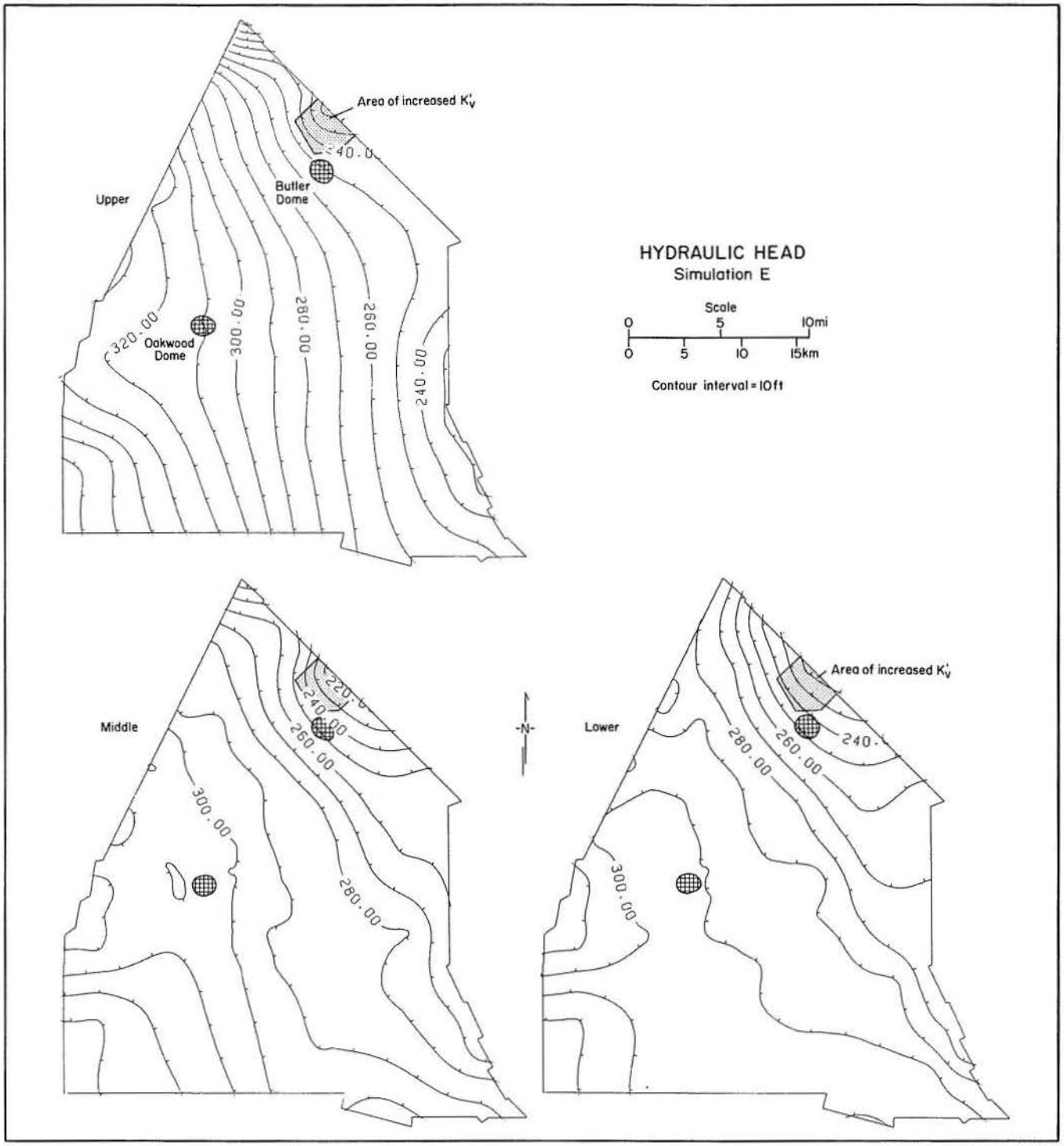

Figure 35. Contour maps of hydraulic head computed in simulation E showing effects of increasing the value of K_v' at a node location near the Trinity River boundary.

happened. Vertical upward flow increased slightly, but heads and lateral velocities remained essentially unchanged. Because $\partial h/\partial z$ is zero at this site, vertical flow will be small, regardless of vertical conductivity. Location of the line of $\partial h/\partial z = 0.00$ is a manifestation of the regional ground-water circulation system, and it therefore may be a fairly predictable, mappable quantity.

The apparently low probability of significant ground-water discharge at that point along Upper Keechi Creek is important because the point

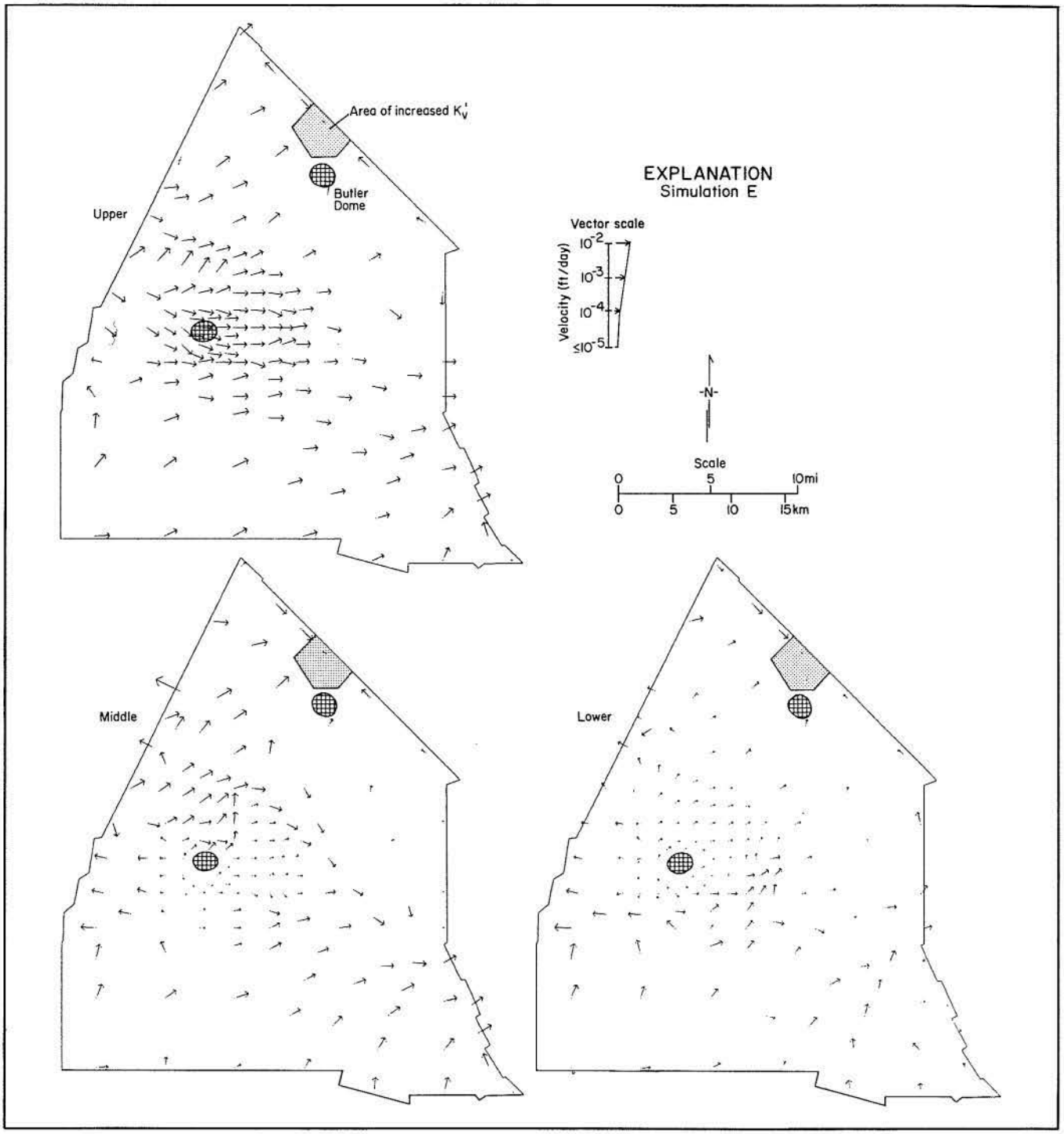

Figure 36. Maps of velocity vectors computed in simulation E showing effects of increasing the value of K_v' at a node location near the Trinity River boundary.

corresponds to the terminus of the brackish-water plume lying northeast of Oakwood Dome. We had previously theorized that the orientation of the plume might be caused by flow toward a discharge area located along the creek. The model proves this theory unlikely.

Comparison of Measured and Computed Heads

Existing measurements of hydraulic head in the Wilcox-Carrizo are insufficient to adequately calibrate and verify the model. The model could be

calibrated to mimic the interpreted potentiometric surface maps, but these maps are too unreliable to serve as a base for worthwhile calibration. Heads computed by the model for run E (fig. 35) are nonetheless plotted with measurement-based potentiometric surfaces for the Wilcox and Carrizo (figs. 5 and 6) in figures 38 and 39. Run E was chosen because it yields the best match with measured heads, owing to partial reproduction of the potentiometric depression that occurs east of Butler Dome. The measured head values primarily represent conditions in the upper half of the system; hence, computed heads from only the upper and middle layers are shown. Hydraulic heads from the upper layer are closest to measured values, whereas those from the middle layer deviate significantly from measured values. This is to be expected because the head control is best in the upper layer.

During construction of the potentiometric surface maps, certain data points were ignored or given less weight because they differed significantly from the regional trend. In some cases the anomalous data are from wells tapping deeper potentials. This is why combined use of the potentiometric surface maps and pressure-depth trends is necessary to approximate the three-dimensional head distribution. For example, we could synthesize a potentiometric surface map of the middle layer based on the pressure-depth data and the potentiometric surface maps that primarily represent the upper layer (figs. 5 and 6). This is how we approximated changes in head with depth where prescribed head boundary conditions were assigned on the sides of the model. The synthesized maps would agree more closely with head values computed by the model. Nevertheless, a major unknown in the model is distribution of head in the lower half of the system.

The best vertical control on head is at site TOH-2, just south of Oakwood Dome (fig. 4). Six pressure measurements at the site yield a pressure-depth slope of 1.02 (fig. 9; table 1), or a vertical hydraulic gradient ($\partial h/\partial z$) of 0.02, which is in close agreement with the corresponding $\partial h/\partial z \cong 0.00$ computed by the model at this site (fig. 37). A more convincing check of $\partial h/\partial z$ values computed by the model could be made if site-specific pressure-depth data were available farther updip and downdip, where $\partial h/\partial z$ should deviate significantly from zero.

Areas of Maximum Potential for Discharge

Areas where there is maximum potential for ground-water discharge are characterized by

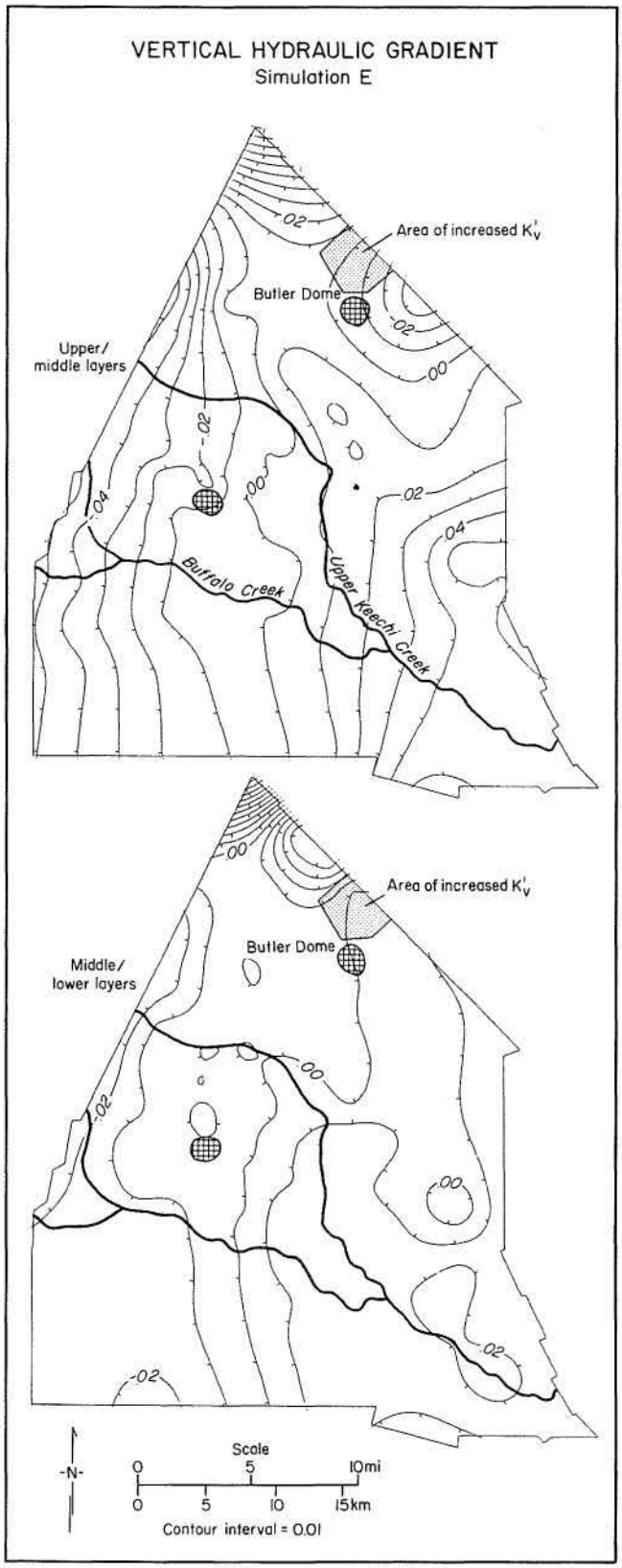

Figure 37. Contour maps of vertical hydraulic gradients ($\partial h/\partial z$) computed in simulation E depicting effects of increasing the value of K_v' at a node location near the Trinity River boundary. The value of $\partial h/\partial z$ approaches 0.0 at the locality.

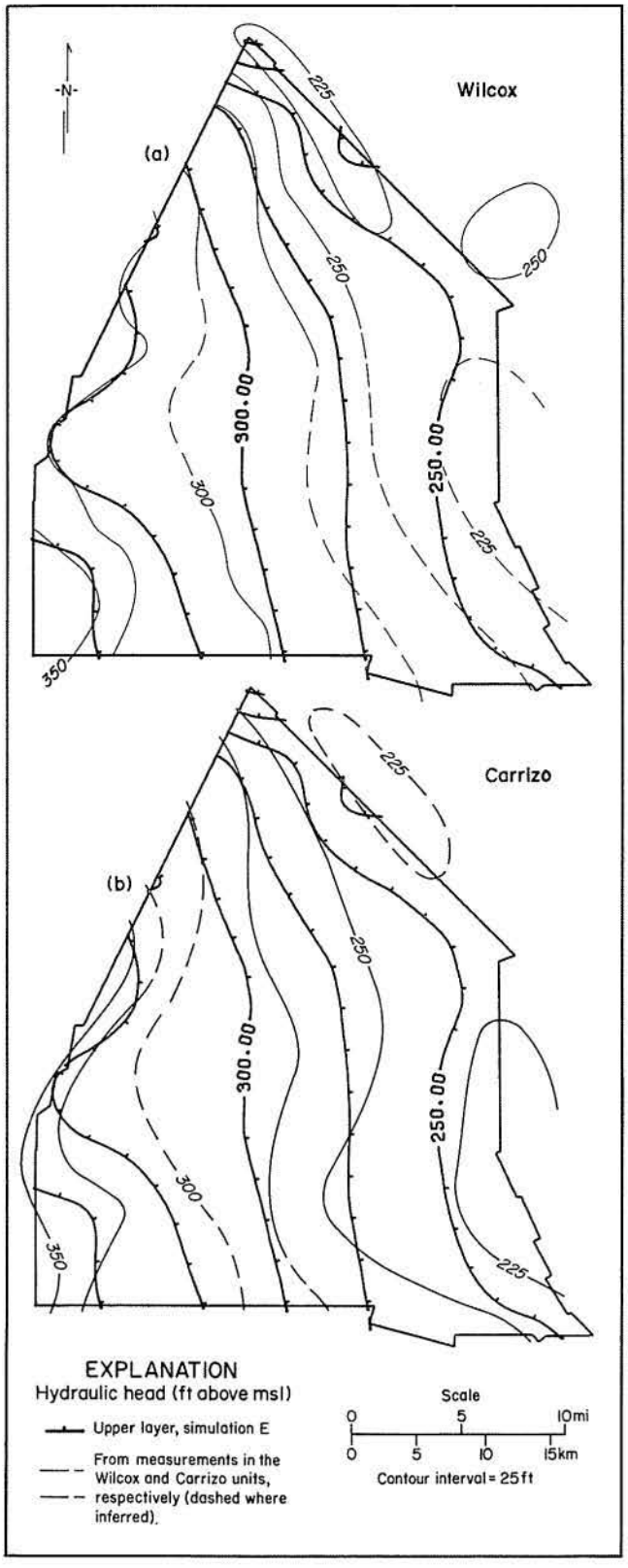

Figure 38. Comparisons of measurement-based and model-generated (simulation E) potentiometric surfaces for (a) upper layer and Wilcox and (b) upper layer and Carrizo. Agreement is best for the upper layer, because the measurement-based maps are primarily from head measurements in the upper half of the system.

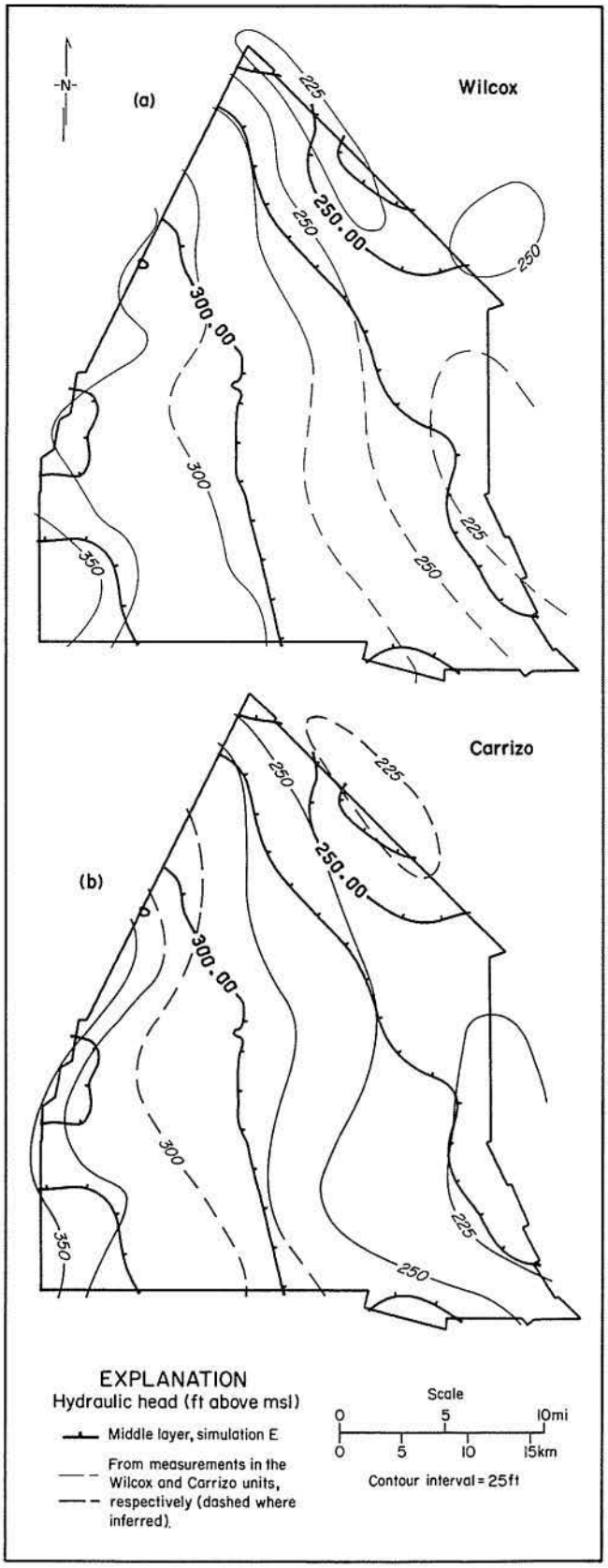

Figure 39. Comparisons of measurement-based and model-generated (simulation E) potentiometric surfaces for (a) middle layer and Wilcox and (b) middle layer and Carrizo.

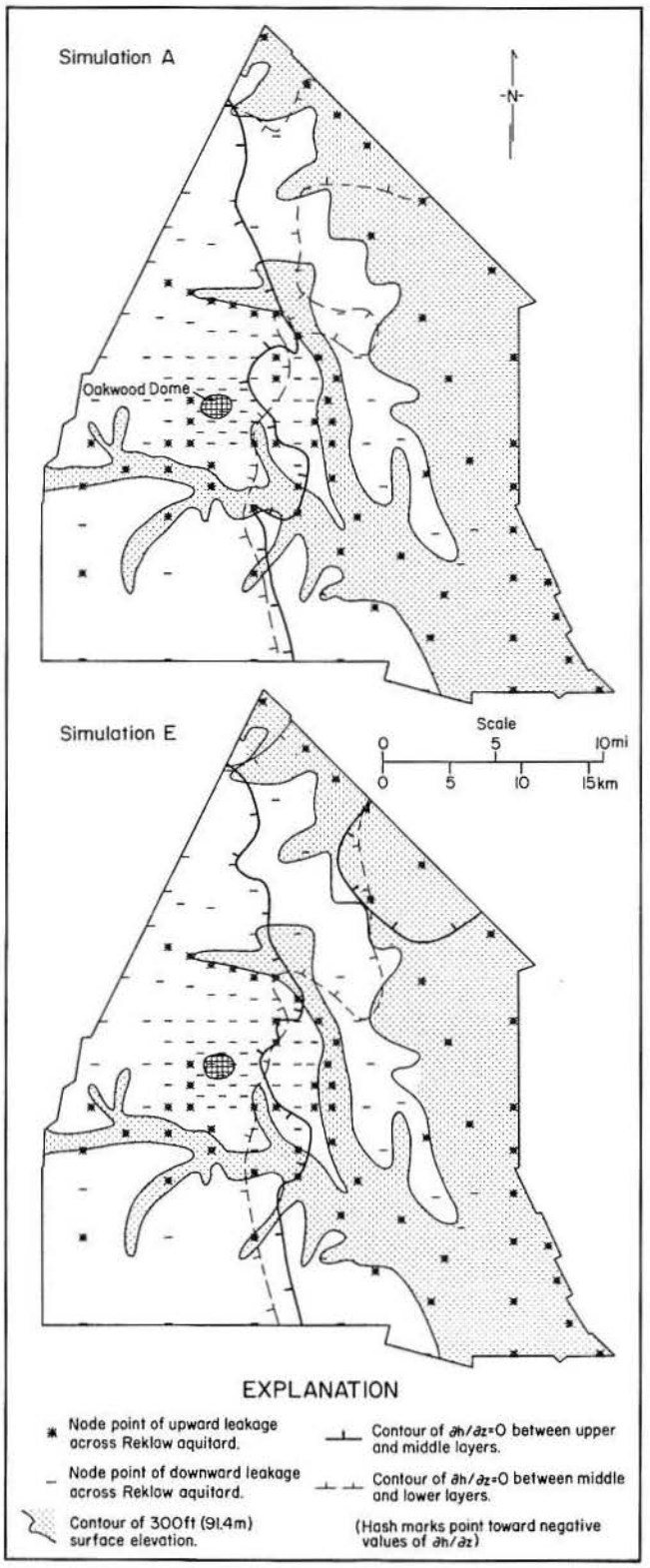

Figure 40. Maps depicting areas of maximum potential for discharge based on simulations A and E (areas where there is potential for both upward leakage across the Reklaw aquitard and upward flow within the Wilcox-Carrizo system). In general, asterisks located east of the ∂h/∂z = 0 contours mark zones of maximum potential for discharge. The 300-ft (91.4-m) surface contour coincides roughly with the ∂h/∂z = 0 contours.

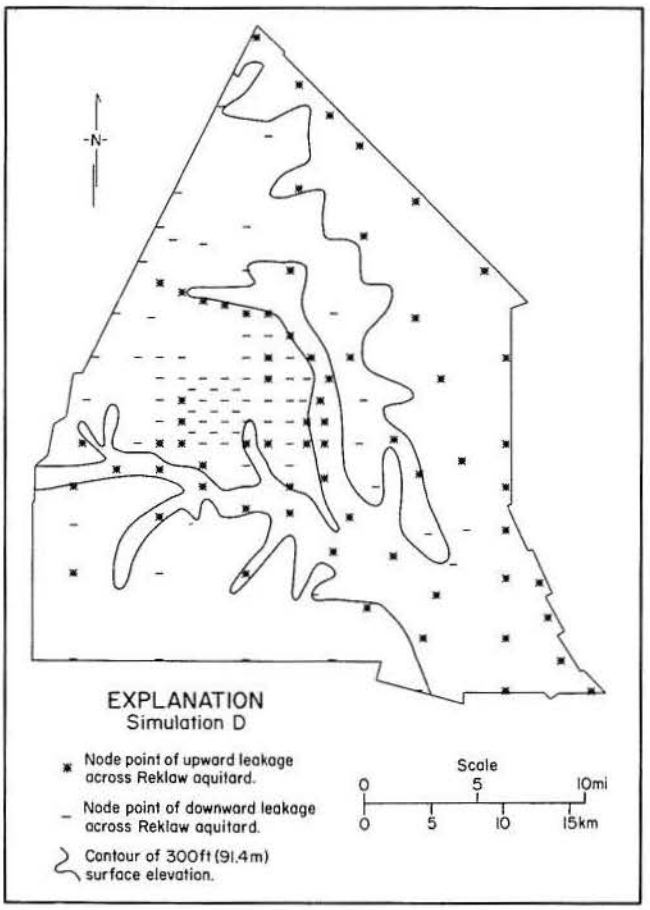

Figure 41. Map showing directions of leakage across the Reklaw aquitard based on simulation D. Values of ∂h/∂z = 0.00 were not contoured for simulation D, but they differ negligibly from those of simulation A.

potential both for upward leakage across the Reklaw aquitard and for upward flow within the Wilcox-Carrizo ($\partial h/\partial z > 0.00$). To locate such areas, directions of vertical flow in the model are shown in figure 40 for simulations A and E. These vertical-flow maps indicate upward and downward leakage across the Reklaw with an asterisk or minus sign, respectively, at each node location. They indicate direction of vertical flow in the Wilcox-Carrizo using the contours of $\partial h/\partial z = 0.00$. East of the contours there is potential for upward flow and west of them is potential for downward flow. Areas of maximum potential for discharge therefore occur where there are asterisks east of the $\partial h/\partial z = 0.00$ contours. Directions of leakage across the Reklaw are also shown for simulation D in figure 41. Although values of $\partial h/\partial z$ were not mapped for simulation D, they differ negligibly from those in simulation A.

Note that simulations A, D, and E (figs. 40 and 41) produce essentially the same distribution of vertical leakage across the Reklaw. In fact, all the

simulations produced the same basic distribution, wherein there is upward leakage along the Trinity River, Upper Keechi Creek, Buffalo Creek, and in a local area just west of Oakwood Dome. Such consistent results stem from the fact that direction of leakage is controlled by heads in the Queen City aquifer and the upper layer of the Wilcox-Carrizo system (refer to figure 26). The former are held constant in the upper boundary condition, and the latter do not change significantly from simulation to simulation, because the homogeneous Carrizo moderates changes in hydraulic gradient in the upper layer of the model.

Directions of leakage in the model are not changed significantly by variation of model input data. Moreover, it is doubtful that any other reasonable model alterations would seriously affect the leakage directions. Treating the Carrizo as a separate layer might have some effect, but it would not change significantly the vertical hydraulic gradients across the Reklaw. Hence, direction of leakage appears rather predictable, and the directions computed by the model are probably valid.

Additionally, positions of the $\partial h/\partial z = 0.00$ contours appear to be reasonable and fairly predictable. The contours do not vary markedly between simulations A, D, and E, and they generally lie in the vicinity of the 300-ft (91-m) land-surface contour (fig. 40). The regional pressure-depth data suggest that the 300-ft (91-m) surface elevation roughly marks a transition from downward to upward flow (Fogg and Kreitler, 1982; fig. 21).

The Trinity River and its tributaries had earlier been identified as areas of potential upward leakage (Fogg and Kreitler, 1981 and 1982), but the local area of upward leakage just west of Oakwood Dome had never been suspected. This area corresponds to a local topographic low (fig. 27), but many other local topographic lows in the system do not produce the same result, suggesting interplay between topography and some other factor, such as the dome itself. Because the dome is a barrier to flow, it may cause a slight increase in head on its northwest side, thereby increasing the potential for upward leakage in the low area.

Ground-Water Budgets Computed by the Model

Ground-water flow rates computed by the model for each simulation are shown in table 4. The major components of the water budget are: (1) inflow along the W-NW boundary, (2) outflow at the SE boundary, and (3) leakage across the Reklaw aquitard. Most of these components are on the order of 10^5 ft^3/d (10^3 m^3/d). Accuracy of the computed flow rates depends almost entirely on accuracy of hydraulic conductivity values and boundary conditions assigned to the model. If all the hydraulic conductivity values or hydraulic gradients imposed on the model were multiplied by a constant, the flow rates would change by the same factor. We believe rates computed in runs A, D, and E are the most reliable.

Table 4 also shows total mass balance (inflow-outflow) for each run. The balance is typically on the order of 10^4 ft/d, which represents a percent error of less than 0.1 percent. Local mass balances (at individual nodes) are equally low.

Recharge over Oakwood Dome is a minor part of the budget and amounts to a meager 0.04 inch/yr (0.10 cm/yr) in run E. Accordingly, recharge over the dome causes no noticeable effects in computed heads and velocities (figs. 30 through 36). Only when K_v'/K_h' is increased to 10^{-2} in run B1 does computed recharge over the dome become significant (table 4).

Since ground water entering the W-NW boundary originates from the outcrop of the Wilcox-Carrizo, we can calculate a recharge rate for the outcrop. On the basis of the regional head map by Fogg and Kreitler (1982), the recharge area that contributes to the model is about 240 mi^2 (380 km^2). Using the W-NW flow rate of 6.02×10^5 ft^3/d (1.70×10^4 m^3/d) from run E, a recharge rate of 0.39 inch/yr (1.0 cm/yr) results. Measurements of recharge rates through the unsaturated zone of the outcrop in Freestone County yield a greater rate of up to 4.0 inches/yr (10.2 cm/yr) (Dutton, 1982). Greater recharge in the shallow outcrop is expected because much of the water that infiltrates the outcrop is discharged relatively quickly to evapotranspiration or local stream valleys, resulting in a much lower rate of recharge to deeper strata.

Ground-Water Travel Times

Ground-water flow paths and travel times from Oakwood Dome to boundaries of the model were determined from the velocity vector data for the middle and lower layers of simulations A and E (figs. 42 and 43). The upper layer was omitted because its travel times would represent a gross average between the Carrizo and Wilcox aquifers. Where flow paths are through the high-sand-percent zones, in which all sands are assumed to be interconnected, travel times are approximately 10^3 to 10^4 yr, but travel times through areas of disconnected sands are 10^5 to 10^6 yr.

Table 4. Ground-water budgets computed by the model. Refer to figure 24 for locations of boundaries.

Simulation	Computed Flow Rates[a], ft^3/d (m^3/d)							
	West-northwest[b, c] boundary (W-NW)		Southeast boundary (SE)	Vertical leakage across Reklaw aquitard	Oakwood Dome[c]		Mass balance	Remarks
A	3.91×10^5 **0.26 in/yr**	(1.11×10^4) **0.6 cm/yr**	-2.56×10^5 (-7.25×10^3)	-1.14×10^5 (-3.23×10^3)	1.19×10^2 **0.03 in/yr**	(3.37×10^0) **0.07 cm/yr**	2.18×10^4 (6.17×10^2)	Vertical leakage is very small locally but because of the large surface area it accounts for 30% of the outflow.
B1	8.89×10^5 **0.58 in/yr**	(2.52×10^4) **1.5 cm/yr**	-4.60×10^4 (-1.30×10^3)	-8.43×10^5 (-2.39×10^4)	1.20×10^4 **2.84 in/yr**	(3.40×10^2) **7.22 cm/yr**	1.22×10^4 (3.45×10^2)	High rates of vertical leakage and recharge at Oakwood Dome are caused by excessively high K_v' values.
B2	2.88×10^5 **0.19 in/yr**	(8.15×10^3) **0.5 cm/yr**	-3.66×10^5 (-1.04×10^4)	$+9.40 \times 10^4$ ($+2.66 \times 10^3$)	6.38×10^{-1} **0.0002 in/yr**	(1.81×10^{-2}) **0.0004 cm/yr**	1.54×10^4 (4.36×10^2)	Low rates of vertical leakage and recharge at Oakwood Dome are caused by excessively low K_v' values.
C1	6.23×10^5 **0.41 in/yr**	(1.76×10^4) **1.0 cm/yr**	-4.67×10^5 (-1.32×10^4)	-1.58×10^5 (-4.47×10^3)	6.57×10^2 **0.16 in/yr**	(1.86×10^1) **0.40 cm/yr**	-7.62×10^2 (-2.16×10^1)	Improved mass balances are due to relatively uniform hydraulic conductivity distributions.
C2	4.88×10^5 **0.32 in/yr**	(1.38×10^4) **0.8 cm/yr**	-3.33×10^5 (-9.43×10^3)	-1.56×10^5 (-4.42×10^3)	1.44×10^2 **0.03 in/yr**	(4.08×10^0) **0.09 cm/yr**	2.32×10^2 (6.57×10^0)	
D	4.38×10^5 **0.29 in/yr**	(1.24×10^4) **0.7 cm/yr**	-3.47×10^5 (-9.83×10^3)	-8.00×10^4 (-2.27×10^3)	2.69×10^2 **0.06 in/yr**	(7.62×10^0) **0.16 cm/yr**	1.10×10^4 (3.11×10^2)	Low leakage rate is due to low hydraulic conductivity assigned to Reklaw aquitard.
E	6.02×10^5 **0.39 in/yr**	(1.70×10^4) **1.0 cm/yr**	-2.42×10^5 (-6.85×10^3)	-3.34×10^5 (-9.46×10^3)	1.74×10^2 **0.04 in/yr**	(4.93×10^0) **0.10 cm/yr**	2.67×10^4 (7.56×10^2)	Vertical leakage includes that for the locality of increased K_v', where the rate is -3.64×10^5 ft^3/day (4.2 CFS).

[a] Positive and negative flow rates indicate flow in and out of the system, respectively. [b] The W-NW values include fluxes passing through the top of the model where the Reklaw aquitard is not assigned (immediately adjacent to the W-NW boundary). [c] Values given in inch/yr and cm/yr are representative recharge rates calculated using the approximate size of the recharge area from which the water originates.

Pore fluid velocities, from which the travel times were computed, were calculated by dividing magnitudes of velocity (specific discharge) shown in the vector plots (figs. 32 and 36) by both porosity and the fraction of sand present (sand percent × 0.01). A porosity of 0.30 was used. Division by the sand fraction yields a flux representative of individual sand bodies, rather than of the composite of sand and mud facies included in the equivalent hydraulic conductivity (K′) term. Where the channel-fill sand bodies were assumed to be interconnected, sand fractions were taken directly from figure 28. Where they were assumed to be disconnected, a sand fraction of 0.50 was used to represent the lower permeability interchannel sands, which generally make up about 50 percent of the section and through which most of the ground water would then be flowing.

Carbon-14 age dates of waters sampled from the channel-fill Wilcox sands are 2,000 to 12,000 yr (Kreitler and Wuerch, 1981b), which supports the 10^3 to 10^4 yr range given by the model. Only one carbon-14 age date is from a low-sand-percent section thought to contain disconnected sands (well TOH-2A; fig. 4), but this well yielded an anomalously young age of 8,000 yr. This age is not reliable, however, because of suspected addition of carbon-14 from an organic-polymer drilling mud used to drill the well.

Thus, probable ages of waters in areas of interchannel sands remain questionable. Ages given by the model for these areas (10^5 to 10^6 yr) at

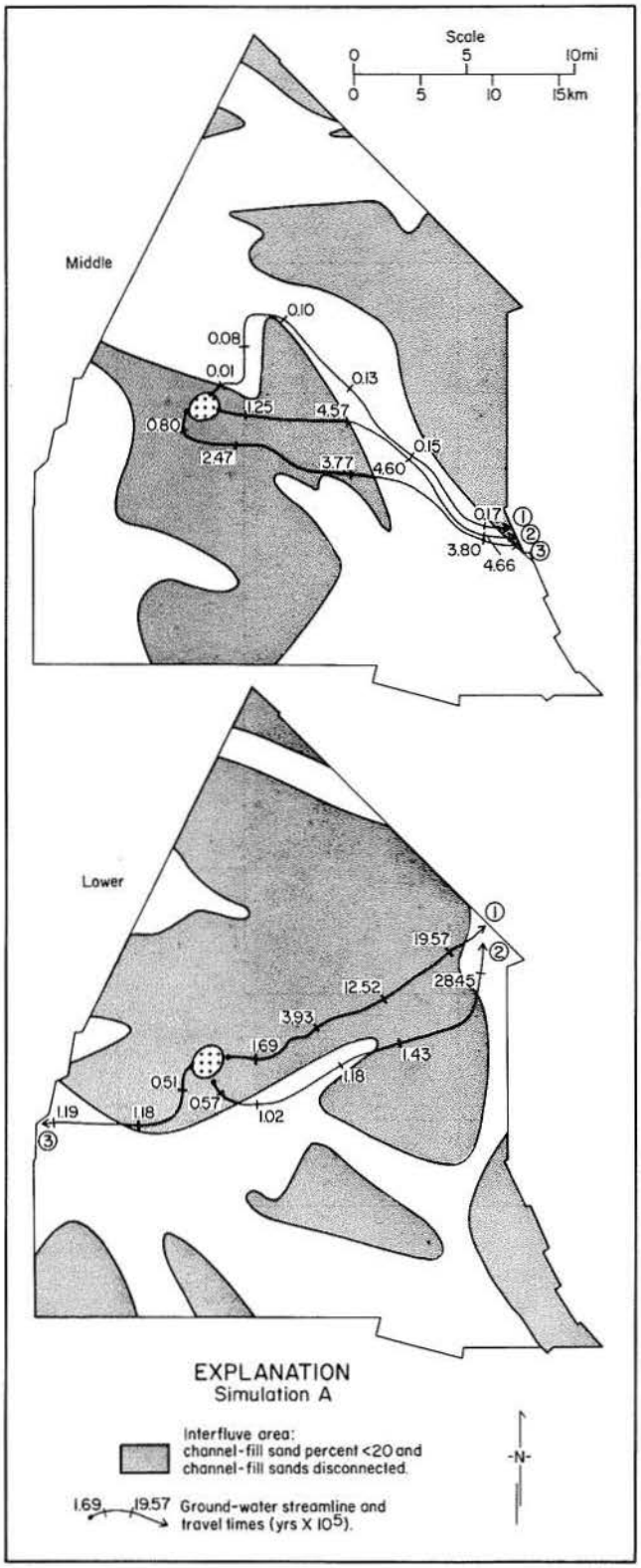

Figure 42. Maps showing ground-water travel times for the middle and lower layers based on simulation A. Flow path 3 (circled number) in the lower layer may be invalid because of possible inaccuracies in boundary conditions assigned to the western boundary. Travel times are lowest in shaded areas, owing to assumptions regarding channel-fill sand-body interconnectedness.

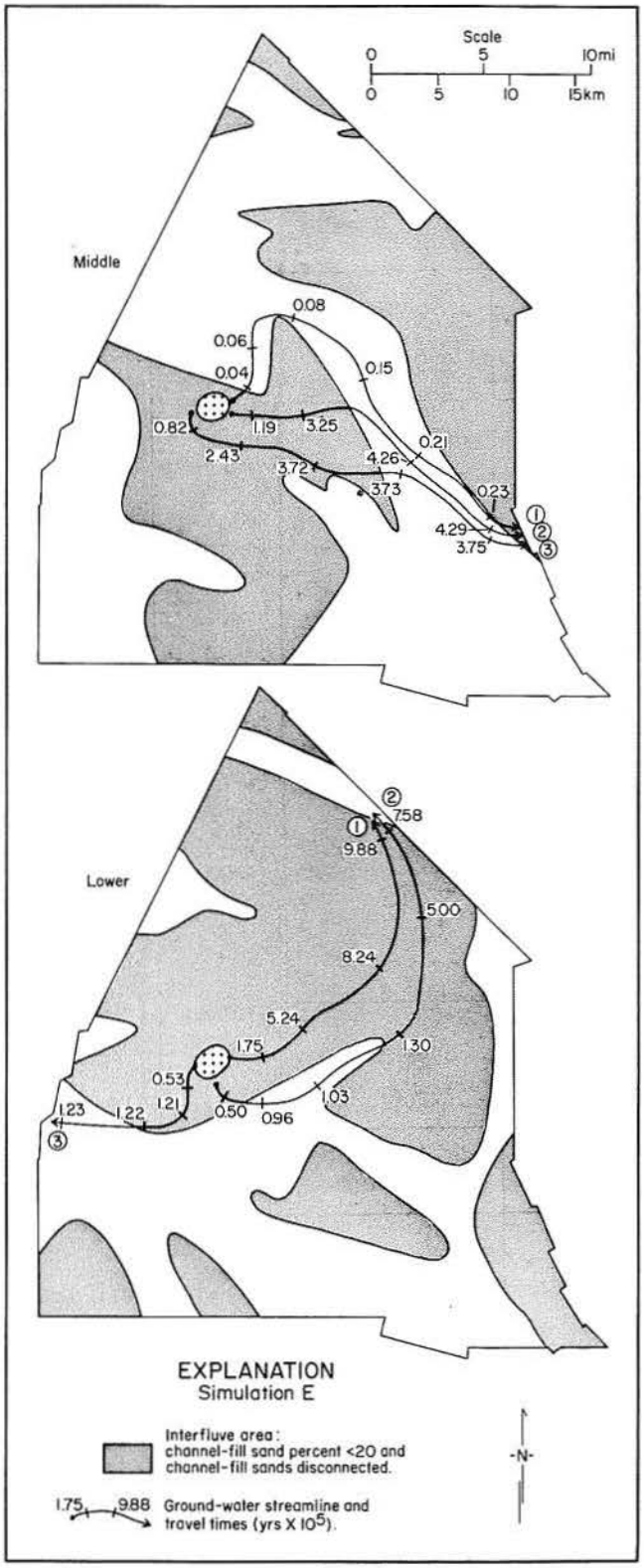

Figure 43. Maps showing ground-water travel times for the middle and lower layers based on simulation E. Flow path 3 in the lower layer may be invalid because of possible inaccuracies in boundary conditions assigned to the western boundary. Flow paths 1 and 2 (circled numbers) in the lower layer terminate at the discharge area that was created by increasing K_v' east of Butler Dome.

first appear too large, but there is no apparent reason why such old waters could not occur in the system. Additional carbon-14 age dating of waters in interchannel sands is needed. The results, however, might prove ambiguous because of potential mixing of waters of much different ages between channel-fill and interchannel facies.

Note that in figure 42 the slowest flow rates occur in the lower layer near the end of the streamlines along the Trinity River. This area corresponds to the topographically controlled depression in the head surface shown in figure 30. Here flow is essentially vertical, and because the cross-sectional area available for vertical flow is very large, the flow rates are very low. In reality, travel times may be much shorter in this area if vertical flow is occurring along local avenues, such as fault zones or vertically connected sand bodies. Recall that vertical hydraulic conductivity is uniformly low throughout the model, except in simulation E just east of Butler Dome.

SUMMARY AND CONCLUSIONS

A three-dimensional steady-state ground-water flow model constructed for the Oakwood Dome vicinity includes salient aspects of the ground-water system: (1) regional ground-water circulation patterns, (2) vertical leakage across the Reklaw aquitard, (3) recharge over Oakwood Dome, and (4) large-scale heterogeneity and anisotropy of the Wilcox-Carrizo aquifer system. Heterogeneity is included as a volume-averaged distribution of horizontal hydraulic conductivity (K_h') based on lab and field measurements of K, borehole resistivity-log data, and assumptions regarding sand-body interconnection. Anisotropy was introduced by lowering the ratio of vertical to horizontal K' (K_v'/K_h') until the model simulated pressure-depth trends that agree reasonably with observed trends. Sensitivity of the model to vertical and horizontal sand-body interconnection was tested by assigning various distributions of K_h' and K_v'/K_h' in different simulations. Sensitivity of the model to K of the Reklaw aquitard was also tested.

The following conclusions can be drawn from the study:

(1) The Wilcox is a multiple aquifer system containing channel-fill sand bodies distributed complexly in a matrix of interchannel sands, silts, and clays of relatively lower permeability.

(2) Key uncertainties in the model are interconnectedness of channel-fill sands and hydraulic conductivity (K) of interchannel sands. If all channel-fill sands are interconnected, there will be little correlation between average ground-water flux and sand distribution. It appears, however, that channel-fill sands are laterally disconnected in low-sand-percent areas and laterally interconnected in high-sand-percent areas, resulting in considerable variations in values of K_h' and ground-water flux. Magnitudes of these variations depend largely on the values of K assumed for the interchannel sands.

(3) The results strongly indicate that sand-body interconnection along the vertical is poor, resulting in an anisotropy ratio (K_v'/K_h') of at most 10^{-4} (and possibly 10^{-3}), reflecting the interbedded sand/mud lithology of the Wilcox. Without such a small ratio, the model will not simulate the observed pressure-depth trends. We can further conclude that *any* aquifer in which heads differ vertically (that is, pressure-depth slope $\neq 1.00$) has a much lower value of K_v' than K_h'. The average ratio of K_v' to K_h' can be determined if K_h' and regional pressure-depth trends are known.

(4) The low value of K_v'/K_h' minimizes vertical flow in the Wilcox-Carrizo system, but vertical flow may be large in local areas where relatively permeable vertical avenues exist (for example, fault planes or vertically interconnected sand bodies). The net effect of a vertical avenue depends on where it is located in the regional flow field. If an avenue is in the regional transition zone between an area of potential downward flow and an area of potential upward flow, little vertical flow will occur, because of the weak or absent driving force. Conversely, if an avenue is located in an area where potential for vertical flow exists, such as along the Trinity River, considerable vertical flow will occur.

(5) The existence and abundance of vertical avenues of flow are extremely difficult to determine, but areas of maximum potential for vertical flow can be mapped through analysis of modeling results and of data on vertical head differentials and pressure-versus-depth trends. Once these areas are delineated, consequences of having such an avenue in a particular location can be evaluated. Maximum potential for vertical upward flow occurs where vertical hydraulic gradients are upward both within the Wilcox-Carrizo and across the Reklaw aquitard. The model indicates that general directions of these gradients are fairly predictable. Oakwood Dome

apparently lies in the transition zone where potential for vertical flow in the Wilcox-Carrizo is relatively small.

(6) One indicator of a local vertical avenue of flow is a pressure-depth slope of 1.00 surrounded by slopes that differ from 1.00. Where ground water can move vertically unimpeded, the vertical hydraulic gradients will approach 0.00 and the pressure-depth slope will likewise approach 1.00.

(7) Correlation between topography and head in a ground-water system does not necessarily indicate good hydraulic communication between the aquifer and shallower intervals. Topographic effects on hydraulic head will be accentuated in strata having a low value of K_h' and may not be evident in overlying strata that have a higher K_h'.

(8) The northeast orientation of the brackish-water plume associated with Oakwood Dome can be attributed to a corresponding northeast ground-water flow direction resulting from variable sand-body distribution and interconnection. The brackish water may originate from salt dissolution occurring where sandy Wilcox facies are near or touching the dome.

(9) The relatively muddy Wilcox strata surrounding Oakwood Dome provide another barrier, in addition to salt dome cap rock, that significantly impedes ground-water flow. Wilcox strata may isolate the dome from the high-permeability, channel-fill sand bodies, except perhaps in the vicinity of the brackish-water plume.

(10) Plotting of model results in the form of hydraulic head contours and velocity vectors demonstrates that local fluxes can differ significantly from regional hydraulic gradients.

(11) Ground-water flow rates may decrease by as much as 10^2 from top to bottom of the Wilcox-Carrizo aquifer system. A more precise estimate of the velocity-depth relationship could be determined with the model if additional pressure-depth data were available for the lower half of the system.

(12) Ground-water ages computed by the model in channel-fill sand belts are approximately 10^4 yr, which is reasonable according to the carbon-14 ages obtained by Kreitler and Wuerch (1981b). However, ages in muddy sands of interchannel areas could approach 10^6 yr. Reliable carbon-14 ages have not been obtained for these sands, but obviously need to be.

(13) Recharge over Oakwood Dome probably is very small and affects only shallow-ground-water conditions directly over the dome.

(14) Of the recharge occurring in the outcrop west of the model area, only a small fraction reaches the artesian section represented by the model. Remaining recharge is discharged in the outcrop area. Ground-water flow rates in the artesian section are consequently sluggish compared to those in the outcrop section.

(15) Flow directions in the transition zone from the outcrop to the artesian section may not always be downdip. Updip flow in the zone may occur in lower segments of the Wilcox in the vicinity of streams that traverse the transition zone.

Applicability to Salt Dome Studies in Louisiana and Mississippi

The applicability of results of the study is not limited to the Oakwood Dome vicinity or the East Texas Basin. The same general methodology of collectively analyzing all available data in a numerical flow model could be applied to nuclear waste isolation studies being carried out in Louisiana and Mississippi. Moreover, those studies could benefit directly from results of the Oakwood model. One general benefit is that more realistic conceptual models can be created of ground-water flow systems around the Louisiana and Mississippi salt domes by analogy to the Oakwood model. The analogy is justified because the basic hydrogeologic components, climate, topography, and aquifer lithology of the three basins are similar.

A more specific benefit is the demonstration of the importance of sand-body interconnectedness, a critical factor affecting ground-water circulation in the Oakwood model. Drilling and testing programs around the domes should focus on this problem. Horizontal interconnectedness can be tested by long-term (several days or weeks) pumping tests in which lateral boundaries of sand bodies might be detected. Similarly, vertical interconnectedness can be tested using leaky aquifer tests, wherein observation wells are constructed in sands that are separated vertically from the pumped interval by the lower permeability interbeds. A cheaper and more versatile method of testing for vertical interconnectedness is to measure pressure-depth profiles in several borings and then to calculate maximum values of the ratio of vertical to horizontal hydraulic conductivity (K_v'/K_h') using model calibration procedures such as those used here. The pressure-depth information can also be used to detect local avenues of relatively rapid vertical flow, which are critical to predicting the rate at which contaminants might escape from a dome. Data on the three-dimensional distribution of hydraulic head (or pressure) is the most important hydraulic information that could be collected.

Finally, the maps of maximum potential for ground-water discharge (fig. 40) are examples of how general ground-water conditions in different salt dome vicinities could be presented and compared meaningfully. A persistent problem with the dome selection process has been the lack of reliable hydrogeologic information that would allow a ranking of domes in order of hydrologic suitability. This problem stems in part from the uncertainty inherent in hydrogeologic data, but it also may stem from our methods of analysis and presentation of the data. Detailed ground-water flow models similar to this one will be constructed for other candidate domes, yet the results will be difficult to compare quantitatively because of differing data bases and ambiguous results. If, for example, the models are used to generate maps of maximum potential for discharge, comparison of results might be easier. Domes located farthest from potential discharge areas are most suitable because of minimum potential for transport of contaminants to the biosphere in the event of a release. Results of this study strongly suggest that conjunctive application of numerical modeling and field testing will lead to fairly reliable maps of potential discharge areas. Even though it may not be possible to accurately determine the actual flow paths, we can clearly compare various dome areas on the basis of potential discharge areas.

ACKNOWLEDGMENTS

Funding for this study was provided by the U.S. Department of Energy, Office of Nuclear Waste Isolation, under contract no. DE-AC97-80ET46617 and by the Texas Energy and Natural Resources Advisory Council, under contract no. IAC(82-83)-0822. L. F. Brown, Jr., R. J. Charbeneau, A. R. Dutton, C. M. Jones, and S. D. Hovorka critically reviewed the manuscript and provided many helpful suggestions. The manuscript was typeset by Fannie M. Sellingsloh, under the supervision of Lucille C. Harrell, and edited by Amanda R. Masterson. Figures were drafted by John T. Ames, under the supervision of Dan F. Scranton, and photographic printing was by James A. Morgan. Micheline R. Davis designed the publication.

REFERENCES

Barnes, V. E., 1967, Palestine sheet: The University of Texas at Austin, Bureau of Economic Geology, Geologic Atlas of Texas, scale 1:250,000.

——1970, Waco sheet: The University of Texas at Austin, Bureau of Economic Geology, Geologic Atlas of Texas, scale 1:250,000.

Bear, J., 1972, Dynamics of fluids in porous media: New York, Elsevier, 764 p.

Collins, E. W., Dix, O. R., and Hobday, D. K., 1981, Oakwood salt dome, East Texas: surface geology and drainage analysis: The University of Texas at Austin, Bureau of Economic Geology Geological Circular 81-6, 23 p.

Cooper, H. H., Jr., and Jacob, C. E., 1946, A generalized graphical method for evaluating formation constants and summarizing well-field history: American Geophysical Union Transactions, v. 27, p. 526-534.

Dutton, A. R., 1982, Hydrogeochemistry of the unsaturated zone at Big Brown lignite mine, East Texas: The University of Texas at Austin, Ph.D. dissertation, 239 p.

Fisher, W. L., and McGowen, J. H., 1967, Depositional systems in the Wilcox Group of Texas and their relationship to the occurrence of oil and gas: Gulf Coast Association of Geological Societies Transactions, v. 17, p. 105-125.

Fogg, G. E., 1981, Aquifer testing and monitoring around Oakwood salt dome, East Texas, *in* Kreitler, C. W., and others, Geology and geohydrology of the East Texas Basin: a report on the progress of nuclear waste isolation feasibility studies (1980): The University of Texas at Austin, Bureau of Economic Geology Geological Circular 81-7, p. 126-135.

Fogg, G. E., and Kreitler, C. W., 1981, Groundwater hydrology around salt domes in the East Texas Basin: a practical approach to the contaminant transport problem: Bulletin of the Association of Engineering Geologists, v. 18, no. 4, 25 p.

Fogg, G. E., and Kreitler, C. W., 1982, Groundwater hydraulics and hydrochemical facies of Eocene aquifers in the East Texas Basin: The

University of Texas at Austin, Bureau of Economic Geology Report of Investigations No. 127, 75 p.

Fogg, G. E., Simpson, E. S., and Neuman, E. S., 1979, Aquifer modeling by numerical methods applied to an Arizona groundwater basin: University of Arizona, Tucson, Technical Reports on Natural Resource Systems, Report No. 32, 140 p.

Freeze, R. A., 1975, A stochastic-conceptual analysis of one-dimensional groundwater flow in nonuniform homogeneous media: Water Resources Research, v. 11, no. 5, p. 725-741.

Freeze, R. A., and Cherry, J. A., 1979, Groundwater: New Jersey, Prentice-Hall, 604 p.

Giles, A. B., and Wood, D. H., in preparation, Oakwood salt dome, East Texas, geologic framework and growth history: The University of Texas at Austin, Bureau of Economic Geology.

Guyton, W. F., and Associates, 1972, Ground-water conditions in Anderson, Cherokee, Freestone, and Henderson Counties, Texas: Texas Water Development Board, 250 p.

Kaiser, W. R., Ayers, W. B., Jr., and LaBrie, L. W., 1980, Lignite resources in Texas: The University of Texas at Austin, Bureau of Economic Geology Report of Investigations No. 104, 52 p.

Kaiser, W. R., Johnston, L. E., and Bach, W. N., 1978, Sand-body geometry and the occurrence of lignite in the Eocene of Texas: The University of Texas at Austin, Bureau of Economic Geology Geological Circular 78-4, 19 p.

Kreitler, C. W., Agagu, O. K., Basciano, J. M., Collins, E. W., Dix, O. R., Dutton, S. P., Fogg, G. E., Giles, A. B., Guevara, E. H., Harris, D. W., Hobday, D. K., McGowen, M. K., Pass, D., and Wood, D. H., 1980, Geology and geohydrology of the East Texas Basin: a report on the progress of nuclear waste isolation feasibility studies (1979): The University of Texas at Austin, Bureau of Economic Geology Geological Circular 80-12, 112 p.

Kreitler, C. W., Davidson, D. E., Dix, O. R., Donaldson, G. A., Dutton, S. P., Collins, E. W., Fogg, G. E., Giles, A. B., Harris, D. W., Jackson, M. P. A., Lopez, C. M., McGowen, M. K., Seni, S. J., and Wood, D. H., 1981, Evaluating the potential of East Texas salt domes for isolation of nuclear wastes: The University of Texas at Austin, Bureau of Economic Geology Geological Circular 81-7, 207 p.

Kreitler, C. W., and Dutton, S. P., 1983, Origin and diagenesis of salt dome cap rock: The University of Texas at Austin, Bureau of Economic Geology Report of Investigations No. 131, 58 p.

Kreitler, C. W., and Wuerch, H. V., 1981a, Water chemistry, Oakwood salt dome, *in* Kreitler, C. W., and others, Geology and geohydrology of the East Texas Basin: a report on the progress of nuclear waste isolation feasibility studies (1980): The University of Texas at Austin, Bureau of Economic Geology Geological Circular 81-7, p. 150-155.

Kreitler, C. W., and Wuerch, H. V., 1981b, Carbon-14 dating of ground water near Oakwood Dome, East Texas, *in* Kreitler, C. W., and others, Geology and geohydrology of the East Texas Basin: a report on the progress of nuclear waste isolation feasibility studies (1980): The University of Texas at Austin, Bureau of Economic Geology Geological Circular 81-7, p. 156-161.

Myers, B. N., 1969, Compilation of results of aquifer tests in Texas: Texas Water Development Board Report 98, 532 p.

Narasimhan, T. N., Neuman, S. P., and Witherspoon, P. A., 1977, Mixed explicit-implicit iterative finite element scheme for diffusion type problems, II, solution strategy and examples: International Journal for Numerical Methods in Engineering, v. 11, p. 325-344.

Narasimhan, T. N., Neuman, S. P., and Witherspoon, P. A., 1978a, Finite element method for subsurface hydrology using a mixed explicit-implicit scheme: Water Resources Research, v. 14, no. 5, p. 863-877.

Narasimhan, T. N., and Witherspoon, P. A., 1977, Numerical model for saturated-unsaturated flow in deformable porous media, 1, theory: Water Resources Research, v. 13, no. 3, p. 657-664.

Narasimhan, T. N., and Witherspoon, P. A., 1978, Numerical model for saturated-unsaturated flow in deformable porous media, 3, applications: Water Resources Research, v. 14, no. 6, p. 1017-1034.

Narasimhan, T. N., Witherspoon, P. A., and Edwards, A. F., 1978b, Numerical model for saturated-unsaturated flow in deformable porous media, 2, the algorithm: Water Resources Research, v. 14, no. 2, p. 255-261.

Neuman, S. P., and Narasimhan, T. N., 1977, Mixed explicit-implicit iterative finite element scheme for diffusion type problems, I, theory: International Journal for Numerical Methods in Engineering, v. 11, p. 309-323.

Peckham, R. C., 1965, Availability and quality of ground water in Leon County, Texas: Texas Water Commission Bulletin 6513, 43 p.

Schlumberger, 1974, Log interpretation, volume II - applications: New York, Schlumberger Limited, 116 p.

Seni, S. J., and Fogg, G. E., 1982, Wilcox Group facies and syndepositional salt dome growth, southern East Texas Basin: The University of Texas at Austin, Bureau of Economic Geology, report prepared for the U.S. Department of Energy, Office of Nuclear Waste Isolation, 33 p.

Tarver, G. E., 1966, Ground water resources of Houston County, Texas: Texas Water Development Board, Report 18, 86 p.

Theis, C. V., 1935, The relation between the lowering of the piezometric surface and the rate and duration of discharge of a well using groundwater storage: American Geophysical Union Transactions, v. 2, p. 519-524.

Unitech, Inc., 1978, CPS-1 users manual: Austin, Texas, CPS-1 support staff, variously paginated.

Weres, O., and Schroeder, R. C., 1978, Documentation for program OGRE: University of California, Lawrence Berkeley Laboratory, report no. LBL-7060, prepared for U.S. Department of Energy under contract W-7405-ENG-48, 58 p.

Wood, D. H., and Guevara, E. H., 1981, Regional structural cross sections and general stratigraphy. East Texas Basin; The University of Texas at Austin, Bureau of Economic Geology Cross Sections, 21 p.

Wright T., ed., 1978, NCAR graphics software: fourth preliminary edition: Boulder, Colorado, National Center for Atmospheric Research, Atmospheric Technology Division.